

Escape from Titan's Atmosphere: Kinetic Monte Carlo Simulations

A Dissertation

Presented to

the faculty of the School of Engineering and Applied Science

University of Virginia

In Partial Fulfillment

of the requirements for the Degree

Doctor of Philosophy Engineering Physics

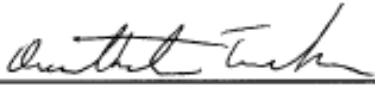
by

Orenthal J. Tucker

May 2012

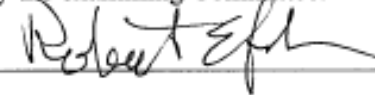
APPROVAL SHEET

The dissertation is submitted in partial fulfillment of the
requirements for the degree of
Doctor of Philosophy Engineering Physics

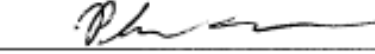
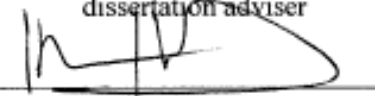


Author

This dissertation has been read and approved by the examining Committee:



dissertation adviser



Accepted for the School of Engineering and Applied Science:



Dean, School of Engineering and
Applied Science

May 2012

Abstract

Loss of atmosphere by molecular escape to space is an important aspect of the evolution of a planetary body. Saturn's moon Titan is a prime candidate for studying atmospheric loss because it possesses an atmosphere thicker than the Earth's but has a much smaller mass. Studies have shown that other satellites similar in size to Titan, like Jupiter's moon Ganymede, lost a Titan-like atmosphere over the age of the solar system. Therefore, a principal goal of the Cassini mission to Saturn has been to investigate atmospheric escape from Titan in order to understand the nature of its present atmosphere. Before Cassini started collecting data on Titan's atmosphere, the escape estimates were consistent with Titan retaining a large atmosphere over its lifetime in the solar system. As indicated by the ratio of its gravitation binding energy to the thermal energy of molecules, known as the Jeans parameter, the two principal species, N_2 and CH_4 , are strongly bound to Titan whereas the trace species, H_2 , is not. Although H_2 escape was assumed to be evaporative, the escape of N_2 and CH_4 was assumed to be driven by non-thermal processes. Surprisingly, a series of recent fluid and diffusion models of Titan's upper atmosphere, constrained to Cassini density data, suggested that the N_2 and CH_4 thermal escape rates were orders of magnitude larger than the pre-Cassini estimates.

A fluid approach, referred to as the slow hydrodynamic escape model, was used to propose that thermal conduction in the most dilute regions of the atmosphere can power a supersonic expansion leading to the significant escape rates. If these rates were correct Titan would have lost a significant portion of its current atmosphere over its lifetime. Because applying fluid models to the rarefied regions is problematic, I used

molecular kinetic Monte Carlo simulations to test the fluid results and to compare with Cassini density data for Titan's atmosphere.

For temperatures characteristic of Titan's upper atmosphere my molecular simulations reproduced the N_2 and CH_4 Cassini density measurements without requiring escape rates orders of magnitude larger than the evaporative rates. This was also the case when the upper atmospheric temperature was significantly increased. Therefore, our computational space science group at the University of Virginia performed a series of simulations to characterize the dependence of the escape rate on the Jeans parameter and the Knudsen number, which is an indicator of the rarefaction of a gas flow. Surprisingly, these simulations confirmed that for very small Knudsen number at the lower boundary of the simulation region the escape rate was evaporative in nature even for Jeans parameters typically considered in the slow hydrodynamic escape models.

Because Pluto's upper atmosphere has a composition similar to that at Titan but with much smaller Jeans parameters, I worked with fellow student Justin Erwin on a combined fluid/ molecular Monte Carlo simulation to model Pluto's upper atmosphere structure and atmospheric escape rate. This method was used to test hydrodynamic models in anticipation of the New Horizon spacecraft encounter with Pluto in 2015. This study also determined that thermal escape from Pluto's atmosphere was evaporative in nature, and the upper atmospheric structure differed significantly from the predictions of the hydrodynamic models.

Finally, Cassini data for varying levels of incident plasma bombarding Titan's upper atmosphere appear to have an effect on the N_2 density vs. altitude, but not on the H_2 density vs. altitude. Therefore, I performed molecular simulations of the diffusion and

escape of H_2 in a background atmosphere of N_2 and CH_4 at temperatures that corresponded to various levels of plasma heating. Over the range of characteristic temperatures of Titan's upper atmosphere used in the molecular model, the H_2 escape rates were similar, but the H_2 densities diffusively separated from the N_2 densities at lower altitudes with decreasing temperatures. This result appears to be contrary to the Cassini density data as I discuss.

Therefore, it appears that to correctly describe escape it is often necessary to couple continuum models for a planet's upper atmosphere with a kinetic model, because neglecting the non-equilibrium nature of the rarefied region can result in inconsistent escape rates and density and temperature structures.

Table of Contents

1. Introduction and Background -----	7
1.1 Origin of Titan's atmosphere -----	9
1.2 Isotope fractionation by atmospheric escape -----	13
1.3 Summary -----	14
2. Cassini data and escape processes -----	18
2.1 Exosphere and exobase -----	18
2.2 Titan: N ₂ , CH ₄ and H ₂ escape estimates -----	20
2.3 Models of thermal escape: Titan -----	23
2.3.1 Jeans Escape – thermal evaporation -----	24
2.3.2 Diffusion in Titan's upper atmosphere -----	25
2.3.3 Slow hydrodynamic escape -----	29
2.3.4 Titan Global Ionosphere and Thermosphere Model T-GITM -----	32
2.4 Non-thermal escape: Titan -----	33
2.5 Summary -----	40
3. Direct Simulation Monte Carlo (DSMC) Model -----	41
3.1 Boundary Conditions -----	42
3.2 Computational Domain and Particle Collisions -----	43
3.3 Sampling Atmospheric Properties -----	45
3.4 DSMC simulations for a trace gas -----	45
3.5 Fluid/DSMC simulations -----	47

3.6	Summary -----	50
4.	DSMC Simulations: Results -----	50
4.1	Thermal Escape of N ₂ and CH ₄ from Titan's Atmosphere-----	51
4.2	Transition from Hydrodynamic to Jeans Escape -----	57
4.3	Thermal escape of N ₂ from Pluto's atmosphere -----	60
4.3.1	Implications for New Horizons and Charon -----	69
4.4	Diffusion and thermal escape of H ₂ from Titan's atmosphere-----	72
4.4.1	INMS density data used in comparisons -----	72
4.4.2	3-component DSMC results for Titan's atmosphere -----	75
4.4.3	Comparison of DSMC and Diffusion model results-----	90
5.	Conclusions and Future Work -----	92

Figure 2-1: Integrated escape flux vs. radial distance.	20
Figure 2-2: Maxwell Boltzmann velocity distributions for $T_x = 160$ K.	21
Figure 2-3: Atmospheric models for particular regions in the upper atmosphere.	23
Figure 2-4: Averaged INMS density profiles.	27
Figure 2-5: Titan plasma interaction.	34
Figure 2-6: INMS density profiles suggestive of non-thermal heating.	36
Figure 2-7: Incident plasma energy spectrums for Titan's atmosphere.	39
Figure 3-1: Schematic of steps involved in DSMC simulation.	42
Figure 3-2: Schematic of the numerical implementation of the fluid/DSMC model.	47
Figure 4-1: SHE vs. DSMC model result for a N_2 Titan atmosphere.	52
Figure 4-2: DSMC results for escape forced to occur at the SHE loss rates.	54
Figure 4-3: DSMC results compared to INMS data for N_2 and CH_4	56
Figure 4-4: Transition from hydrodynamic to Jeans escape.	59
Figure 4-5: Pluto DSMC simulations for (HS, HS-LB, VHS, VHS-LB) models.	63
Figure 4-6: DSMC result for Pluto $\beta_0 = 0$ heating conditions.	66
Figure 4-7: DSMC result for Pluto $\beta_0 = 1.5 \times 10^{-3} \text{ erg cm}^{-2} \text{ s}^{-1}$ heating conditions.	68
Figure 4-8: Charon's influence on molecular escape from Pluto.	70
Figure 4-9: Averaged INMS densities for inbound Cassini trajectories.	74
Figure 4-10: Multi-component DSMC results compared to INMS data.	77
Figure 4-11: Density profiles for DSMC- H_2 simulations.	82
Figure 4-12: DSMC- H_2 simulations showing the effect of diffusion at various T_{N_2}	85
Figure 4-13: Individual INMS N_2 and H_2 density profiles.	87

Figure 4-14: DSMC results compared to T29 and T41 flybys.	89
Figure 4-15: Diffusion model fits of the INMS data.	90
Figure 4-16: DSMC-H ₂ velocity distributions.	91

Acronyms, Symbols and Definitions

CAPS – Cassini Plasma Spectrometer
 DSMC – direct simulation Monte Carlo
 DSMC-H₂ – DSMC model of H₂ in static background gas
 EUV – extreme ultraviolet radiation
 Fluid/DSMC – combined fluid and DSMC model
 GCMS – Gas Chromatograph Mass Spectrometer
 HS – hard sphere
 IR – infrared radiation
 INMS – ion neutral mass spectrometer
 LB – Larsen Borgnakke approximation (translational and internal energy transfer)
 lobe – low plasma flux conditions
 plasma sheet – high plasma flux conditions
 SHE – slow hydrodynamic escape
 TA – T41 – Cassini encounters with Titan’s atmosphere
 T-GITM – Titan Global Ionosphere and Thermosphere model
 UV – ultraviolet radiation
 VHS – variable hard sphere

C_p – constant pressure heat capacity per molecule

D_{12} – molecular diffusion coefficient

f - mixing ratio

G – gravitational constant

H – scale height

K – eddy diffusion coefficient

k – Boltzmann gas constant

Kn – Knudsen number

ℓ_{mfp} – mean free path

M_p – planetary mass

m – molecular mass

n – number density

p – pressure

Q – net heating/cooling rate per volume of the atmosphere

r – radial distance

T – temperature

T_{N_2} – background N_2 temperature used in DSMC- H_2 simulations

u – bulk flow velocity

v – molecular velocity

v_{esc} – escape velocity

$\langle v_{\text{th}} \rangle$ – mean thermal velocity

v_{r} – relative velocity

$\langle E\phi \rangle$ – average energy per time carried off by escaping molecules

$d\phi/dr$ – production of escaping molecules

α_{12} – thermal diffusion factor

β – column integrated heating rate of the atmosphere

κ – thermal conductivity

λ – Jeans parameter

ω – viscosity exponent

σ – collision cross-section

Φ/Φ_{00} – dimensionless escape rate

ϕ – molecular escape rate

Φ_{g} – gravitational potential

ϕ_{D} – diffusion flow rate

ϕ_{DL} – diffusion limited flow rate

ϕ_{J} – Jeans escape rate

Subscripts

0 – reference altitude or lower boundary

J – Jeans

x – exobase

1. Introduction and Background

The ongoing and very successful Cassini mission (2004 - 2017) to study the Saturn system has given planetary scientists a wealth of new data on its moons, rings and magnetosphere. Modeling of the data for the atmosphere of Saturn's largest moon Titan has required those who study the evolution of atmospheres to reconsider how to apply models for the thermal escape of molecules from the atmosphere of Titan and other astronomical bodies. In this dissertation, I investigate the results of recent models for atmospheric escape from Titan, and show the importance of using a molecular kinetic approach to model the uppermost regions of its atmosphere. The results have implications to planetary atmospheres in general, and to that end, I also analyze models of thermal escape from Pluto.

Titan possesses a terrestrial-like atmosphere with a surface pressure ~ 1.5 times that of the Earth and a surface temperature $\sim 1/3$ times of the Earth. The atmosphere is composed of $\sim 98\%$ N_2 , $\sim 1\%$ CH_4 , $\sim 0.1\%$ H_2 and sparse populations of complex organic molecules, which give Titan its unique orange haze. As a result of its low gravitational binding energy, 0.03 eV at the surface ($1/20$ of Earth's), a pressure of 1.5 times the Earth's is equivalent to a total column density that is about ten times that at Earth even though Titan has a radius ($R_T = 2575 \text{ km}$) only ~ 0.4 times that at Earth.

Molecular escape from Titan's atmosphere can occur thermally at characteristic temperatures, $\sim 100 - 200 \text{ K}$, of the upper atmosphere as a result of solar UV/EUV heating and heating due to bombardment by the plasma in Saturn's magnetosphere. In addition, atmospheric loss via non-thermal mechanisms is induced by a variety of

processes such as photochemistry, atmospheric sputtering, dissociative recombination, ionospheric sweeping, etc. which lead to the escape of neutral and ionized molecules (e.g., Cravens et al., 1997; Johnson, 1990; Johnson, 1994; Strobel and Shemansky, 1982). Pre-Cassini it was concluded that H_2 would escape most efficiently at thermal rates $\sim 10^{28} \text{ s}^{-1}$ (e.g., Hunten, 1973; Lebonnois et al., 2003). However, the escape of the heavier molecules N_2 and CH_4 was considered to be driven by non-thermal processes, and to occur at rates at least two orders of magnitude less than the H_2 rates, $< 10^{26} \text{ s}^{-1}$, consistent with Titan retaining much of its original atmosphere over 4 – 5 Gyr (e.g., Gan et al., 1992; Johnson, 2004; Michael and Johnson, 2005; Michael et al., 2005; Lammer et al., 1993; Shematovich et al., 2003; Strobel, 1992).

Surprisingly, using the Cassini data for the neutral densities in Titan's upper atmosphere, recent continuum models (e.g., Yelle et al., 2008; Strobel, 2008a, 2009, 2010) proposed that methane escape occurs thermally, in a hydrodynamic manner, at rates 100 times larger than the pre-Cassini non-thermal estimates. Molecular hydrogen escape estimates obtained from recent diffusion models remain consistent with the pre-Cassini rates, and the general consensus is that hydrogen escape is diffusion limited (e.g., Cui et al., 2008, 2009; Yelle et al., 2006, 2008). In these continuum models one solves the Navier-Stokes equations and/or the diffusion equation for an upward flux of molecules assumed to be escaping. This flux is a boundary condition used to fit the neutral density data versus altitude, and not an intrinsic result of the continuum models.

The continuum approach is most suitably applied to dense gas flows that exhibit small deviations from the equilibrium Maxwell Boltzmann velocity distribution (Bird, 1994; Chapman and Cowling, 1970). However, escape from planetary atmospheres

occurs from the uppermost regions of the atmosphere where the gas flow is rarefied. In this region the local velocity distribution of molecules can be significantly non-Maxwellian due to escape. Furthermore the different molecular species in the atmosphere, as well as the translation and rotational energy modes of a molecule, can attain different temperatures in this rarefied region. These non-equilibrium effects are the result of a decline in the frequency of collisions as the atmosphere becomes increasingly sparse with altitude. Therefore a kinetic approach is more suitable for describing escape from planetary atmospheres.

In this dissertation I examine how thermal escape affects the structure of Titan's upper atmosphere using a kinetic Monte Carlo model, commonly referred to as the Direct Simulation Monte Carlo (DSMC) model (Bird, 1994), calibrated to Cassini data. The results have implications for the evolution of Titan's atmosphere specifically, and ramifications on how continuum models are applied to the thermal escape problem in general. Because the atmosphere of Pluto has the same principal constituents as that of Titan, but the energy necessary to escape its gravity is an order of magnitude smaller, it provides an important test of many aspects of the modeling carried out here. Therefore, a hybrid DSMC–continuum model was also developed to describe escape from Pluto's atmosphere. In this introductory section, I will discuss how and why the current understanding of the origin and evolution of Titan's atmosphere is directly related to atmospheric escape.

1.1 Origin of Titan's atmosphere

Titan is the only moon in the solar system that possesses a thick terrestrial like atmosphere; in fact its surface pressure is larger than that at Mars and Earth and its total

column abundance is comparable to Venus's. Furthermore, it is also interesting that both of Jupiter's largest moons Ganymede and Callisto, which are similar in size to Titan, have surface pressures many orders of magnitude smaller. Therefore three questions emerge: How was the atmosphere formed? How has the atmosphere changed over time? Lastly, why does Titan still possess a significant atmosphere? These considerations are why Titan is considered an important endpoint in the study of the atmospheric evolution.

A planetary body can obtain an atmosphere by means of gravitational capture, cometary delivery or outgassing. In order to determine the origin of a planetary atmosphere the abundances and ratios of stable isotopes that compose the atmosphere are typically compared to corresponding solar and cometary values, see Table 1-1. For Titan the gravitational capture of N_2 has been ruled out by the lack of abundance of neon in the upper atmosphere compared to solar values, and the comet delivery of the N_2 and CH_4 have been ruled out because comets are probably deficient in the amount of N_2 needed to produce the atmosphere. In addition, comets have a D/H ratio 2 – 10 times that determined from hydrogen bearing molecules in Titan's atmosphere (e.g., Atreya et al., 2009; Bockelée-Morvan et al., 2004; Owen 1999; Lunine et. al., 2009). It is important to point out the N_2 isotope measurements for comets and the Sun, on which these considerations are based, are still ongoing (Owen et al., 2001). Nevertheless there is consensus that the dominant amount of Titan's atmosphere originated through the outgassing of volatiles that condensed on the planetesimals in Saturn's subnebula from which Titan was formed.

For the characteristic temperature (~75 K) of the ices that made up the planetesimals in Saturn's subnebula before Titan was formed, experiments have shown

that the trapping of ^{36}Ar and N_2 gas molecules in the ice, referred to as clathrate hydrates, would have occurred (Bar-Nun et al., 1988; Owen 1999). Therefore, it was suggested that if the N_2 in the Titan's current atmosphere is primordial the isotope ratio would be similar to the solar value $^{36}\text{Ar}/\text{N}_2 \sim 0.11$ (Grevesse et al., 2005). Measurements taken by the Cassini Huygens probe Gas Chromatograph Mass Spectrometer (GCMS) in the well mixed region of the atmosphere obtained an isotope ratio of $^{36}\text{Ar}/\text{N}_2 \sim 3 \times 10^{-7}$, suggesting that molecular nitrogen in Titan's atmosphere is not primordial (Atreya et al., 2009).

Subsequently many planetary formation models have been aimed at determining how Titan obtained its N_2 atmosphere. These models of the outer solar system suggest that ammonia was the principal source of primordial nitrogen incorporated into the planetesimals that formed Titan even though N_2 is the present dominant nitrogen bearing species. N_2 is volatile in comparison to NH_3 which more bonds readily with water ice at low temperatures (Loeffler and Baragiola, 2012); therefore, it's likely that ammonia rather than N_2 was incorporated in the planetesimals that formed Titan (e.g., Lewis, 1971; Lunine et al., 2009; Prin and Fegley, 1981). There are four competing ideas about the subsequent source and conversion of the NH_3 to the N_2 : photolysis, endogenic processes, comet delivery and asteroid impacts (e.g., Atreya et al., 2009; Sekine et al., 2011). In the various photochemical scenarios, it is assumed that during accretion NH_3 was released into the atmosphere. For a temperature range of 150 K – 200 K and over time periods of 2 – 30 Myr photolytic decomposition into N_2 and H_2 could result in an initial N_2 surface pressure up to 20 bar on Titan (Atreya et al., 2009). In the endogenic scenario, heat generated within Titan's interior over time decomposes NH_3 to N_2 and H_2 , which subsequently led to the formation of N_2 clathrate hydrates in Titan's ice mantle and crust

that are periodically outgassed to form the atmosphere (Atreya et al., 2009). Lastly several plausible impact schemes involving comets and asteroids have been considered. Here I list a few: shock-induced dissociation of NH_3 during accretion (McKay et al., 1988), comet delivery of NH_3 (e.g., Mandt et al., 2009) and conversion of NH_3 by impacts occurring during the late heavy bombardment period (Sekine et al., 2011). The various ideas on the origin of Titan's N_2 atmosphere each have difficulties resolving the current $^{14}\text{N}/^{15}\text{N}$ isotope ratio, which is 60-70 % of that at Earth (Table 1-1) (e.g., Atreya et al., 2009; Sekine et al., 2011).

The origin of the methane in Titan's atmosphere remains unsolved as well. Based on measurements by the GCMS, the carbon isotope ratios $^{12}\text{C}/^{13}\text{C}$ are ~92 % of the terrestrial value (e.g., Niemann et al., 2005; Owen and Encrenaz, 2003). Therefore, several formation models conclude that present day Titan possesses a subsurface inventory of CH_4 (e.g., Lunine et al., 2009 and references therein). For example, photochemistry occurring in Titan's present atmosphere leads to the formation of H_2 , nitriles, hazes and heavy hydrocarbons that would deplete the current abundance of methane in the atmosphere in ~30 Myr (Atreya et al., 2009). The issue that remains unclear is whether the methane was native to Titan or produced in situ during Titan's formation.

Measurements of isotopic ratios in carbon bearing molecules detected on comets suggest that CO and CO_2 were more abundant than CH_4 in the solar nebula (Bockelée-Morvan et al., 2004), which is in agreement with the results of certain Titan formation models (e.g., Ailbert and Mousis, 2007; Hersant et al., 2008; Mousis et al., 2002; Prinn and Fegley, 1981). In these models N_2 , CO and CO_2 are dominant in the solar nebula but

NH_3 and CH_4 become dominant in Saturn's subnebula due to favorable chemical/transport processes. However the same models also predict that these processes would result in a solar abundance of the heavy primordial noble gases Kr, Xe and Ar on Titan (Mousis et al., 2002). Unfortunately, Cassini has detected little to no amounts of the noble gases in Titan's atmosphere (Niemann et al., 2005). Other scenarios have been suggested in which CO_2 and CO were converted to CH_4 in Titan's interior (Atreya et al., 2006), but it is unclear if such processes can reproduce the sub-solar D/H ratio determined in Titan's methane (Cordier et al., 2008).

Table 1-1: Cassini isotope ratios and mole fractions in Titan's atmosphere

Ratio	Homosphere measurements	Titan/Earth
$^{14}\text{N}/^{15}\text{N}$ (* N_2 ,)	183 ± 5	0.67
$^{12}\text{C}/^{13}\text{C}$ (* CH_4)	82.3 ± 1	0.92
D/H (* H_2 , # CH_4)	$(1.3 \pm 0.11) \times 10^{-4}$, $(2.3 \pm 0.5) \times 10^{-4}$	1.44
$^{36}\text{Ar}/(\text{N}_2 + \text{CH}_4)$	$(2.8 \pm 0.3) \times 10^{-7}$	7.0×10^{-3}
$^{40}\text{Ar}/(\text{N}_2 + \text{CH}_4)$	$(4.3 \pm 0.1) \times 10^{-5}$	3.6×10^{-3}

(Niemann et al., 2005) * GCMS(Gas Chromatograph mass spectrometer), # CIRS(Composite Infrared spectrometer) The homosphere is a well mixed region of the atmosphere where the mole fractions are nearly constant with altitude.

1.2 Isotope fractionation by atmospheric escape

Isotope fractionation in atmospheres refers to the preferential separation of isotopes by effects such as chemistry, condensation, diffusion, gravity and escape. In a strongly bound atmosphere, low mass isotopes, on average, will diffuse over time to higher altitudes and the processes that drive escape in the upper atmosphere will preferentially deplete the original inventory of light isotopes. The current surface pressure of 1.5 bar and nitrogen isotope ratio, $^{14}\text{N}/^{15}\text{N} \sim 143 - 183$, is considered by many researchers to be the result of escape (Lammer et al., 2000; Lunine et al., 1999; Niemann

et al., 2005; Owen, 2000). For example, Earth's nitrogen isotope ratio is considered to be primordial is $^{14}\text{N}/^{15}\text{N} \sim 270$ suggesting that Titan has undergone severe fractionation, assuming they both formed with the same inventory of elements. Using Cassini measurements for the N_2 isotopes and considering diffusive fractionation, the original inventory of nitrogen would have been $\sim 2 - 10$ times the current amount (e.g., Atreya et al., 2009).

Whether or not escape over Titan's history can explain the current isotope ratios is still unresolved. Models have shown that a hydrodynamic mass loss from Titan would be an efficient escape mechanism. However, it would be inefficient at fractionating the atmosphere, because it is a bulk loss process that is initiated near or below the altitudes where the molecules have not diffusively separated (Mandt et al., 2009). In the upper regions of the atmosphere, where molecules are diffusively separated, evaporative and non-thermal escape mechanisms are efficient fractionators, but it is unclear if such processes are robust enough to account for the current fractionation (e.g., Johnson, 2004; Mandt et al., 2009; Lammer et al., 2000; Lunine et al., 1999). In order to constrain these models, it is important to be able to correctly describe the physics of the current state of atmospheric loss from Titan, tested against the large Cassini database.

1.3 Summary

Understanding the origin and evolution of Titan's atmosphere represents an important endpoint in the study of the various ways planets, planetary satellites or the newly discovered exoplanets can obtain and lose their atmospheres. The ongoing Cassini mission (2004 - 2017), in which there have been to date more than 79 passes through Titan's upper atmosphere, is providing a plethora of data for atmospheric scientist to

refine computational models on atmospheric evolution and escape. Current measurements of the isotopic ratios for carbon, nitrogen and hydrogen are enhanced in the light isotope in comparison to the terrestrial values. Therefore many studies are aimed at determining whether or not Titan formed within the same inventory of primordial elements as Earth. One approach to resolve this issue is by properly characterizing the present escape of Titan's atmosphere to space, then to infer whether fractionation by escape is sufficient to account for the present isotopic ratios during periods of higher solar activity.

In this dissertation I will not try to solve the isotope ratio problem. Rather I will examine the role of N_2 , CH_4 and H_2 mass loss from Titan's atmosphere by escape to space with an emphasis on resolving issues that have arisen in describing thermal escape using a kinetic Monte Carlo model. Currently, there is considerable disagreement on the nature of escape between continuum models, which suggest a hydrodynamic type of loss, and kinetic models, that suggest an evaporative type of loss (e.g., Johnson, 2010; Johnson et. al., 2009). Here I demonstrate using the 'so-called' direct simulation Monte Carlo model that thermal escape of N_2 and CH_4 is insignificant at present, in comparison to the non-thermal escape estimates. And, while the H_2 does escape Titan's gravity at large rates, I will show it essentially occurs close to the theoretical Jeans rates. It is also shown that the continuum approach can result in inaccurate results for the escape flux and/or resulting macroscopic properties of the atmosphere as a result of improperly considering the heat transport in the rarefied region of the atmosphere. It is possible to accurately consider the heat flow into the rarefied region using continuum models only if such models are coupled to results obtained or verified by a kinetic approach in the non-equilibrium region of the atmosphere. My emphasis is on atmospheric escape from Titan

for comparisons to Cassini data, but the implications of the results on thermal escape in general are considered and examined in detail for Pluto, which has a similar composition but very different gravitational binding energy.

My PhD work has led to 5 publications on which I am first author and 8 publications on which I am a co-author. My early work focused on the effect of the incident plasma on Titan's atmosphere. However, realizing that continuum models were giving surprisingly large thermal escape rates, my focus shifted to correcting these results using a kinetic model for the regions of an atmosphere from which escape is occurring. Included below is a list of my most relevant publications pertaining to this dissertation followed by a list of other publications.

Most relevant publications:

Tucker, O. J. and Johnson, R. E., 2009, Thermally driven atmospheric escape: Monte Carlo simulations for Titan's atmosphere. Planet Space Sci. 57, 1889-1894.

Tucker, O. J., Erwin, J. T., Deighan, J. I., Volkov, A. N., Johnson, R. E., 2012. Thermally driven escape from Pluto's atmosphere: combined fluid/kinetic model. Icarus 217, 408-415.

Volkov, A. N., Johnson, R. E., Tucker, O. J. and Erwin, J. T. 2011a. Thermally-driven atmospheric escape: Transition from hydrodynamic to Jeans escape. Astrophys. J. 729, L24 1-5

Tucker, O. J., Johnson, R. E., Deighan, J. I., Volkov, A. N., 2012. Diffusion and thermal escape of H₂ from Titan's atmosphere: direct Monte Carlo simulations. To be submitted.

Related publications:

- Tucker, O. J., Erwin, J. T., Volkov, A. N., Cassidy, T. A., Johnson, R. E., 2011. *Escape from Pluto's atmosphere: Fluid/DSMC hybrid simulation. Proc. 27th International Symposium on Rarefied Gas Dynamics, Pacific Grove, USA, 2010, AIP Conf. Proc. 759 1333, pp. 1145–1150.*
- Johnson, R.E., Tucker, O.J., Michael, M., Sittler, E.C., Smith, H.T., Young, D.T., Waite, J.H., 2009. *Mass Loss Processes in Titan's Upper Atmosphere, Chapter 15 in Titan from Cassini-Huygens. (eds. R.H. Brown et al.) pp 373-391.*
- Volkov, A.N., Tucker, O.J., Erwin, J.T., Johnson, R.E., 2011b. *Kinetic simulations of thermal escape from a single component atmosphere. Phys. of Fluids 23, 06601.*
- Shah, M.B., Latimer C.J., Montenegro, E.C., Tucker, O.J., Johnson, R.E., Smith, H.T., 2009. *The implantation and interaction of O⁺ in atmosphere: Laboratory measurements of collision-induced of N₂ and Modeling of positive ion formation. ApJ 703:1947-1954 2009.*

Non-related publications

- Johnson, R.E., H.T. Smith, O.J. Tucker, M. Liu, and R. Tokar 2006. *The Enceladus and OH Tori at Saturn. Astrophys. J. Letts. 644:L137-L139.*
- Smith, H.T., R.E. Johnson, E.C. Sittler, M. Shappirio, D. Reisenfeld, O. J. Tucker, M. Burger, F.J. Crary, D.J. McComas, D.T. Young, 2007. *Enceladus The likely dominant nitrogen source in Saturn's magnetosphere. Icarus 188, 356-366.*
- Burger, M.H., E.C. Sittler Jr., R.E. Johnson, H.T. Smith, O.J. Tucker, and V.I. Shematovich 2007. *Understanding the escape of water from Enceladus. JGR 112, A0621.*

Cassidy, T.A., R.E. Johnson, and O.J. Tucker, 2009. Trace constituents of Europa's atmosphere", Icarus 201, 182-190.

Tucker, O.J., D.S. Ivanov, R.E. Johnson, L.V. Zhigilei, and E.M. Bringa, 2005. Molecular dynamics simulation of sputtering from a cylindrical track: EAM versus pair potentials", Nucl. Instrum. and Methods B 228, 163-169.

2. Cassini data and escape processes

2.1 Exosphere and exobase

As a result of gravity, the density a planetary atmosphere typically decreases with increasing distance from the planet center r according to the hydrostatic law, $d(nkT_0)/dr = -n/H(r)$, where n is the density, k is Boltzmann's constant, $T_0 = T(r_0)$ is temperature and $H(r)$ is the atmospheric scale height. The hydrostatic density profile in an isothermal atmosphere decreases exponentially with increasing altitude according to its scale height:

$$n(r) = n_0(r_0) \exp \left[-\frac{r_0}{H(r_0)} + \frac{r}{H(r)} \right]. \quad \text{Equation 2-1}$$

Chamberlain (1963) reviewed atmospheric 'evaporation' from the most tenuous regions of an atmosphere by defining a critical layer above which collisions could be ignored. This region of the atmosphere, where molecular escape is most efficient, is often referred to as the outermost atmosphere, planetary corona or exosphere (Chamberlain, 1963). In this region a molecule will have a high probability to escape to space if its motion is directed outward and it has an energy greater than the planet's gravitational binding energy $\Phi_g(r) = GM_p m/r$ (where G is the gravitational constant, M_p is the planet mass and m is the molecule mass). Quantitatively, the rarefaction of a gas flow at a particular altitude can be expressed by the local Knudsen number Kn which is the ratio of

the mean free path for a collision ℓ_{mfp} to a corresponding macroscopic length scale. For a hydrostatic atmosphere this length scale is the atmospheric scale height, $H(r) = kT_0 r / \Phi_g(r)$ and $Kn = \ell_{\text{mfp}} / H(r)$. The exosphere is typically defined as the region of atmosphere where the Knudsen number is $Kn \geq 1$, and the lower boundary is referred to as the nominal exobase where $Kn = 1$ (e.g., Chamberlain, 1963; Banks and Kockarts, 1973; Jeans, 1916; Spitzer, 1949). Hence on average a molecule that suffered its previous collision near the exobase can travel a distance over which the density will decrease by a factor $1/e$ without suffering another collision. In terms of the hydrostatic column density, N , this critical level occurs at the altitude where $N \sim c/\sigma$, for the collision cross-section between molecules, σ with c of the order of unity (Johnson et al., 2008).

Molecules that obtain relatively high kinetic energies from interactions with the incident plasma or by photochemical reactions can escape from depths well below nominal exobase. These molecules as well as those in the tail of a Maxwellian distribution, referred to as suprathermal, can have kinetic energies much greater than the gravitational binding energy. Johnson (1990, 1994) used realistic potentials to determine the mean free path when considering the deflections of suprathermal molecules within a background gas and analytically derived an average escape column resulting in $c \sim 1.3$, with σ equal to the diffusion (momentum transfer) cross section (e.g., Johnson et al., 2008). Therefore, it should be kept in mind that escape occurs from a broad region of altitudes in real planetary atmospheres with the most energetic molecules being able to escape from depths several scale heights below the exobase as shown by the mass integrated escape flux profiles in Figure 2-1. The energetic H_2 molecules (Figure 2-1(a)) obtain escaping trajectories primarily through thermal collisions (Lebonnois et al., 2003),

and the N atoms (Figure 2-1(b)) are suprathermal particles produced from non-thermal interactions (Johnson et al., 2008; Shematovich et al., 2003).

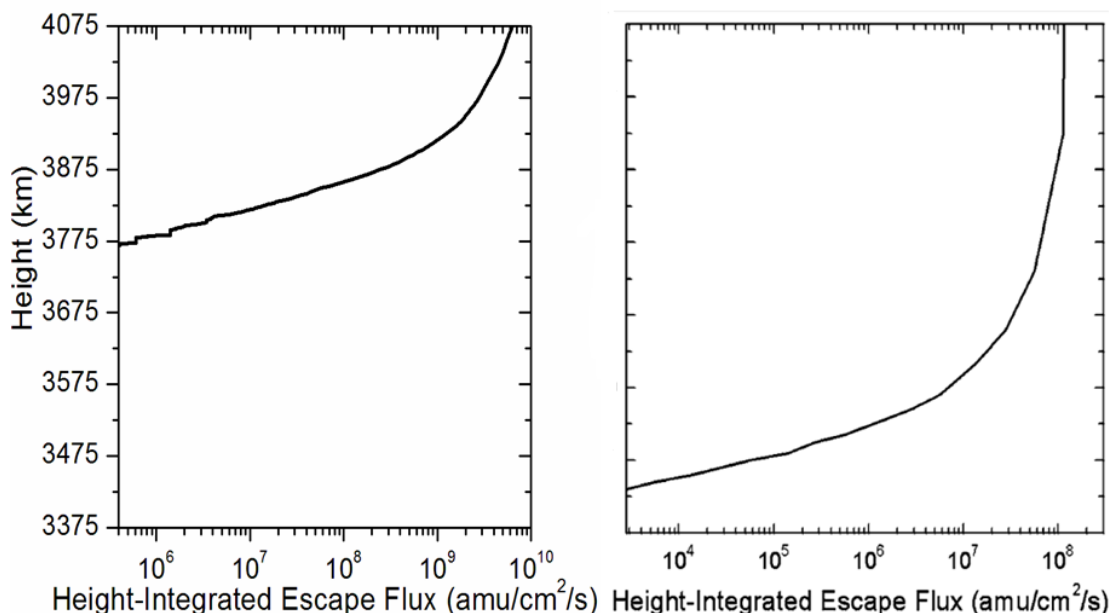


Figure 2-1: Integrated escape flux vs. radial distance.

Left frame: Integrated thermal escape flux of H₂. Right frame: Integrated escape flux of N atoms, non-thermal induced escape (Shematovich et al., 2003). Molecular escape is seen to occur over a broad range of altitudes about the exobase depending on the driving mechanism. (Titan radius $R_T = 2575$ km and the averaged exobase radial distance is $r_x \sim 4075$ km)

2.2 Titan: N₂, CH₄ and H₂ escape estimates

Prior to Cassini it was concluded the escape of N₂ and CH₄ would be driven principally by non-thermal processes and H₂ escape occurred essentially at the Jeans theoretical rates (e.g., Johnson et al., 2009) as discussed in more detail below. If it is assumed the molecules have a Maxwell Boltzmann distribution of velocities at inferred temperatures for Titan's exosphere (100 – 200 K), the N₂ and CH₄ molecules will have a very low probability of having an escape velocity because of their much larger masses in comparison to H₂ (Figure 2-2). Shown in Table 2-1 are the pre-Cassini estimated escape

rates presented as mass loss rates, based on Voyager 1 data, for the non-thermal induced escape of nitrogen and carbon atoms $\sim 1 - 6 \times 10^{26} \text{ amu s}^{-1}$. If these loss rates are applied since its formation, then the overall mass loss rates are consistent with Titan only losing a small fraction of its current atmospheric mass $\sim 1\%$ over 4.5 Gyr (Johnson, 2004).

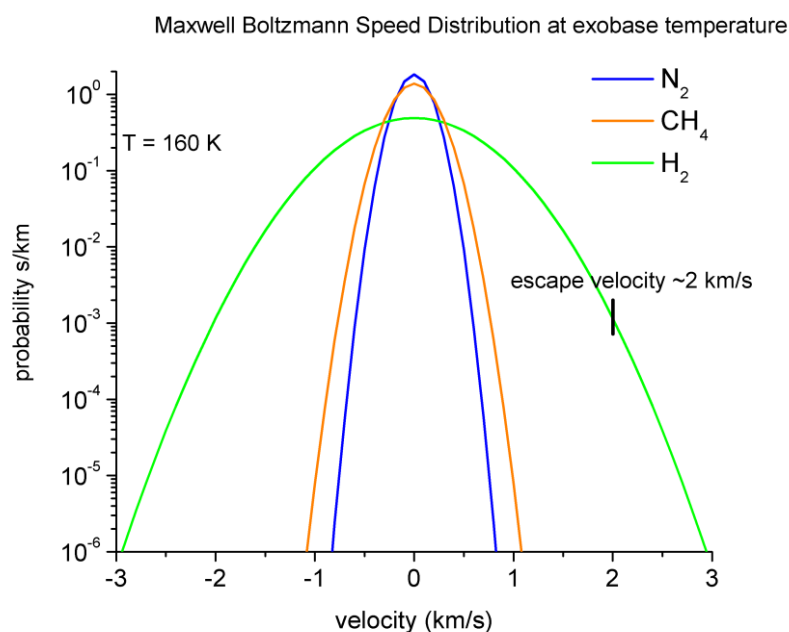


Figure 2-2: Maxwell Boltzmann velocity distributions for $T_x = 160 \text{ K}$.

At thermal speeds characteristic of the temperature in Titan's exosphere molecular nitrogen and methane have very low probabilities of obtaining an escape velocity via thermal collisions.

Surprisingly, in contrast to the pre-Cassini estimates, recent calculations of the structure of Titan's thermosphere calibrated to density versus altitude measurements made by the Ion Neutral Mass Spectrometer (INMS) instrument led to substantially larger mass loss estimates for N_2 and CH_4 $0.3 - 5 \times 10^{28} \text{ amu/s}$ (e.g., Strobel, 2008a, 2009, 2010; Yelle et al., 2008), as summarized in Table 2-1. Furthermore, these loss rates were

assumed to be driven by thermal conduction in the upper atmosphere and not via non-thermal processes. At these rates a significant fraction of the present atmospheric mass would have been lost over Titan's lifetime. The loss of hydrogen was found to be consistent with pre-Cassini estimates as confirmed by the Cassini data of density vs. altitude data for H₂ (e.g., Garnier et al., 2007; Waite et al., 2005; Yelle et al., 2006). However, the processes driving H₂ escape are not well understood. In summary, the estimates presented in Table 2-1 highlight the uncertainty in both the mass loss rates to space for N₂ and CH₄ as well as a dominant loss mechanisms driving escape for all 3 principal species. In Sections 2.3 and 2.4, I review some of the models for thermal and non-thermal escape from Titan's atmosphere used to obtain the loss rates.

Table 2-1: Escape processes and estimated rates for Titan's atmosphere

Atmospheric Component	Escape Process	Loss Rate
<i>(in 10²⁸ amu/s ≈ 0.2 Titan Atmospheric Masses/4Gyr)</i>		
Pre Cassini		
a. H ₂	Jean's Escape	~ 1 –3
b. CH ₄	Destruction/Precipitation	~ 10 –30
c. C, N	Photochemistry & Sputtering	~ 0.01 – 0.06
Based on Cassini Data		
d. Ions	Pickup/ Outflow	~ 0.01- 0.05
e. H ₂	Thermal Escape	~ 0.8 -2
f. CH ₄	Destruction/Precipitation	~ 24
g. N ₂ /CH ₄	Corona Fits (1450 -2000km)	~ 0.00 - 0.16
h. N ₂ /CH ₄	Sputtering	~ 0.3 - 3.6
i. CH ₄	Hydrodynamic	~ 4 –5
j. CH ₄ + H ₂	Hydrodynamic	~ 4.5
a. (e.g., Lebonnois et al., 2003), b. (Wilson and Atreya 2004); c. (Michael et al., 2005; Shematovich et al., 2003; Cravens et al., 1997; Lammer and Bauer, 1993; Strobel et al., 1982; Gan et al., 1992; etc.), d. (Hartle et al. 2006; Coates et al., 2007; Ma et al., 2006; Sillanpaa et al. 2006; Wahlund et al., 2005; etc.), e. (Cui et al., 2008 ; Garnier et al., 2008; Bell et al., 2010a,b), f. (based on the H ₂ data in Cui et al., 2008 and model of Wilson and Atreya, 2004; Mandt et al., 2009), g. (DeLaHaye et al., 2007a ; Bell et al., 2009 ; based on kappa fits), h.(DeLaHaye et al., 2007a; average for 5 passes based on analytic model and coronal structure), i. (Yelle et al., 2008), j. (Strobel 2008a, 2009)		

2.3 Models of thermal escape: Titan

The thermal escape estimates discussed in Section 2.1 were obtained by considering models of the thermosphere and the exosphere (Figure 2-3). In the thermosphere, $Kn < 1$, molecular collisions are frequent allowing molecules to maintain a Maxwell Boltzmann distribution of velocities. Therefore, the diffusion equation and the Navier Stokes fluid equations can be applied to this region in order to infer the net upward flux of molecules typically assumed to be escaping. At higher altitudes in the exosphere, $Kn > 1$, infrequent collisions and molecular escape result in a non-Maxwellian velocity distribution. Therefore, in this region, the escape flux is estimated at the molecular level using concepts from the kinetic theory of gases by obtaining solutions to the collisionless Boltzmann equation or performing Monte Carlo simulations. In principle, the full Boltzmann equation can be applied to the thermosphere and exosphere to obtain the macroscopic atmospheric properties in a self-consistent manner but is often a difficult task (e.g., Chamberlain, 1963; Shizgal and Blackmore, 1986).

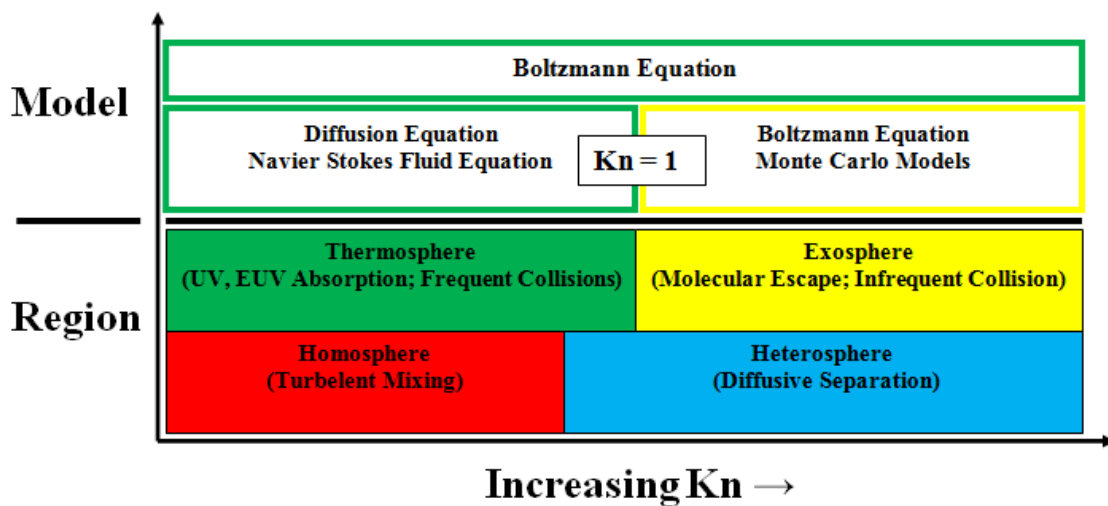


Figure 2-3: Atmospheric models for particular regions in the upper atmosphere.

2.3.1 Jeans Escape – thermal evaporation

At the beginning of the 20th century interest emerged in applying concepts of kinetic theory to the thermal ‘evaporation’ or the escape of planetary atmospheres. This was assumed to occur from the exobase above which the atmosphere is assumed to be collisionless. Jeans (1916) popularized the analytical expression for thermal escape from the exobase for molecules assumed to possess Maxwell Boltzmann distribution of velocities.

$$f_{mb}(v) = \left(\frac{m}{2\pi kT} \right)^{3/2} \exp\left(\frac{-mv^2}{2kT} \right); v \text{ is the molecular velocity} \quad \text{Equation 2-2}$$

For such conditions it was shown that thermal escape depends on the ratio of the gravitational energy to the thermal energy of molecules, $\lambda = \Phi_g(r)/kT$, commonly referred to as the Jeans parameter. Integrating over those molecules that cross the exobase with total energy such that their speeds exceed the escape speed, $v \geq v_{esc}$, results in the following equation, commonly referred to as the theoretical Jeans escape rate:

$$\varphi_J = 4\pi r_x^2 n_x \int_0^{2\pi} \int_0^\pi \int_{v_{esc}}^\infty v^3 f_{mb}(v) dv \sin \phi d\phi d\theta = \pi r_x^2 n_x \langle v_{th,x} \rangle (1 + \lambda_x) \exp(-\lambda_x) \quad \text{Equation 2-3}$$

where subscript ‘x’ refers to quantities evaluated at the exobase distance r_x and

$\langle v_{th,x} \rangle = (8kT_x/\pi m)^{1/2}$ is the mean thermal speed. The above integration is performed in spherical coordinates for polar angle ϕ and azimuthal angle θ . The concomitant energy per unit time carried away by escaping molecules (e.g. diatomic) is:

$$\langle E\varphi \rangle_J = \varphi_J (kT_x) \left(2 + \frac{1}{1 + \lambda_J} \right) \quad \text{Equation 2-4}$$

For large Jeans parameters the atmosphere is strongly bound so that ϕ_J and $\langle E\phi \rangle_J \rightarrow 0$ with $\lambda_x \rightarrow \infty$. However, for small Jeans parameters the escape flux, $\phi_J / 4\pi r_x^2 \rightarrow \frac{1}{4} n_x \langle v_{th,x} \rangle$, and energy flux, $\langle E\phi \rangle_J / 4\pi r_x^2 \rightarrow (3kT_x) \left(\frac{1}{4} n_x \langle v_{th,x} \rangle \right)$, of molecules is similar to that of free expansion. The Jeans parameters at Titan's exobase distance, $r_x \sim 4075$ km with $T_x = 150$ K, would be $\lambda_x(\text{N}_2, \text{CH}_4, \text{H}_2) = (48, 27, 3)$, and with approximate exobase densities of $n_x(\text{N}_2, \text{CH}_4, \text{H}_2) \sim (10^7, 5 \times 10^6, 1 \times 10^6) \text{ cm}^{-3}$ the corresponding Jeans rates are $\phi_J \sim 10^{10}, 10^{18}$ and 10^{28} molecules/s ($\sim 10^{11}, 10^{19}$ and 10^{28} amu/s).

2.3.2 Diffusion in Titan's upper atmosphere

In the Jeans treatment, the atmosphere is assumed to be isothermal and in hydrostatic equilibrium, with the constituents possessing density gradients representative of their individual scale heights. However atmospheric turbulence at lower altitudes tends to drive the scale height of a low mass trace constituent to that of the heavier background gas (Banks and Kockarts, 1973). For example, this is seen in the averaged INMS density data set (Figure 2-4(a)) where the H_2 density profile has a similar gradient to the N_2 density profile below 3775 km but above diffusive separation occurs.

Assuming a hydrostatic background atmosphere of density n_2 , the diffusion rate, ϕ_D , of a trace gas of density n_1 through the background gas can be written as the following:

$$\phi_D = -4\pi r^2 D_{12} n_1 \left[\frac{1}{n_1} \frac{dn_1}{dz} + \frac{1}{H_1(r)} + \left(\frac{1 + \alpha_{12}}{T} \right) \frac{dT}{dz} \right] \quad \text{Equation 2-5}$$

where α_{12} is the thermal diffusion factor, $D_{12} = \left(\frac{b}{n_1 + n_2} \right)$ is the binary diffusion

coefficient and $b \propto T^\omega$ where $\omega \sim (0.7 - 1.0)$ is related to the viscosity exponent (Chapman and Cowling, 1970). The thermal diffusion factor is a gas parameter which depends on the intermolecular forces, and typically for models of Titan's atmosphere, this factor or the temperature gradient is assumed to be negligible (e.g., Cui et al., 2008, 2009; Hunten, 1973; Yelle et al., 2006, 2008) giving

$$\varphi_D = -4\pi r^2 n_1 D_{12} \left(\frac{1}{n_1} \frac{dn_1}{dr} + \frac{1}{H_1(r)} \right) \quad \text{Equation 2-6}$$

Rewriting Equation 2-6 in terms of the mixing ratio $f = n_1/n_2$ leads to the expression:

$$\varphi_D = \left[\varphi_{DL} - 4\pi r^2 D_{12} n_2 \frac{df}{dr} \right] \quad \text{Equation 2-7}$$

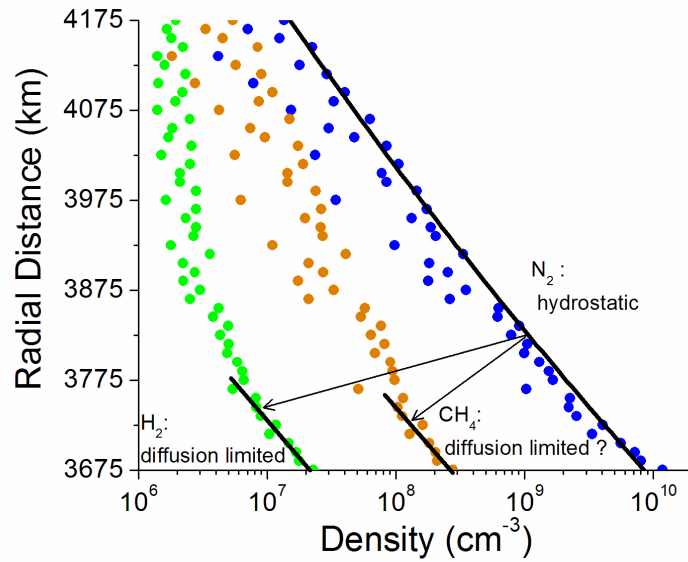
where φ_{DL} is referred to as the diffusion limited flow rate.

$$\varphi_{DL} = 4\pi r^2 f_{12} b \left(\frac{1}{H_2(r)} - \frac{1}{H_1(r)} \right) \quad \text{Equation 2-8}$$

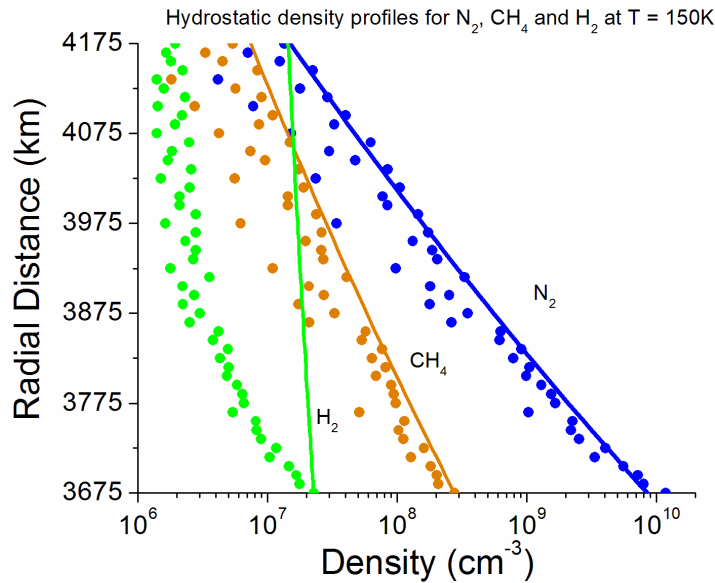
If mixing ratio, f , is nearly constant with altitude, diffusion occurs at the limiting rate, $\varphi_D = \varphi_{DL}$, likewise, for $\varphi_D \rightarrow 0$ the density profile of n_1 will follow the hydrostatic law.

The result in Equation 2-8 is insensitive to temperature, as the temperature dependence in the scale height nearly cancels with that in the diffusion coefficient (Hunten, 1973).

The diffusion equation is typically used to model the transition region between the homosphere, where molecular species are well mixed, and the heterosphere where molecular species diffusively separate.



(a)



(b)

Figure 2-4: Averaged INMS density profiles.

The data (filled circles) for N_2 (blue), CH_4 (orange) and H_2 (green) was taken during inbound trajectories of Cassini into Titan's atmosphere. a) Below 3775 km the density gradient for the trace component H_2 tracks with N_2 , because the gases are well mixed (black lines). The N_2 density profile can be fit with the hydrostatic law for $T \sim 150$ K; however, the H_2 density profile above ~ 3770 km is best fit with the diffusion equation (Equation 2-7). b) Hydrostatic density profiles (colored lines) for $T \sim 150$ K: N_2 (blue), CH_4 (orange) and H_2 (green).

Several diffusion models have been used to infer CH₄ and H₂ escapes rates constrained by the globally averaged INMS data and all have obtained similar results (e.g., Cui et al., 2008, 2009; Cui et al., 2011; Waite et al., 2005; Yelle et al., 2006, 2008). In these approaches the N₂ density profile is assumed to be hydrostatic, and the diffusion equation (Equation 2-7) is fit to the INMS density data for CH₄ and H₂ by choosing an upward diffusive flow rate, ϕ_D , that is assumed to be the globally averaged escape rate for each species. As discussed above, inspection of the INMS globally averaged density data clearly indicates that H₂ escape is limited by diffusion as pointed out in Yelle et al. (2006), and several models infer that H₂ escapes at the limiting rate enhanced over the theoretical Jeans rate by up to factor of ~ 3 (Cui et al., 2008; Yelle et al., 2006).

However, the inferred methane escape rates obtained by diffusion models applied to the methane density profiles are highly uncertain. That is, depending on the particular Cassini flyby, or averaged data set, it is possible to roughly fit the CH₄ density profile to the hydrostatic equation or to several different values of the diffusion rate (Yelle et al., 2006). Between individual Cassini flybys and even for inbound and outbound trajectories within individual flyby event, the density profiles for methane and molecular nitrogen have been shown to exhibit significant variations considered to be suggestive of horizontal transport and/or energy deposition directly into the thermosphere above the homopause (e.g., Müller-Wodarg and Yelle, 2002; Yelle et al., 2006; Westlake et al., 2011). These processes can drive turbulence at high altitudes, which are often modeled as eddy diffusion. Turbulence tends to keep the atmosphere well mixed and can be included in the diffusion equation in a form similar to molecular diffusion (e.g., Banks and Kockarts, 1973). Similar to the binary diffusion coefficient for molecular diffusion,

turbulent mixing can be characterized by an eddy diffusion coefficient K . Yelle et al., (2006) was able to fit the diffusion equation including eddy diffusion to an averaged INMS CH_4 density set using a range of methane escape fluxes and eddy diffusion coefficients, with the large eddy diffusion coefficients requiring small escape fluxes and vice versa. Later, Yelle et al., (2008) constrained the eddy diffusion coefficient, $K(r) \sim 2-5 \times 10^7 \text{ cm}^2 \text{ s}^{-1}$, using the INMS Ar density data. Based on this, they inferred that methane also escapes approximately at the diffusion limited rates, $2-2.5 \times 10^{27} \text{ CH}_4/\text{s}$ ($3-4 \times 10^{28} \text{ amu/s}$). This escape rate is many orders of magnitude larger than the corresponding Jeans rate for the suggested exobase temperatures. Therefore, it was concluded that horizontal transport due to thermospheric winds and energy input into the upper thermosphere region drives an upward flow of CH_4 molecules limited by vertical mixing below the homopause (Yelle et. al., 2008).

2.3.3 *Slow hydrodynamic escape*

Strobel (2008a, 2009, 2010) postulated that the escape flux is the result of a slow hydrodynamic expansion of Titan's atmosphere that leads to the escape of CH_4 and H_2 , driven by the conduction of heat from solar UV and EUV radiation. The slow hydrodynamic escape (SHE) model, considered intermediate to Jeans escape and the hydrodynamic outflow has been suggested to be applicable to a dense, tightly bound atmosphere for which the Jeans parameter at a radial distance, r_0 , below the exobase is $\lambda(r_0) > \sim 10$ (e.g., Parker, 1964b; Watson et al., 1981). The flow is referred to as slow because near r_0 the gravitational energy $\Phi_g(r)$ dominates the thermal energy ($C_p T$), which also dominates the flow energy ($\frac{1}{2} m u^2$), where C_p is the heat capacity per molecule and $u(r)$ is the flow speed. However, in this model the flow velocity can become larger than

the isothermal sound speed, $c_s = (kT/m)^{1/2}$, so that the outflow becomes supersonic at distances far above the exobase, resulting in escape rates much larger than the Jeans rate.

Using the SHE model, solutions were obtained to the Navier Stokes fluid equations for continuity, momentum and energy for $n(r)$ and $T(r)$. The 1D steady-state continuity equation leads to a constant molecular flow given here as a flow rate, ϕ , vs. radial distance:

$$\phi = 4\pi r^2 n(r) u(r) = 4\pi r_0^2 n(r_0) u(r_0) \quad \text{Equation 2-9}$$

The radial momentum equation, in which the viscous term is dropped, is:

$$\frac{dp}{dr} = n \left(\frac{d(\Phi_g - 1/2 mu^2)}{dr} \right) \quad \text{Equation 2-10}$$

with the gas pressure $p = nkT$. Finally, the corresponding energy equation is:

$$\frac{d}{dr} \left\{ \phi \left(\frac{1}{2} mu^2 + C_p T - \Phi_g \right) - 4\pi r^2 \kappa(T) \frac{dT}{dr} \right\} = 4\pi r^2 Q(r) \quad \text{Equation 2-11}$$

where $\kappa(T)$, is the thermal conductivity and $Q(r)$ accounts for the solar heating and IR cooling rates. Knowing the number density, n_0 , and temperature, T_0 , at the lower boundary, i.e. $n(r_0) = n_0$, $T(r_0) = T_0$, Equation 2-10 and Equation 2-11 are solved. A unique solution requires two additional parameters at the lower boundary, u_0 (or ϕ) and $(dT/dr)_0$. In order to find u_0 and $(dT/dr)_0$, one needs to impose assumptions about the behavior of density and temperature at $r \rightarrow \infty$. The typical upper boundary conditions when solving the fluid equations in the SHE model are $n, T \rightarrow 0$ as $r \rightarrow \infty$ (Parker, 1964a,b). Since the flow is slow, the standard procedure is to integrate Equation 2-10 and Equation 2-11 neglecting the u^2 terms (Parker, 1964a,b). Therefore, although $\phi \neq 0$ in

Equation 2-9, u^2 is set equal to 0 in Equation 2-10 and Equation 2-11 below an upper boundary where $1/2 mu^2 \ll C_p T$, and T and n are only regarded as valid out to an r where the u is a small fraction of the local sound speed (e.g., McNutt, 1989; Krasnopolsky, 1999; Strobel, 2008a,b).

The pressure and the heat flow are determined from the integration of Equation 2-10 and Equation 2-11 using the total heating rate $\beta(r) = r_0^{-2} [\int_{r_0}^r Q(r) dr]$ with $\beta \rightarrow \beta_0$ as $r \rightarrow \infty$, as defined in Strobel (2008a), and ϕ and $\langle E\phi \rangle_{r_0}$ are constants of integration.

Energy conservation requires that the energy carried off by escaping molecules, $\langle E\phi \rangle$, is replaced by a flow of energy into the lower boundary, $\langle E\phi \rangle_{r_0}$,

with $\langle E\phi \rangle = \langle E\phi \rangle_{r_0} + 4\pi r_0^2 \beta_0$:

$$p = p_0 \exp \left[- \int \frac{\lambda(r)}{r} dr \right] \quad \text{Equation 2-12}$$

$$\phi(C_p T - \Phi_g) - 4\pi r^2 \kappa(T) \frac{dT}{dr} = \langle E\phi \rangle_{r_0} + 4\pi r_0^2 \beta(r) \quad \text{Equation 2-13}$$

In the SHE model, the flow energy to infinity is assumed to be negligible $\langle E\phi \rangle = 0$.

Therefore to find a solution one varies the parameters ϕ and $(dT/dr)_0$ to find a solution with the right asymptotic behavior, zero total energy flux at $r \rightarrow \infty$ and consistent with density data, when available.

Strobel (2008) numerically solved Equation 2-10 and Equation 2-11 for a N_2 atmosphere including the heat deposited by solar UV radiation primarily absorbed by methane molecules. Assuming a single representative species, N_2 , he obtained a mass loss rate $4\text{--}5 \times 10^{28}$ amu/s ($1\text{--}2 \times 10^{27}$ N_2 /s) that he subsequently attributed to CH_4 and H_2

escape. Later in Strobel (2009), he re-wrote the continuity and momentum equation for a 3-component atmosphere to directly obtain the CH_4 and H_2 loss rates. In this study, he included ion-chemistry which results in a net destruction of CH_4 and net production of H_2 , as well as the effects of eddy diffusion considered in Yelle et al. (2008). Again he concluded, using data averaged over a number of passes through Titan's upper atmosphere, that escape occurred many orders of magnitude larger than the Jeans rates: e.g., $1.7 \times 10^{27} \text{ CH}_4/\text{s}$ ($2.7 \times 10^{28} \text{ amu/s}$) and $9.2 \times 10^{27} \text{ H}_2/\text{s}$ ($1.8 \times 10^{28} \text{ amu/s}$). It was determined that ion chemistry and non-thermal processes had a negligible effect on the escape rates.

2.3.4 Titan Global Ionosphere and Thermosphere Model T-GITM

Solar UV radiation ionizes molecules in the thermosphere and exosphere and the region over which these charged particles are produced is referred to as the ionosphere. Bell et al. (2010a,b) solved the steady state radial Navier Stokes fluid equations for neutral molecule and ion densities in Titan's thermosphere using his Titan Global Ionosphere and Thermosphere (T-GITM) model. There are differences between T-GITM and the SHE model in Strobel (2009): (1) the equations are integrated to the exobase, (2) sub-sonic solutions are permitted, and (3) diffusive equilibrium is enforced at the exobase. Under similar conditions the T-GITM and SHE model yield the same results for escape rates and densities; however, Bell et al. (2010a,b) emphasizes that the high escape rates, if correct, are produced by external mechanisms and not via upward thermal heat conduction as suggested by the SHE model. In fact, when the densities were scaled upward by a factor of 3 due to recalibration of the INMS instrument, Bell et al. (2010a,b)

determined the CH_4 density profiles could be fit with Pre-Cassini rates for non-thermal induced escape.

2.4 Non-thermal escape: Titan

In the exobase region molecules can escape thermally or via non-thermal processes as discussed earlier. For instance, non-thermal processes associated with the interaction of Saturn's magnetosphere with Titan's atmosphere can both drive escape and modify the upper atmospheric structure. Saturn's magnetosphere, composed primarily of electrons, protons and water group ions (i.e., H^+ , H_2^+ , O^+ , O_2^+ etc), has a complex configuration. The localized ion compositions, densities and energies vary significantly depending on Titan's orbital position and orientation with respect to Saturn's magnetospheric plane (e.g., Sittler et al., 2010; Mauk et al., 2009) At Titan's orbital position Saturn's magnetosphere is non-isotropic as a result of the interaction with the solar wind. The field configuration is dipole like when Titan is on the sunward facing side of Saturn and disk like when Titan is on the anti-sun side. The trapped heavy ions are primarily confined to the disk or near the magnetic equator in the dipolar region typically referred to as the plasma sheet (Figure 2-5(a)). When Titan orbits within the plasma sheet it is most exposed to the heavier water group ions but outside the plasma sheet it is exposed primarily to the trapped protons. In addition, Titan has a 16 day orbital period, but the magnetic field revolves every 10 hours, leading to a fluid like flow of the plasma about Titan (Figure 2-5(b)). Finally, sometimes Titan can orbit outside of Saturn's magnetosphere where it is instead exposed to shocked solar wind plasma.

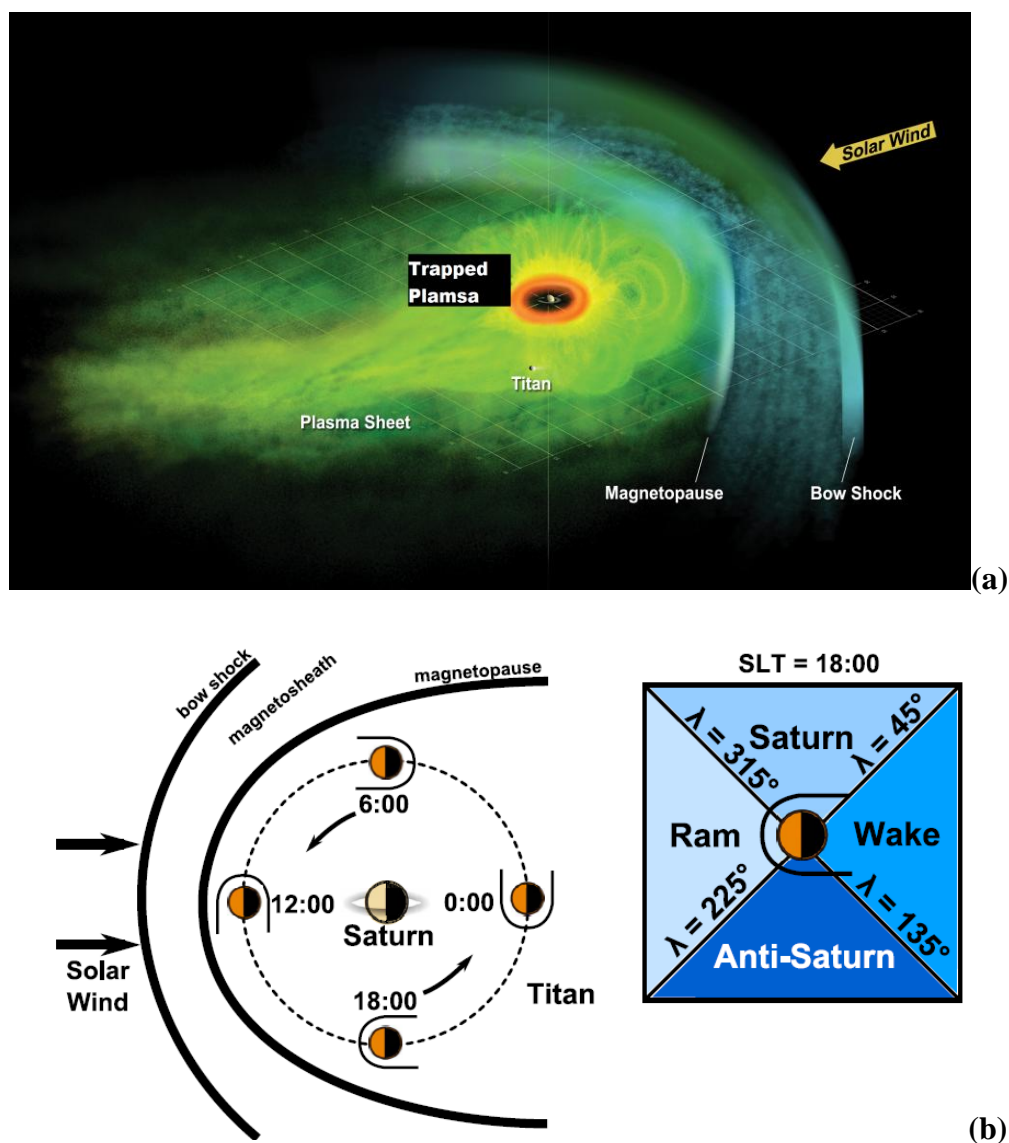


Figure 2-5: Titan plasma interaction.

a) Artistic image of Titan's interaction with Saturn's magnetosphere. Over Titan's orbit the plasma composition and temperatures in Saturn's magnetosphere are highly variable (image credit NASA/JPL/JHUAPL). b) Titan's position versus Saturn local time SLT. Titan orbits Saturn every 16 days counter clockwise and Saturn's magnetic field rotates every 10 hours (image from Westlake et al. 2011).

Solar UV radiation, plasma from Saturn's magnetosphere, and the solar wind ions can all interact with molecules in Titan's thermosphere/exosphere driving complex chemistry that ionizes, excites and dissociates Titan's main atmospheric components. This in turn produces suprathermal molecules which quickly thermalize in the collision

dominated regions but can lead to direct escape if produced near the exobase (e.g., Cravens et al., 1997; De La Haye, 2007b; Krasnopolsky, 2010; Vuitton et al., 2007). The water group ions in Saturn's magnetosphere bombard Titan's exosphere and induce escape by electron impact ionization, charge exchange ionization and via direct and knock-on sputtering: i.e., a single ion collision ejects a molecule from the atmosphere, and indirect or recoil sputtering occurs when an ion collides with several molecules along its path and creates a cascade of collisions leading to heating and escape (Johnson 1994; Johnson, 2009). The aim of many detailed studies is to characterize the most important chemical and momentum transfer processes that affect Titan's atmospheric structure and drive escape (e.g., Johnson, 2009; Johnson et al., 2009; Strobel and Cui, 2012).

For example, De La Haye et al. (2007a) examined INMS N_2 and CH_4 density profiles for individual Cassini flybys in the upper thermosphere, $r \sim 3700$ km up to distances above the exobase $r \sim 4500$ km, and concluded the exospheric densities exhibited a suprathermal component based on the change in the density gradient above the exobase (i.e., Figure 2-6(a)). In the region between $r = 3700 - 4025$ km, which is below the exobase, the density data were fit with the diffusion equation assuming a large eddy diffusion coefficient $K = 10^9 - 10^{10} \text{ cm}^2 \text{ s}^{-1}$, and above the exobase the densities were fit using a kappa or analytical power function energy distribution (i.e., Figure 2-6(b)) with a method developed from the Liouville theorem (e.g., Banks and Kockarts, 1973; De La Haye et al., 2007a). These distributions are nearly Maxwellian at low energies, but the tail of the distributions become less steep at higher energies than the Maxwellian. This enhanced tail of the distributions is considered characteristic of a non-thermal component or suprathermal molecules. Using the energy distributions at the

exobase for suprathermal N_2 and CH_4 molecules, it was determined that the density profiles suggested an averaged energy deposition rate of $\sim 70\text{--}140 \text{ eV cm}^{-3} \text{ s}^{-1}$ and the inferred escape rate was $1.6 \times 10^{26} \text{ N/s}$ ($2.2 \times 10^{27} \text{ amu/s}$) and $5.7 \times 10^{25} \text{ CH}_4/\text{s}$ ($9.1 \times 10^{26} \text{ amu/s}$).

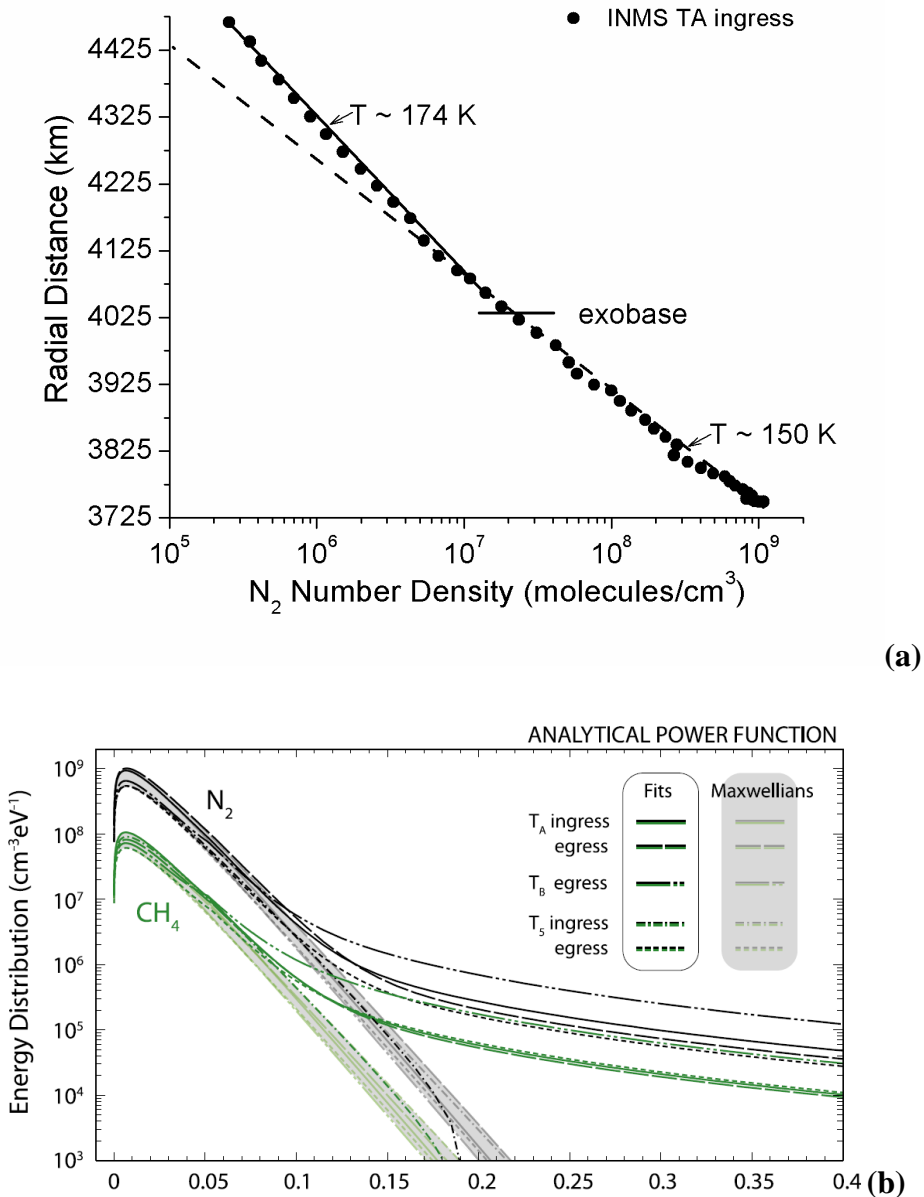


Figure 2-6: INMS density profiles suggestive of non-thermal heating.

a) INMS ingress density data (filled circles) vs. radial distance for an early Titan flyby referred to as TA. The dashed line is a hydrostatic fit to the densities below the exobase 4025 km for $T = 150 \text{ K}$, and above the exobase the densities are fit using $T = 174 \text{ K}$

suggestive of a suprathermal component (De La Haye et al., 2007a). b) N_2 and CH_4 energy distributions characteristic of a suprathermal population (analytical power function (De La Haye et al. 2007a)) and corresponding Maxwellian energy distributions for 3 different flybys. The energy distributions including suprathermal densities have a flat tail compared the corresponding Maxwellian energy distributions due to a larger population of higher energy molecules.

In another study using the known exothermic reactions occurring in Titan's exosphere/thermosphere, De La Haye et al. (2007b) investigated the ability of photochemistry, neutral chemistry and ion chemistry to produce the suprathermal densities characteristic of the above mentioned energy deposition and escape rates. An exhaustive list of reactions can be found in De La Haye et al. (2007b) and the references therein. When considering all of the exothermic reactions collectively, ion-neutral chemistry was deemed to be an insufficient source for the production of the necessary suprathermal. Therefore, bombardment by the incident heavy ions was suggested to be the source of the suprathermal neutrals inferred from the density profiles.

At the time this dissertation was completed, the most detailed studies on the effect of plasma bombardment on Titan's exosphere were completed prior to Cassini (e.g. Lammer and Bauer 1993; Lammer et al., 1998; Michael and Johnson 2005; Michael et al., 2005; Shematovich et al., 2003). For example, Michael et al. (2005) used kinetic Monte Carlo models to simulate fluxes for deflected and pick-up ions impinging on Titan's atmosphere that were based on the Voyager spacecraft data (Figure 2-7(a)) (Brecht et al., 2000). Such models suggested an energy deposition rate of $\sim 20 \text{ eV cm}^{-2} \text{ s}^{-1}$ at the exobase, which corresponded to an escape rate of $\sim 3.6 \times 10^{25} \text{ N/s}$ ($5.0 \times 10^{26} \text{ amu/s}$). However, data from the Cassini plasma spectrometer (CAPS) instrument suggests that the ion spectrum is dominated by heavy ions at lower energies than that used to calculate the

energy deposition in Michael et al. (2005) (e.g., Figure 2-7(a)). Therefore, Johnson et al. (2009) rescaled the energy deposition rates in Michael et al. (2005) to account for the corresponding ion energy spectrum shown in Figure 2-7(b) and obtained an updated energy deposition rate at the exobase of $\sim 300 \text{ eV cm}^{-3} \text{ s}^{-1}$. Considering this energy deposition rate with the analysis of De La Haye et al. (2007a) an upper bound of the N_2 and CH_4 loss rate was obtained $\sim 0.3 - 4 \times 10^{28} \text{ amu/s}$, which is much larger than the estimates prior to Cassini. As indicated by Saturn's magnetosphere configuration and the different ion energy spectra, the plasma interaction with Titan's upper atmosphere is non-isotropic, and the estimated non-thermal escape rates are highly variable depending on local plasma conditions throughout Titan's orbit.

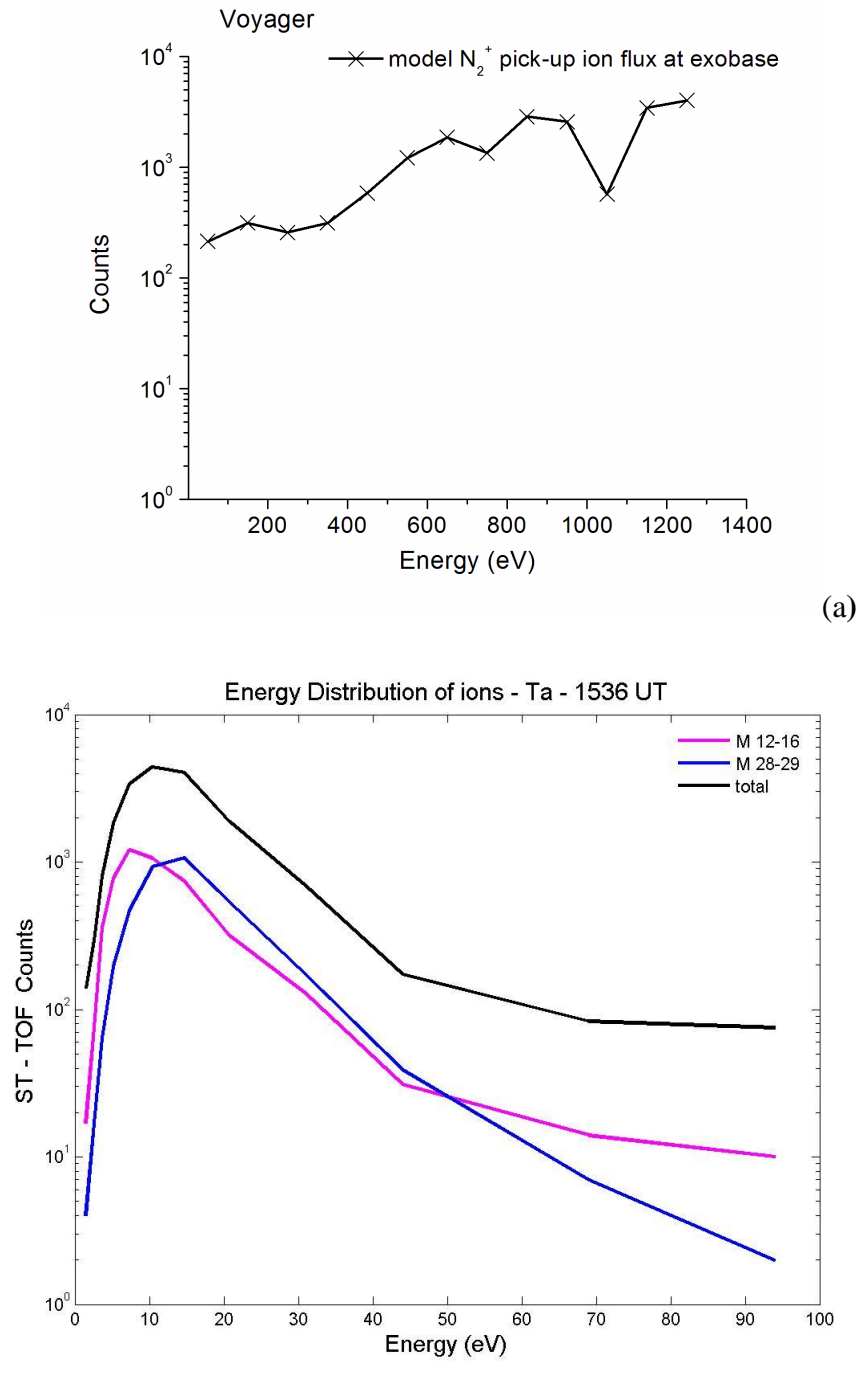


Figure 2-7: Incident plasma energy spectrums for Titan's atmosphere.

a) Energy spectrum for an inferred voyager like flux for deflected and pick up N_2 ions (Brecht et al., 2000). b) Energy spectrum from CAPS data for mass 12-16 amu and 28-29 ions. This spectrum is considered to be dominantly composed of pickup ions (Johnson et al., 2009). The low energy heavy ions are most efficient at heating and sputtering Titan's exosphere.

2.5 Summary

Prior to Cassini's arrival at Saturn nitrogen and carbon atoms were thought to escape at modest rates via non-thermal interactions occurring in Titan's upper atmosphere, and molecular hydrogen was considered to escape thermally close to the Jeans rates. At temperatures characteristic of Titan's upper atmosphere the Jeans parameter at the exobase for methane and molecular nitrogen is large so thermal escape should be negligible. Therefore, once the present nitrogen atmosphere formed, Titan would retain it over its lifetime in the Solar System. However thermal escape of molecular hydrogen, which is produced by dissociation of CH_4 , is efficient because of its relatively small Jeans parameter.

Some estimates obtained using continuum models suggested that Titan could have lost a significant amount of its current atmosphere by thermal escape in 4 Gyr. For example, fits to the Cassini INMS density data versus altitude using the diffusion equation or the slow hydrodynamic model suggested a much larger methane loss rate. However, model fits to the escape region and a different hydrodynamic model of Titan's thermosphere and ionosphere suggested the upward diffusive flux of methane was driven by non-thermal processes. The simulations described above cannot self consistently model the transition from collisional to collisionless flow of the upper atmosphere, on which escape depends. Therefore, the additional modeling described here is important both for understanding the processes driving escape and to constrain loss rate estimates.

3. Direct Simulation Monte Carlo (DSMC) Model

Several studies of Earth's atmosphere have shown the importance of using Monte Carlo techniques or models which solve the Boltzmann equation to derive the evolution of the molecular velocity distribution from the thermosphere ($Kn < \sim 1$) where it is Maxwellian to the exosphere ($Kn > 1$) where it is non-Maxwellian (e.g., Brinkmann, 1970; Chamberlain, 1967; Chamberlain and Smith, 1971; Shizgal and Blackmore, 1986). Here I use the 'so-called' Direct Simulation Monte Carlo (DSMC) method, a general model for dilute gas flows which has been shown to be consistent with solving the Boltzmann equation. (Bird, 1994). The DSMC method applied in the kinetic region $Kn > 0.1$ directly models the stochastic nature of the molecular motion and collisions in a gas flow using Monte Carlo techniques for a set of modeling molecules that represent the atmosphere in order to calculate the gas properties at a molecular level (Figure 3-1). Collisions between molecules are calculated in discrete radial cells based on the local values of the relative speed, cross section and density. Therefore, the method is a direct approach for describing the transition in an atmosphere from the collisional to collisionless regime. The atmosphere structure is driven by heat transport from the lower boundary via collisions and molecular escape from the upper boundary. The general requirements for a DSMC simulation are: the time step is chosen to be much smaller than the mean collision time and the cell widths in the flow direction are kept much smaller than mean free path for collisions and the atmospheric scale height (Bird, 1994). In this section, I describe the application of the DSMC model to the problem of thermal escape from planetary atmospheres.

DSMC Method

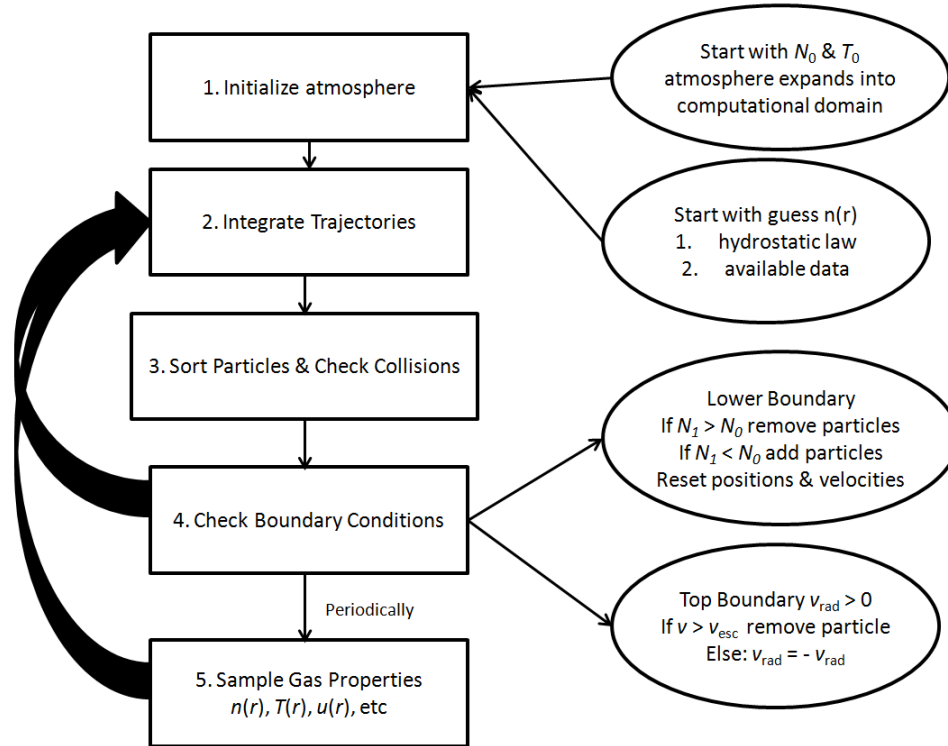


Figure 3-1: Schematic of steps involved in DSMC simulation.

V_{rad} is the radial velocity component, N_0 is the amount of representative molecules that correspond to the density at the lower boundary n_0 and N_1 is the number of representative particles in the bottom cell.

3.1 Boundary Conditions

A detailed summary of the DSMC method applied to thermal escape from planetary atmospheres is given in Volkov et al. (2011a). At the lower boundary, the number density $n(r_0) = n_0$ and temperature $T(r_0) = T_0$ are kept constant and the number of simulation particles is given by $N = (n_0 \cdot V_0)/W$ where W is the particle weight and V_0 is the volume of the bottom cell. The density in the lower boundary cell is maintained by randomly deleting particles when too many enter or creating particles when too many exit the bottom cell at each simulation step. The lower boundary temperature is maintained by sampling the particle velocities from the Maxwell Boltzmann velocity distribution and

isotropically redistributing the particles throughout the lower boundary cell every simulation step. At the upper boundary, if a particle is traveling radially outwards and has a velocity larger than the escape velocity it is removed, otherwise the radial component of the velocity vector is reversed. Since collisions can occur above the exobase which may promote particles to escaping speeds it is important to choose an upper boundary high enough to include the dominant portion of escaping molecules. This altitude can be determined by trial and error; however, suggestions are given in Volkov et al. (2011a).

3.2 Computational Domain and Particle Collisions

To compare the DSMC results with 1-D continuum models results and globally averaged INMS data sets, the computational domain is a 3-dimensional space composed of radial cells. That is, the particles positions and velocities are followed in 3-dimensional space, but the macroscopic properties of the atmosphere are only considered in the radial flow direction. This grid is divided in evenly spaced cells or cells of varying size which increase with increasing mean free path. Typically, the cell lengths range in sizes from $1/3$ to 1 mean free path but once the mean free path becomes equivalent to the atmospheric scale height cell lengths are capped. The trajectories of the simulations particles are obtained by integrating their equations of motion including the gravitational force of the planet.

In a gas flow, molecules experience forces of attraction and repulsion due to the presence of other molecules. For tenuous planetary atmospheres the spacing between molecules is significant and these intermolecular interactions can be approximated using binary collisions. For example, using $\text{Kn} \sim \ell_{\text{mfp_HS}}/H$, where $\ell_{\text{mfp_HS}} = 1/(2^{1/2}n\sigma)$ for hard sphere (HS) collisions and $H = r/\lambda$, with the N_2 density measurements from averaged

INMS (ingress lobe data) in Titan's upper atmosphere one finds that at $r = 3575$ km, $n_{\text{N}_2} \sim 1 \times 10^{10} \text{ cm}^{-3}$ and $\text{Kn} \sim 10^{-2}$. The average intermolecular spacing at this density is $> 10^{-4}$ cm compared to an average molecular diameter $d \sim 10^{-8}$ cm. Additionally for Pluto using the inferred stellar occultation density of $n_{\text{N}_2} \sim 4 \times 10^{12} \text{ cm}^{-3}$ at $r = 1450$ km, $\text{Kn} \sim 10^{-6}$ and the spacing is $> 10^{-6}$ cm. Therefore, only binary collisions are considered, and each collision is a statistical event dependent upon the time step, cell density, relative velocity of particles and collision cross sections (e.g. Bird, 1994 *section 11.1*). In each cell and at every simulation step collisions are evaluated, therefore at every step it is necessary to determine whether or not a particle changed cells. To evaluate a collision between particles within a cell they are both rotated to a common radial axis, and the post-collision velocities are determined from the pre-collision velocities in the center of mass frame. For the HS model particles scatter at random isotropic angles in the center of mass frame.

In this study, we use both the hard sphere model and the variable hard sphere atmospheres of Titan and Pluto. Because the collision cross section for the HS model is independent of temperature, it provides a crude approximation to the effect of temperature on the viscosity of a gas flow. The collision cross section in the VHS model provides a better description. In this model $\sigma = \sigma_0 (\langle v_{r0} \rangle / \langle v_r \rangle)^{2\omega}$, so that the cross section is proportional to mean relative velocity, $\langle v_r \rangle$, in a collision raised to the viscosity exponent, ω . This parameter is obtained from real gas measurements, where subscript '0' represent reference parameters obtained from data (e.g. Bird 1994, *section 2.6*).

The Larsen-Borgnakke (LB) model is used to approximate the transfer of energy between internal and translational modes using both the HS and VHS models (e.g., Bird,

1994, *section 5.3-5.4*). In the LB approximation, the translation and internal energy modes are considered collectively. At temperatures characteristic for Titan's (N_2 , CH_4 , H_2) and Pluto's (N_2) upper atmosphere, the molecular vibrational modes are assumed not to be excited so that in this thesis the LB model is used only for rotational degrees of freedom. The initial internal energy for each molecule is set in the lower boundary of cell based on a Maxwell-Boltzmann energy distribution and changes in rotational levels due to IR cooling between collisions are neglected.

3.3 Sampling Atmospheric Properties

The macroscopic properties of the atmosphere, e.g., density, temperature, flow velocity, molecular flux and heat flux, at each altitude are calculated using the molecular velocity distributions in each cell. It is best to sample the gas flow once the simulation is approximately steady state, so the simulation process is twofold, first obtaining a steady state result and secondly sampling the macroscopic properties. The macroscopic properties are taken as rolling averages over the simulation time. Therefore, the statistical scatter in the results depends upon both the number of representative molecules used and the sampling average.

3.4 DSMC simulations for a trace gas

For Titan's atmosphere I used two different types of DSMC simulations for thermal escape to compare with INMS data and to test the results of escape obtained by the SHE and diffusion models. The 3-component DSMC simulations for Titan's atmosphere are computationally demanding as a result of the small H_2 mixing ratio i.e., $f_{\text{H}_2}(3685 \text{ km}) = n_{\text{H}_2}/n_{\text{N}_2} = 0.004$. If 6000 particles represent the density in a cell only 24 particles would represent the H_2 species. Therefore, after considering the results for the

steady state atmosphere using 3 components, I modified the code to also dynamically track the H_2 molecules in a stationary background gas composed of the dominant species N_2 (e.g., Brinkmann, 1970; Chamberlain and Campbell, 1967; Chamberlain and Smith, 1971). I will refer to these simulations as DSMC- H_2 . The DSMC- H_2 simulations are completed in significantly less time than the 3-component DSMC simulations and provide better statistics. Using the full 3-component DSMC it is seen that the N_2 and CH_4 temperatures and densities are affected by H_2 escape which will be discussed further in Section 4. However having obtained a good description of the principal components investigating H_2 escape in the background gas is sufficient. In the DSMC- H_2 model, when a collision occurs between a H_2 molecule and the background gas molecule, an artificial N_2 or CH_4 molecule is created with a velocity and internal energy sampled from a Maxwell Boltzmann distribution. After the collision, only the subsequent motion and internal energy change of the H_2 particle is tracked.

3.5 Fluid/DSMC simulations

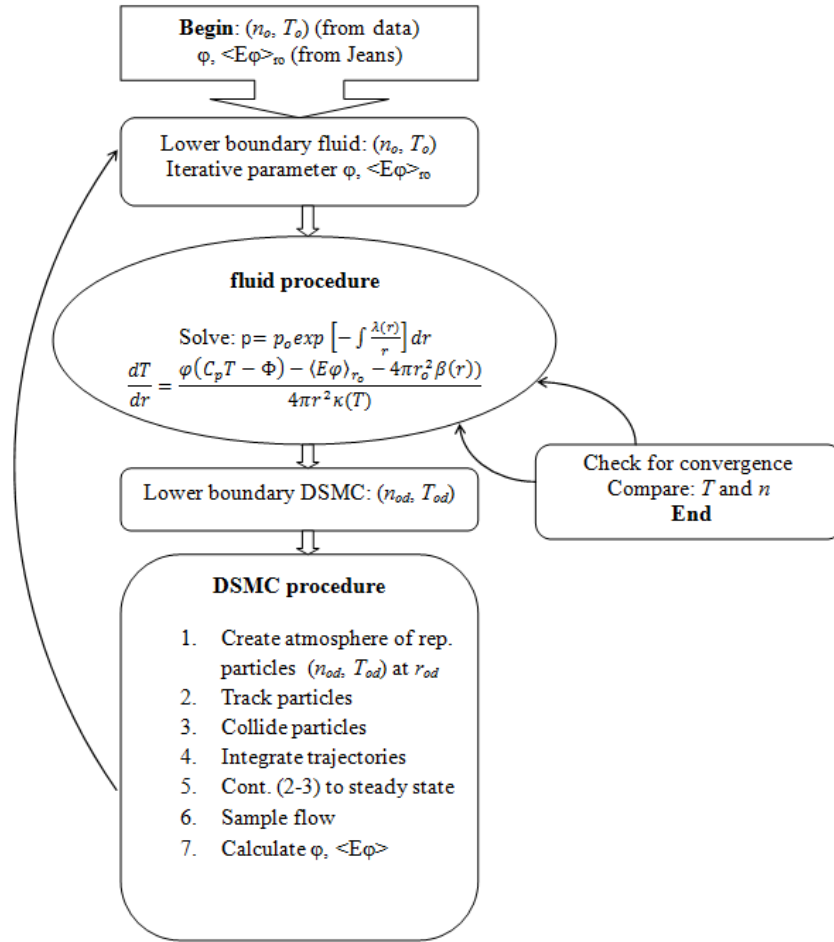


Figure 3-2: Schematic of the numerical implementation of the fluid/DSMC model.

To obtain solutions of the hydrodynamic equations at r_0 where $Kn \ll 0.1$, n_0 and T_0 are given, and ϕ and $\langle E\phi \rangle_{r_0}$ are obtained iteratively using the DSMC method. An initial guess of the energy flow into the lower boundary of ϕ and $\langle E\phi \rangle_{r_0}$ is used to solve Equation 2-12 and Equation 2-13 up to $Kn \sim 1$. The n_{od} and T_{od} from the fluid solution at $Kn_{od} \sim 0.1$ are used in the DSMC simulation up to describe the atmosphere up to $Kn \gg 0.1$ and to obtain improved values of ϕ and $\langle E\phi \rangle_{r_0}$. The iterations are continued until temperature and density are consistent between the fluid and DSMC solutions in the overlap region of $0.1 < Kn < 1$.

For a couple of decades thermal escape from Pluto's atmosphere has been modeled hydrodynamic ally (e.g., Hunten and Watson, 1982; Krasnopolsky, 1999;

McNutt, 1989; Strobel, 2008b). I used a combined fluid/DSMC approach for Pluto's atmosphere to directly compare with SHE model results. The DSMC model can in principle be applied to the entire atmosphere, but it is computationally expensive when applied to a dense region of the atmosphere. In the dense region of the atmosphere where collisions are frequent the flow can be treated as a continuum and the use of a fluid model is most efficient. In the fluid models the hydrodynamic equations are solved to obtain the mass flow rate through the atmosphere but are unable to account for relatively infrequent collisions of upwardly moving molecules or returning molecules that regulate escape in the upper atmosphere. Therefore, they cannot correctly calculate the amount of heat transported through the atmosphere. A combined fluid/DSMC model applied to dense and rarefied parts of the atmosphere respectively avoids these difficulties and provides a computationally efficient tool for simulation of the atmosphere (e.g., Marconi et al., 1996).

The atmosphere is divided into two regions, a fluid region where the hydrodynamic equations are applicable from r_0 where $Kn \ll 1$ to an intermediate boundary r_{od} chosen to correspond to $Kn \sim 0.1$, and a DSMC from r_{od} to r_1 where $Kn \gg 1$. When solving the fluid equations no constraints are placed on the density and temperature at infinity and unlike the SHE model, the energy flow at infinity is not set to zero. However, consistent with the SHE model, the $u(r)^2$ terms are dropped in Equation 2-10 and Equation 2-11. Such terms have also been included and do not affect the conclusions presented here. For instance, for a dense gravitationally bound atmosphere $u(r)^2$ can be safely neglected below the exobase (Parker, 1964b). The lower boundary conditions in the fluid region are n_0 and T_0 , while the parameters ϕ and $\langle E\phi \rangle_{r_0}$, the

particle and energy flow across r_0 , in Equation 2-12 are determined by the DSMC part of the model. Since the fluid model requires initial values for ϕ and $\langle E\phi \rangle_{r_0}$, for the $\beta_0=0$ case the simulations are begun assuming an isothermal, hydrostatic atmosphere and the DSMC model for such an atmosphere starting at $Kn(r_{od}) \sim 0.1$ is used to obtain the initial estimates.

Numerical solutions of the fluid equations, carried out by fellow student Justin Erwin, for $\beta_0 \neq 0$ are *very sensitive* to the choice of the input escape parameters, especially the energy carried away by escape, $\langle E\phi \rangle$. Therefore, an initial solution was achieved by incrementally adding in a small fraction of the heating rate and solving the fluid equations iteratively, but assuming Jeans escape at the exobase, $Kn=1$. Having achieved a converged solution in this manner, we used the calculated $n(r_{od})$ and $T(r_{od})$ evaluated at $Kn(r_{od}) = 0.1$ as the starting point for the first DSMC iteration.

As schematically presented in Figure 3-2, we solve the Equation 2-12 and Equation 2-13 for the density and temperature up to the exobase and iteratively obtain ϕ and $\langle E\phi \rangle_{r_0}$. From that solution the resulting n_{od} and T_{od} at a radius r_{od} , where $Kn \sim 0.1$, which is about two scale heights below the nominal exobase, are used in the DSMC simulation up to an altitude many scale heights above the exobase, $Kn \gg 1$. At the upper boundary of the DSMC domain, as stated above, the molecular escape rate, ϕ , and the energy flow through the 1D system, $\langle E\phi \rangle$. Values of $\langle E\phi \rangle$ and ϕ from the upper boundary are used to update corresponding values in the fluid part of the model and then used to solve Equation 2-12 and Equation 2-13 up to $Kn=1$ during the next iteration. Likewise the results from the new simulation of the hydrodynamic equations provide

updated n_{od} and T_{od} at $Kn(r_{\text{od}}) \sim 0.1$ for the kinetic model, which are then used to obtain new values of ϕ and $\langle E\phi \rangle$.

3.6 Summary

Thermal escape from a planetary atmosphere results in a non-equilibrium gas flow in the upper atmosphere. In order calculate, the evolution of the velocity distribution from regions in the thermosphere where it is Maxwellian to regions in the exosphere where it can be non-Maxwellian, solutions to the Boltzmann equation are required. The DSMC method is equivalent to solving Boltzmann equation, in that particle motions are directly modeled and particle collisions are treated as binary random events. Often the SHE model and diffusion models are applied up to the nominal exobase. However, these models approximate the velocity distribution functions with a Maxwellian. Therefore, the DSMC model or the fluid/DSMC hybrid simulations provide a suitable test of a purely fluid simulation.

4. DSMC Simulations: Results

One of the principal goals of the Cassini mission to Saturn is to characterize the mechanisms driving escape of the major molecular species in Titan's atmosphere. As stated above, prior to the availability of Cassini data, thermal escape from Titan was assumed to occur at the theoretical Jeans rate, in which case only H_2 had a significant escape rate, and any significant escape of N_2 and CH_4 was considered to be driven by non-thermal processes. However, there are significant differences in estimates of escape rates obtained by fluid models and DSMC models each of which appears to be consistent with the density structure of the upper atmosphere. Fluid models were used to infer

thermal escape rates for N_2 and CH_4 that are orders of magnitude larger than the corresponding Jeans rates as seen in Table 2-1, and they also suggested that H_2 escape is diffusion limited and independent of temperature in Titan's thermosphere. The results to be discussed for Titan and Pluto have important implications for how fluid models are applied to rarefied atmospheres in general.

4.1 Thermal Escape of N_2 and CH_4 from Titan's Atmosphere

The DSMC model in Tucker and Johnson (2009) fixed the temperature and density at the lower boundary, ($r_0 = 3875$ km, $T_0 = 141$ K, $\lambda_0 \sim 53$ and $n_0 = 1.8 \times 10^8 \text{ cm}^{-3}$), to that obtained by the SHE model in Strobel (2008a). Figure 4-1 compares the results from a DSMC simulation and the SHE model for a N_2 atmosphere. In the DSMC simulations the HS model for collisions was used with a collision cross section of $3.1 \times 10^{-15} \text{ cm}^2$ (Bondi, 1964) appropriate for the temperatures near the exobase, $r_x \sim 4000$ km. It is seen that, unlike the temperature profile in Strobel (2008a) the atmosphere is isothermal throughout the transition region. In addition, since no representative particles escaped during the simulation, consistent with the estimate of the Jeans escape rate and the simulation time, an upper limit on the escape rate is obtained. If one representative particle would have escaped, the simulated escape rate would be more than six orders of magnitude less than the rate, $\sim 1.0 \times 10^{27} \text{ N}_2/\text{s}$, estimated in Strobel (2008). Test simulations were also carried out for the other cases that included EUV and UV in Strobel (2008) by normalizing to the temperatures and densities at 4000 km, and using the appropriate heating rates. In all cases, purely thermal escape of N_2 was negligible.

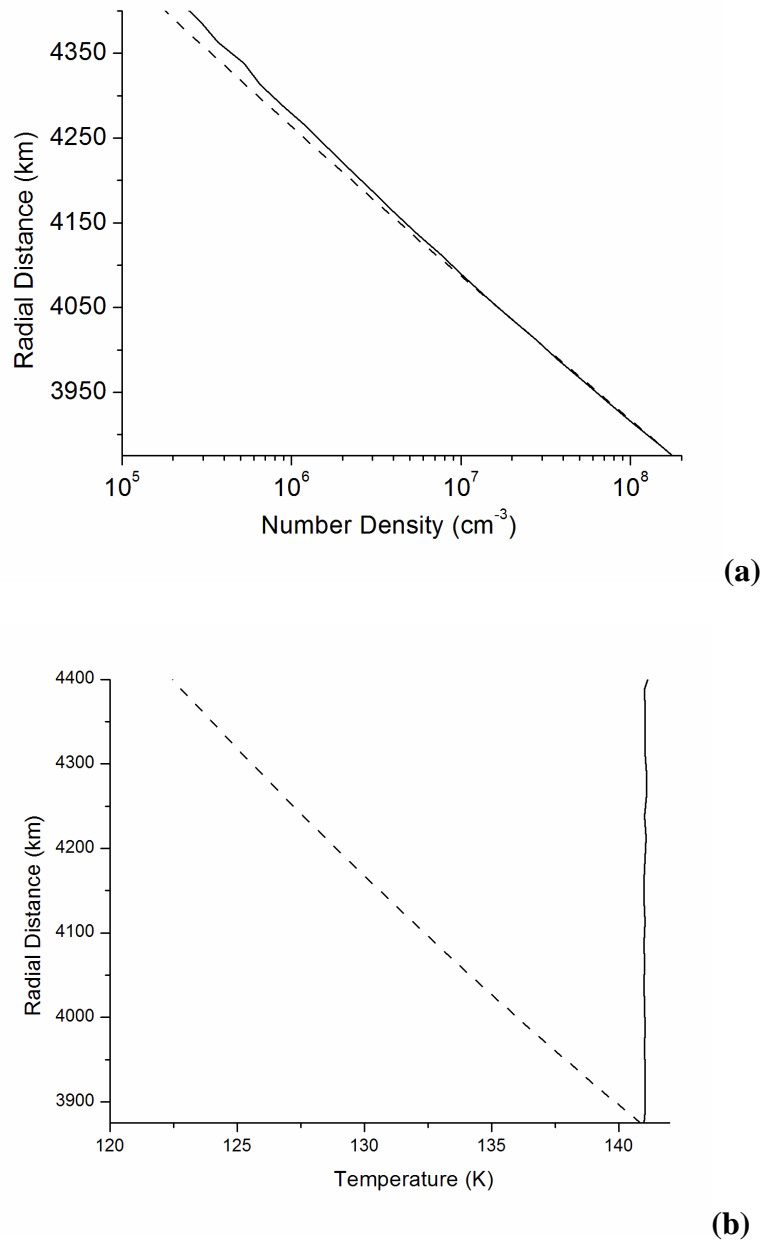


Figure 4-1: SHE vs. DSMC model result for a N_2 Titan atmosphere.

Density (a) and temperature (b) profiles for DSMC (solid curve) using lower boundary conditions at 3875 km ($n_0 = 1.8 \times 10^8 \text{ cm}^{-3}$, $T_0 = 141 \text{ K}$) obtained from the case with no heating in Strobel (2008) (solid curve). Nominal exobase is at ($r_x = 4000$, $\lambda_x \sim 50$ km).

Even for a DSMC simulation performed for the conditions, ($r_0 = 3900$ km, $T_0 = 183$ K, $\lambda_0 = 41$ and $n_0 = 3 \times 10^8 \text{ cm}^{-3}$) consistent with the temperature of the heating peak for solar medium heating in Strobel (2008), no representative N_2 particles escaped.

Therefore, in similar DSMC simulation, I artificially removed particles from the upper boundary $r = 4750$ km at a rate of the 1.0×10^{27} N₂/s to consider the effect of a large escape rate on the temperature and density structure (Figure 4-2). Removing particles in this manner is qualitatively similar to the effect of sputtering of N₂ by magnetosphere particles. For this simulation there is a modest cooling of ~ 6 K from the lower boundary to the top boundary, where the particles are removed. It is seen that the density versus altitude for the DSMC simulations with and without escape is essentially the same. The results from these DSMC simulations are consistent with the INMS density measurements for both negligible thermal escape and significant non-thermal escape indicating that density vs. altitude is not a strong constraint.

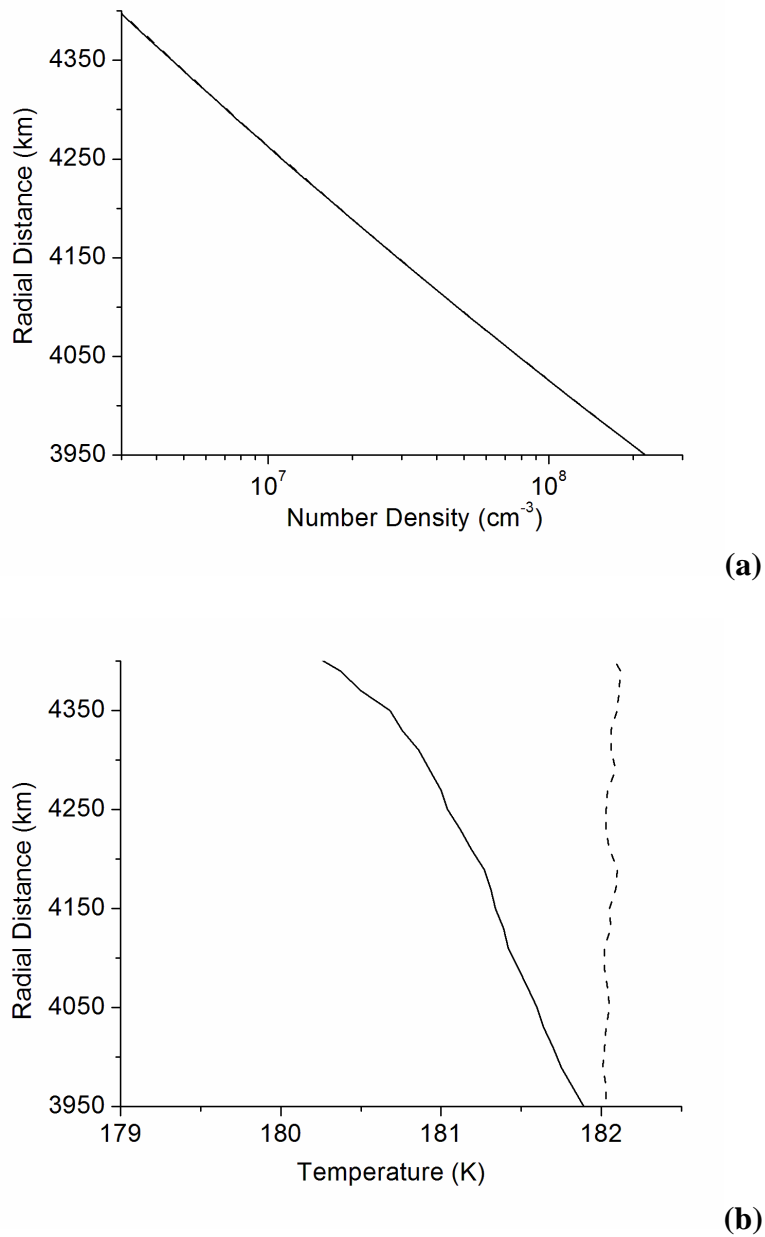


Figure 4-2: DSMC results for escape forced to occur at the SHE loss rates. Density (a) and temperature (b) profiles for DSMC simulation with forced escape at $1.0 \times 10^{27} \text{ N}_2/\text{s}$ and without escape (solid and dashed curves respectively) using lower boundary conditions at 3900 km ($n_0 = 3 \times 10^8 \text{ cm}^{-3}$, $T_0 = 182 \text{ K}$; $\lambda_x \sim 50$).

In the results of Tucker and Johnson (2009), thermal escape does occur in the simulations when the T is increased significantly. However, unlike the SHE model applied to Pluto and Titan, even if the temperature at the lower boundary of the

simulation region becomes as high as 500K or 600K ($\lambda_x \sim 14$ and ~ 11 at the exobase), the escape rate is only ~ 1.5 that of Jeans escape rate calculated using the exobase temperature and exobase density. That is, for this simulation, $\lambda_x \sim 11$ at the exobase (indicated in both panels) giving a Jeans rate of 4.6×10^{25} N₂/s. The actual (simulated) escape rate is 7.0×10^{25} N₂/s.

Although Strobel (2008) solved the approximate fluid equations for a single component atmosphere with a net mass flux, he subsequently assumed that the principal escaping component was CH₄. Yelle et al. (2008) solved the coupled diffusion equations for CH₄ and N₂ and came to roughly the same conclusion. That is, they found an upward flow of $\sim 4 \times 10^{28}$ amu/s for CH₄ which they assumed escaped to space. Therefore, we carried out another set of DSMC simulations for an atmosphere having both methane and molecular nitrogen. At the lower boundary, in this case $r = 3800$ km, the temperature and the density of each species were fixed to the values used in the model in Yelle et al. (2008), and escape was allowed at the upper boundary, about 2.5 N₂ scale heights above the exobase. Hard sphere cross sections were again used for simplicity. Molecular diffusion, included here explicitly by the molecular collisions, dominates over eddy diffusion above ~ 3400 km (Yelle et al. 2008). As seen in Figure 4-3, the model can reproduce the INMS averaged density measurements. Again, only an upper bound on the escape rate for CH₄ is obtained from these simulations and this is many orders of magnitude smaller than the suggested rate. Therefore, the conclusion that thermal conduction can drive large escape rates at these values of λ_x is not supported.

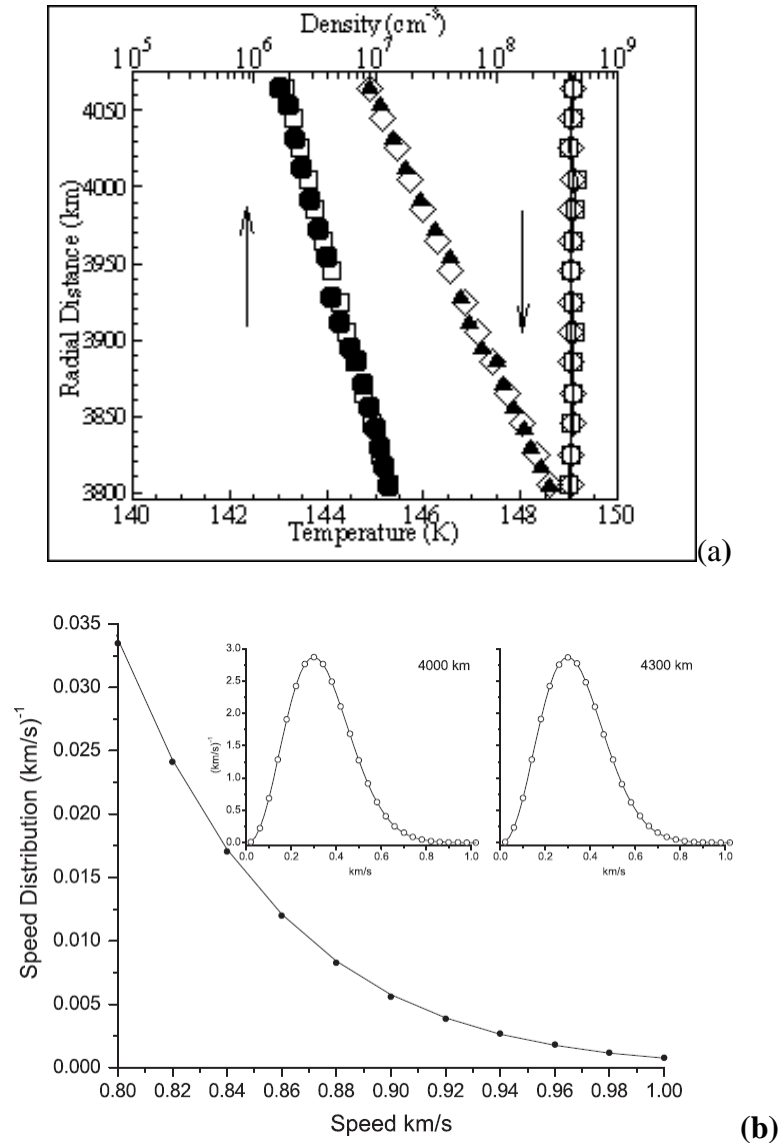


Figure 4-3: DSMC results compared to INMS data for N_2 and CH_4 .

a) The resulting profiles (filled triangles N_2 and filled circles CH_4) are compared to the averaged INMS data (open diamonds N_2 open squares CH_4). Densities and temperatures at the lower boundary are fixed to those in Yelle et al. (2008). Temperature is essentially the same, within the DSMC uncertainties, for both species. No test particles escaped over the DSMC run consistent with the Jeans estimate. b) Velocity distributions from DSMC simulations for an N_2 atmosphere. Insert: distributions for 2 altitudes at the exobase 4000km and above 4300km. Main figure: the tail of the distribution averaged over 4 altitudes, $r = 4000, 4100, 4200$ and 4300 km. The Maxwell velocity distribution is shown by the solid line.

As shown in Figure 4-3b, the velocity distributions obtained by the DSMC model for the exosphere are essentially Maxwellian. Also, there is no evidence for a significant enhancement in the tail of the speed distribution, as suggested by the SHE model, so that the Jeans model is a good approximation to the N_2 escape rate.

4.2 Transition from Hydrodynamic to Jeans Escape

Three regimes of escape have typically been characterized using the Jeans parameter. If a planetary atmosphere has a relatively large Jeans parameter at the exobase for the dominant atmospheric species, thermal escape occurs on a molecule by molecule basis similar to evaporation. At small Jeans parameters the thermal energy of molecules is comparable to or larger than the gravitational binding energy of the planet at the exobase, so the bulk atmosphere can escape as a hydrodynamic outflow (e.g., Öpik, 1963; Hunten, 1973). This has been suggested to occur when $\lambda_x < \sim 2$ at the exobase altitude or below, resulting in escape rates much larger than the Jeans rate (Hunten, 1973; Watson et al., 1981). The intermediate regime was recently described as the Fourier regime (Gruzinov, 2011) as thermal conduction dominates.

Parker (1958) used the hydrodynamic equations to model the thermal expansion of the solar wind in the vicinity of $\lambda_0 \sim 2$. He subsequently extended that model to describe the expansion of a stellar wind from a star with a tightly bound corona with $\lambda_0 > \sim 10$ for which no or very little heat is deposited above r_0 (Parker 1964a, b). This was the regime in which the SHE model was intended. In this formulation, escape is powered by the heat flow from below r_0 and the conditions imposed are $T, n \rightarrow 0$ as $r \rightarrow \infty$. He then showed that the dense atmosphere must expand according to a critical solution, in which the flow velocity gradually increases above the isothermal speed of sound. Purely

subsonic solutions were not permitted because they resulted in a finite pressure at infinity.

Chamberlain (1960, 1961) re-considered the expansion of the solar wind for subsonic velocities with the condition $T \rightarrow 0$ as $r \rightarrow \infty$. He deemed this approach to be a slow hydrodynamic expansion of the solar wind, and showed it is possible to obtain a subsonic solution with the hydrodynamic equations if the energy flux at infinity is 0. In this formulation the number density n approaches a constant as $r \rightarrow \infty$. Later, Parker (1964b) acknowledged this result is a limiting case to supersonic expansion. He determined that this approximation would only occur in the limit that the density at the lower boundary, n_0 , goes to infinity. He showed for sufficiently large densities at r_0 , the energy flux carried to infinity is non-zero for the condition $T \rightarrow 0$ and, hence, the expansion can proceed supersonically. This is the typical approach used in applying the SHE model to planetary atmospheres (e.g., Krasnopolsky, 1999; Strobel, 2008a, b; Watson et. al., 1981). Particular emphasis has been placed on Pluto's atmosphere which is widely thought to be escaping hydro-dynamically (e.g., McNutt, 1989; Krasnopolsky, 1999; Strobel, 2008b; Tian and Toon, 2005).

In light of the DSMC results for Titan that determined that escape was evaporative in nature even for Jeans parameters as low as $\lambda_x \sim 10$, Volkov et al. (2011a,b) used a DSMC model to characterize the set of parameters Kn_0 and λ_0 for which escape transitioned from occurring on a molecule by molecule basis to a bulk hydrodynamic outflow. In this study, the Knudsen number was defined as ℓ_{mfp}/r_0 . The study was conducted for a single component atmosphere using both the HS and VHS-LB cross sections and assuming no solar heating above r_0 . The DSMC simulations do not require

boundary conditions for density and temperature at infinity, therefore both subsonic and supersonic solutions are permitted.

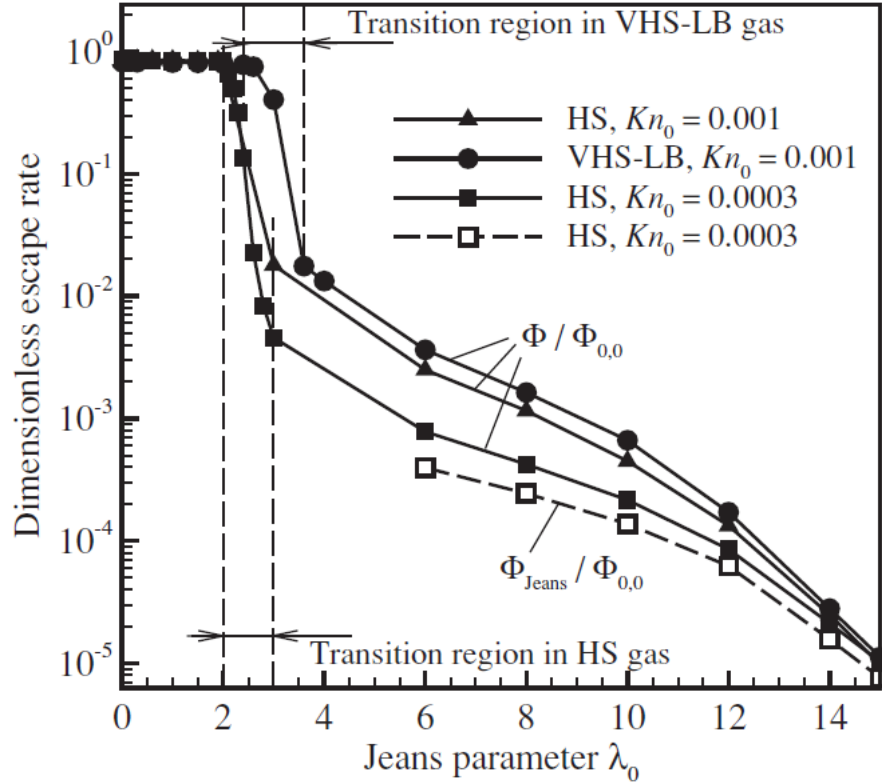


Figure 4-4: Transition from hydrodynamic to Jeans escape.

The dimensionless $\Phi/\Phi_{0,0}$ escape rate versus the Jeans parameter at the source surface, λ_0 , for various $Kn_0 = \ell_{\text{mfp}}/r_0$ and collision models labeled on the graph, where Φ is the DSMC escape rate and $\Phi_{0,0} = \pi r_0^2 n_0 \langle v_0 \rangle$ is free molecular flow rate in the absence of gravity from a Maxwell Boltzmann velocity distribution.

Shown in Figure 4-4 is a plot of the dimensionless escape rate versus Jeans parameter at the planetary surface for Knudsen numbers at the lower boundary of $Kn_0 = 0.001$ and 0.003 . The dimensionless escape rate is the ratio of the actual DSMC escape rate, Φ , to the escape rate for free molecular flow in the absence of gravity, $\Phi_{0,0} = \pi r_0^2 n_0 \langle v_0 \rangle$, which is the thermal flow rate across a spherical surface for a Maxwell Boltzmann velocity distribution. The maximum possible escape would be $\Phi/\Phi_{0,0} = 1$. For

Jeans parameters $\lambda_0 \leq 2$ the maximum rate is about ~20% less than the free molecular flow rate, as a result of collisions generating a return flow of molecules to the surface. More interesting when Kn_0 is small ($= 0.001$) is the dramatic decrease of the dimensionless escape rate over Jeans parameters $2 < \lambda_0 < \sim 3$, i.e., 3 orders of magnitude for the HS model. This region expands to slightly larger λ_0 when the rotational modes are included. The decrease in the escape rate is directly related to how the population of molecular escape velocities decreases with increasing Jeans parameter. For $\lambda_0 \geq 6$ the escape rate is found to be close to the theoretical Jeans rates as indicated. The results of these simulations are quantitatively consistent with those just described for N_2 at Titan.

The SHE model solution was thought to be valid to distances above the exobase where the flow velocity is a fraction of the isothermal sound speed (e.g. Parker 1964; Strobel 2008 a,b). However, the DSMC results show, not surprisingly, that the translational and internal energy modes are not in equilibrium near and above the nominal exobase when significant escape occurs (e.g., for Pluto, Figure 4-5 (a) and Titan, Figure 4-10(b, d)).

4.3 Thermal escape of N_2 from Pluto's atmosphere

Table 4-1: Parameters for fluid/kinetic model

Parameter	HS model	VHS model
heat capacity/molecule: C_p	$(5/2)k$	$(7/2)k$
viscosity exponent: ω ($\kappa(T) = \kappa_0 T^\omega$)	$1/2$	*1
collision cross section: σ ($\times 10^{-15}$) cm^2	$\sigma_0 = 9.0$	$^+ \sigma = \sigma_0 (\langle v_{r0} \rangle / \langle v_r \rangle)$

Parameters for N_2 used in the fluid/kinetic. The lower boundary radial distance is $r_0 = 1450$ km where $n(r_0) = 4 \times 10^{12} \text{ cm}^{-3}$ ($Kn_0 \sim 10^{-6}$), $T(r_0) = 88.2$ K. * The viscosity exponent for the VHS model and $\kappa_0 = 9.37 \text{ erg cm}^{-1} \text{ s}^{-1} \text{ K}^{-2}$ are taken from Strobel (2008b). $^+$ The average relative velocity at r_0 is defined by $\langle v_{r0} \rangle = (16kT_0/\pi m)^{1/2}$.

Since the hydrodynamic models, like the SHE model have often been applied to Pluto's atmosphere, a combined fluid/DSMC approach was used to model thermal escape from Pluto. Two cases were considered: no heating above a lower boundary and a case for the solar rate in the upper atmosphere that is about what is expected when the New Horizon spacecraft encounters Pluto (Tucker et al., 2012). The collision model parameters used in the Pluto simulations are listed in Table 4-1. The 1D radial fluid/DSMC model is applied from $r_0 = 1450$ km, where the density and temperature are estimated from occultation data (Elliot et al., 2007), up to $r_1 = 30000$ km: i.e., for $n_0 = 4 \times 10^{12}$ N₂/cm³ ($Kn_0 = \ell_{\text{mfp}}/H \sim 10^{-6}$) and $T_0 = 88.2$ K consistent with Strobel (2008b). Pluto's orbital axis is nearly parallel to its orbital plane which results in the structure of the atmosphere being non-isotropic over the globe. In addition, because of its eccentric orbit the solar heating rate is variable, as it depends upon the relative abundances of CH₄ and CO present in the primarily N₂ atmosphere. However, for the purpose of this study a globally averaged N₂ atmosphere is assumed with heating rates near the solar minimum level. The heating/ cooling data given in Strobel (2008b) are used for the solar heating due to N₂ and CH₄ absorption bands (including UV, EUV, and near-IR) and CO radiative cooling. Since the heating and cooling rates depend on the temperature and column of gas above a given radial position in the atmosphere, the radial dependence in the net heating rate is recalculated at each step as the density profile approaches steady state.

In the combined fluid/DSMC model of Pluto's atmosphere, the VHS-LB collision model was used in order to have a thermal conduction and heat capacity consistent with that used in the SHE model. We also compared the effect of using the HS, HS-LB, VHS and VHS-LB collision models on ϕ , $n(r)$, $T(r)$ and $u(r)$. In these DSMC simulations, the

following lower boundary conditions were first used: $r_{od} = 2836$ km where $\lambda_{od} = 12$, $n_{od} = 2.9 \times 10^7$ cm³ and $T_{od} = 85.5$ K. The reference value used for the cross section is $\sigma_0 = 9.0 \times 10^{-15}$ cm². The mean free paths at the lower boundary for a collision for HS and VHS molecules are $\ell_{mfp} = (\sqrt{2}n\sigma_0)^{-1}$ and $\ell_{mfp} = (\langle v_{th} \rangle / n\sigma_0 \langle v_{r0} \rangle)$ respectively (Bird 1994), but the values of ℓ_{mfp} and $Kn(r_{od})$ for this particular case are similar: ~ 27 km and ~ 0.1 respectively. The resulting temperature profiles and escape rates were slightly different: e.g., the escape rates are $4.4, 5.1, 4.3$ and 4.8×10^{25} N₂/s for the HS, HS-LB, VHS and VHS-LB models respectively. Above the exobase, as seen in Figure 4-5(a), the translational temperature decreases faster than the rotational temperature, and the perpendicular temperature decreases faster than the radial temperature. This disequilibrium between temperature modes is an effect of infrequent collisions.

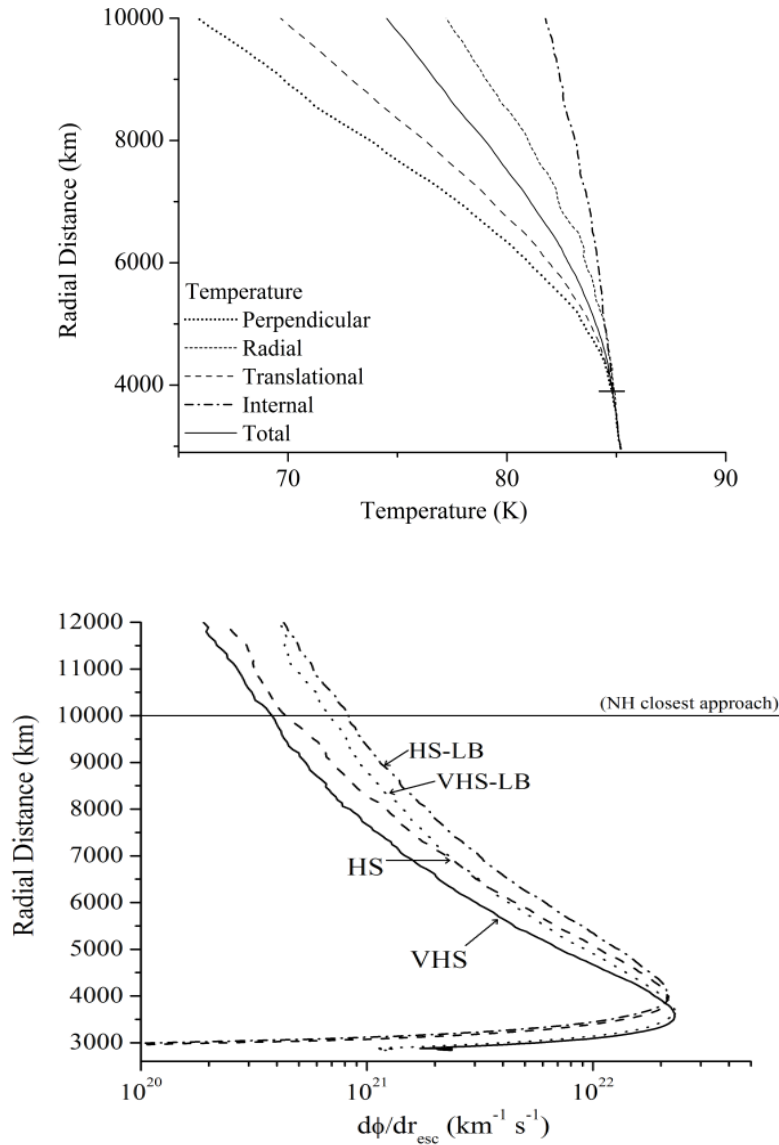


Figure 4-5: Pluto DSMC simulations for (HS, HS-LB, VHS, VHS-LB) models.

(a) $T(\text{K})$ in VHS-LB model: short dashed curve perpendicular temperature, T_{perp} , dotted curve radial temperature, T_r , dashed dotted curve rotational temperature, T_{rot} , dashed curve translational temperature, $T_{\text{trans}} = (T_r + 2T_{\text{perp}})/3$, solid curve total temperature, $T = (3T_{\text{trans}} + 2T_{\text{rot}})/5$. ($Kn(r_{od})=0.1$ and $\beta(r) = 0$) The exobase altitude is ~ 3900 km, indicated by short horizontal curve. (b) Production of escaping molecules, $d\phi/dr_{\text{esc}}$ ($\text{km}^{-1} \text{s}^{-1}$) vs. r : HS (dashed curve), VHS (solid curve), HS-LB (dashed dotted curve), VHS-LB (dotted curve). The New Horizons spacecraft distance of closest approach to Pluto will be 10000 km.

In the transition region there is an altitude where it is most efficient for molecules to acquire escape trajectories. Below this altitude collisions inhibit escape and above there are too few collisions to produce escape. In the DSMC region the average number of escaping molecules produced in each radial cell, $d\phi/dr_{\text{esc}}$, is calculated by noting the altitude at which molecules that eventually traverse the top of the simulation domain $r_1 = 30000$ km, first attained an escape velocity. Molecules that later lose their escape velocity are dropped from the inventory, so the total escape rate is given

by $\phi = \int_{r_0}^{r_1} (d\phi/dr)_{\text{esc}} dr$. The peak in the escape rate production, Figure 4-5(b), for the HS ($r \sim 4090$ km) and VHS ($r \sim 3680$ km), occurs at the essentially same altitude for models with and without the internal degrees of freedom. The difference in the peak altitude is determined by the conductivity, which differs between the VHS ($\kappa \propto T$) and HS models ($\kappa \propto T^{1/2}$).

Table 4-2: SHE vs. fluid/DSMC

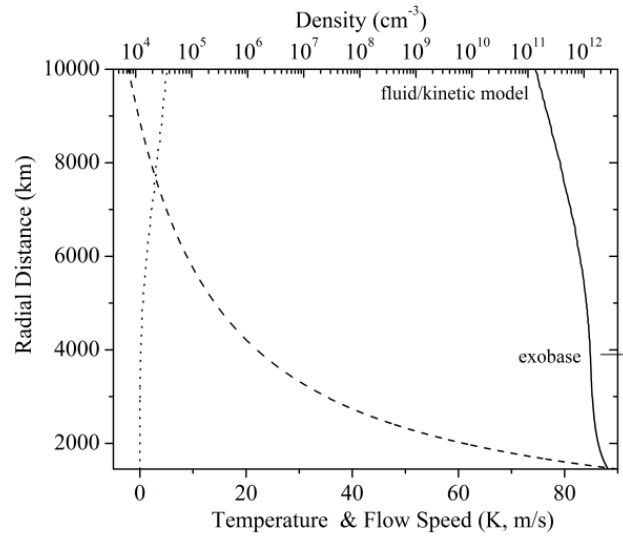
β_0 (10^{-3} erg cm $^{-2}$ s $^{-1}$)	No heating		1.7	1.5
	SHE*	fluid/kinetic~	SHE*	fluid/kinetic~
r_x (km)	2700	3900	3530	6200
n_x ($\times 10^5$ cm $^{-3}$)	53	17	53	6.7
T_x (K) [$H_x(100\text{km})$]	48[1.2]	85 [4.5]	65 [2.6]	87 [12]
u_x (m s $^{-1}$)	1	5×10^{-4}	2	4
λ_x	23	8.8	13	5.4
ϕ (10^{25} s $^{-1}$)	54	4.8	180	120
ϕ/ϕ_J	$\sim 10^7$	1.6	$\sim 10^3$	2.0
$\langle E\phi \rangle / kT_0\phi$	0	1.8	0	1.8
$\langle E\phi \rangle_J / kT_0\phi_J$	~ 1.11	2.02	~ 1.53	2.12

The exobase altitude r_x is defined by $Kn = \ell_{\text{mfp}}/H = 1$ using $\ell_{\text{mfp}} = \langle v_{\text{th}} \rangle / (n\sigma_0 \langle v_{r0} \rangle)$.

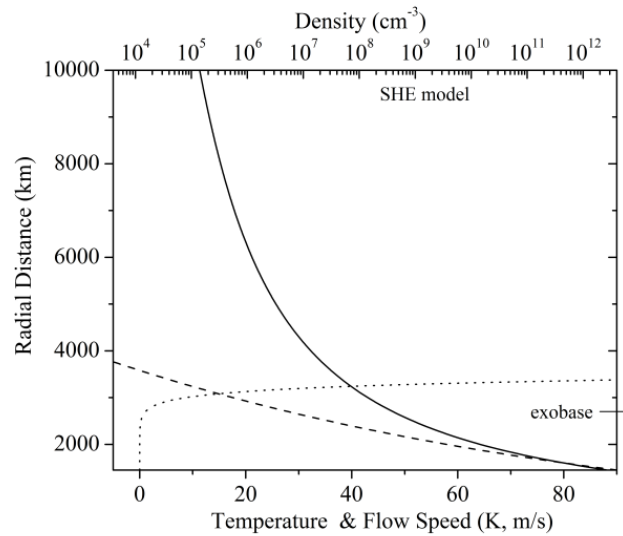
In the fluid/DSMC simulations performed for $\beta_0=0$ and solar minimum conditions, we used the VHS-LB model. Given in Table 4-2 are exobase values for the

density, temperature, bulk velocity, escape rate ϕ and average energy carried off, $\langle E\phi \rangle$, including the corresponding values for the theoretical Jeans escape rate and energy flow rate (ϕ_J , $\langle E\phi \rangle_J$). The lower boundary radial distance is at $r_0 = 1450$ km where $n(r_0) = 4 \times 10^{12} \text{ cm}^{-3}$ ($Kn_0 \sim 10^{-6}$) and $T(r_0) = 88.2$ K, $\lambda(r_0) = 23$.

In the first case, it is assumed no solar heating occurs in the simulation region: i.e., $Q(r) = 0$ above r_0 so that $\beta_0 = 0$ in Equation 2-13. We then carry out a second set of simulations using approximate solar minimum conditions where the net heating/cooling above r_0 is such that $\beta_0 = 1.5 \times 10^{-3} \text{ erg cm}^{-2} \text{ s}^{-1}$. This is similar to the value used in the SHE model $\beta_0 = 1.7 \times 10^{-3} \text{ erg cm}^{-2} \text{ s}^{-1}$ (Strobel, 2008b). The escape rate obtained for the $\beta_0 = 0$ case, $4.8 \times 10^{25} \text{ s}^{-1}$, is $\sim 1.6 \times \phi_J$, where ϕ_J is the Jeans rate for $T_x = 85$ K and the heat flow out is $\sim 1.4 \times \langle E\phi \rangle_J$ both evaluated at the exobase, $r_x = 3900$ km. These results differ significantly from those obtained in the SHE model (e.g., $r_x = 2700$ km, $n_x \sim 5.3 \times 10^6 \text{ cm}^{-3}$, $T_x = 48$ K and $\lambda_x \sim 23$; Strobel, 2008b) resulting in very different atmospheric profiles as seen in Figure 4-6. The change in temperature with increasing r is seen to fall off much faster in the SHE solution consistent with an overestimate in the adiabatic cooling due to the escape rate being an order of magnitude larger than that obtained with the fluid/DSMC model.



(a)

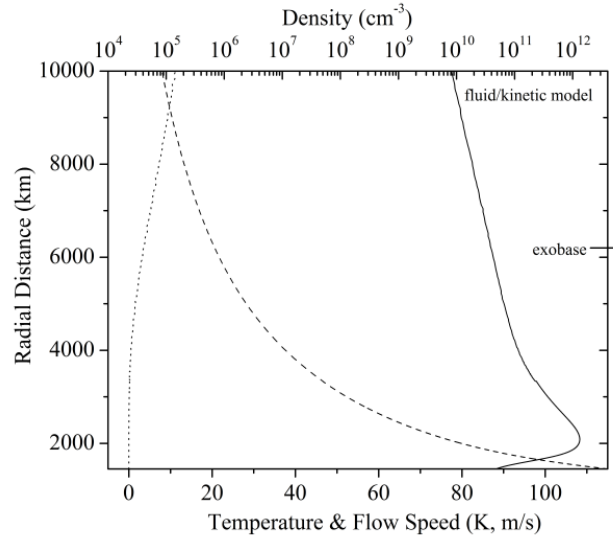


(b)

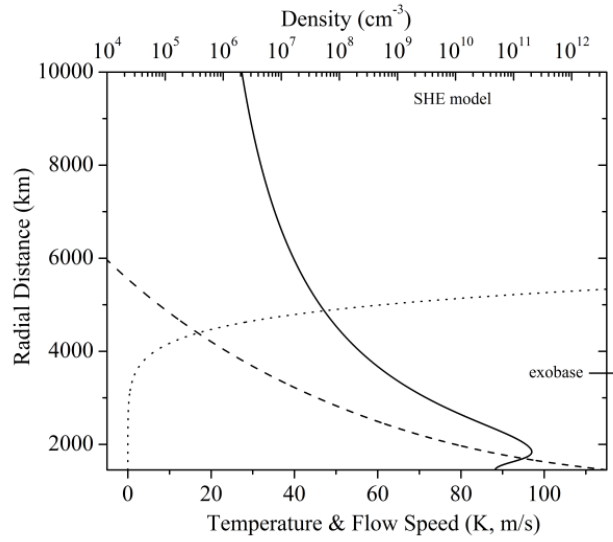
Figure 4-6: DSMC result for Pluto $\beta_0 = 0$ heating conditions.

$n(\text{cm}^{-3})$ (top axis), $T(\text{K})$ and $u(\text{m/s})$ (bottom axis) vs. radial distance: Comparison of fluid/kinetic (a) n (dashed curves), T (solid curves) and u (dotted curves) to SHE model results (b) from Strobel (2008b) for no heating above r_0 ($\beta_0 = 0$). The exobase distance is indicated by the solid curve on right axis: 3900 km fluid/DSMC model and 2700 km SHE model.

As seen in Table 4-2, the resulting escape rate for the solar minimum case was $1.2 \times 10^{27} \text{ s}^{-1}$ with $r_x \sim 6200 \text{ km}$, $n_x \sim 7 \times 10^5 \text{ cm}^{-3}$, $T_x \sim 87 \text{ K}$ and $\lambda_x \sim 5$. Although, the escape rate is fortuitously close to the SHE result, $1.8 \times 10^{27} \text{ N}_2/\text{s}$, the structure of the exobase region for the SHE model is *very* different: $r_x \sim 3530 \text{ km}$, $n_x \sim 5.3 \times 10^6 \text{ cm}^{-3}$, $T_x \sim 65 \text{ K}$ and $\lambda_x \sim 13$. Therefore, although the SHE escape rate was suggested to be $>10^3 \times \phi_J$, based on the temperature and density at the exobase obtained, the escape rate is actually $2.0 \times \phi_J$ and the energy flux rate is $1.7 \times \langle E\phi \rangle_J$. The size of this enhancement to the Jeans rate is similar to that found above for Titan and in Figure 4-4.



(a)



(b)

Figure 4-7: DSMC result for Pluto $\beta_0 = 1.5 \times 10^{-3} \text{ erg cm}^{-2} \text{ s}^{-1}$ heating conditions.

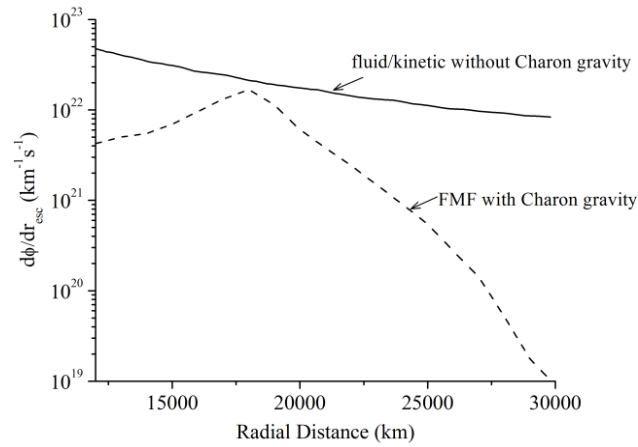
(a) $n(\text{cm}^{-3})$ (top axis), $T(\text{K})$ and $u(\text{m/s})$ (bottom axis) vs. radial distance: Comparison of fluid/kinetic (a) n (dashed curves), T (solid curves) and u (dotted curves) to SHE model results (b) from Strobel (2008b) for solar minimum heating conditions above r_0 . The exobase distance is indicated by the solid curve on right axis: 6200 km fluid/kinetic model and 3530 km SHE model.

4.3.1 *Implications for New Horizons and Charon*

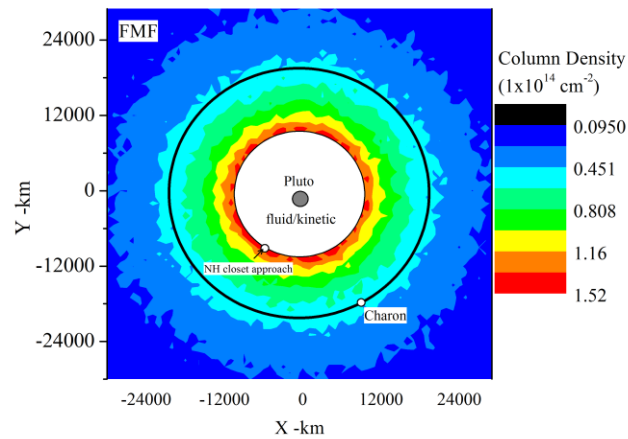
Equally important to the comparisons between the DSMC and fluid model results are the implications for the measurements at the time of the New Horizon encounter in 2015. That is, the first spacecraft measurements of the density structure of the upper atmosphere are expected to characterize the upper atmosphere and show the effect of Pluto's moon Charon and the interaction with the solar wind. To this end, the DSMC results, which obtain an atmosphere density profile much more extended than the SHE model were reevaluated accounting for the effect of Charon's gravity, and were also compared to recent telescope observations of the upper atmosphere.

The region of space where the gravitational attraction of Charon begins to dominate that of Pluto is referred to as the Hill sphere. Charon has $\frac{1}{2}$ the diameter and $\frac{1}{10}$ mass of Pluto and orbits at a distance of 19500 km from Pluto. The Hill sphere radius about Charon is ~ 6300 km which is a radial distance approximately 13000 km from Pluto. For the solar minimum case the atmospheric density at this distance is $< \sim 10^5 \text{ cm}^{-3}$, Figure 4-7a. Ignoring here any tidal effect on Pluto's lower atmosphere the effect of Charon's gravity on the molecular trajectories and escape rate was investigated. We used the DSMC results for solar minimum conditions to perform free molecular flow (FMF) simulations in which molecules move under the influence of gravity from both Pluto and Charon but without inter-molecular collisions. Charon is assumed to have a circular orbit about Pluto and the molecular trajectories are tracked in a 3D region from 10000 km to 30000 km about Pluto. The FMF simulation is begun by emitting molecules at $r = 10000$ km with radial velocities obtained from the fluid/DSMC model for solar minimum heating conditions. Molecules escaping from Pluto are either emitted initially with a

speed above the escape speed or they gain an escape speed under the gravitational influence of Charon. After several Charon orbits we obtained a steady-state morphology of the gas density in the Pluto-Charon system and the integrated escape rate produced versus radial distance, as shown in Figure 4-8(a, b).



(a)



(b)

Figure 4-8: Charon's influence on molecular escape from Pluto.

(a) Production of escaping molecules from Pluto $d\phi/dr_{\text{esc}}$ ($\text{km}^{-1}\text{s}^{-1}$) vs. r . (b) Contour plot of column density in the z plane Charon's northern and southern hemispheres in FMF simulations including Charon's gravitational influence: black curve represents Charon's orbit.

For solar minimum heating conditions it was estimated that molecules from Pluto's atmosphere impinge upon Charon at a rate of 10^{25} N₂/s. With Charon's surface temperature of ~50 K these molecules would stick and are equivalent to the deposition of a monolayer of molecules over 4 Charon orbits (25.5 days). Charon's gravitational pull perturbs the trajectories of molecules in Pluto's expanded atmosphere, accelerating them to or decelerating them from escaping Pluto's gravity. The above conclusions were determined by performing FMF simulations with and without the gravitational influence of Charon. I found that the escape rate decreased by 3 % in simulations that included Charon. This is opposite to the change in the escape rate that would have occurred if the energy to reach the Hill sphere of Charon was used as the escape criterion. A contour plot of the averaged total column densities over the north and south hemispheres when including Charon's gravitational influence is shown in Figure 4-8(b). The relevance of Charon is likely more significant at solar maximum heating conditions and when Pluto is close to perihelion.

The fluid/DSMC model of Pluto's atmosphere only considered the dominant molecular component, N₂. Although CO is minor species <~0.5% near the surface (e.g., Lellouch et al., 2010), having a similar mass, the CO should roughly track the N₂ profile described here. The solar activity during the recent observations of Greaves et al. (2011) in 2009/10 for CO emissions was close to that used for our assumed solar minimum conditions. The observations found CO at altitudes ~4500 km indicating that the atmosphere is more robust than indicated by the SHE model results in Strobel (2008b). However, based on an assumed mixing ratio of ~0.5% the CO tangential column density at 4500 km would be $\sim 6 \times 10^{11}$ CO cm⁻², but the temperature at this altitude is 91 K as

opposed to 50 K suggested by the observations. The tangential column density of the atmosphere refers to a line of sight column density through the atmosphere at the altitude of 4500 km.

Solar maximum conditions are expected to occur in 2013, so that the New Horizon encounter with Pluto and Charon in 2015 will occur somewhere between solar maximum and minimum conditions. At a distance from the sun of 33 AU the integrated heating rate $\beta_0 \sim 1.7$ times that used here ($\sim 2.5 \times 10^{-3} \text{ erg cm}^{-2} \text{ s}^{-1}$). Therefore, accurate simulations of the atmospheric density at the encounter distance 10000 km from Pluto, and the atmospheric structure and the escape rates expected during the encounter will require the use of a fluid/DSMC model such as that described here.

4.4 Diffusion and thermal escape of H₂ from Titan's atmosphere

Recent molecular hydrogen escape estimates from continuum models are consistent with pre-Cassini values, but the role of diffusion and the effect of the varying plasma environment on the density structure of the upper atmosphere is still unclear. In this section, I compare results of DSMC simulations to INMS density data and continuum model results to understand the role of thermal escape and diffusion of H₂ in Titan's upper atmosphere.

4.4.1 INMS density data used in comparisons

The INMS density profiles used in this dissertation were provided by collaborator Jared Bell at the South West Research Institute, (e.g., Magee et al., 2009; Westlake et al., 2011). The collective N₂ density profiles are indicative of hydrostatic temperatures ranging from 100 K to 200 K in Titan's upper atmosphere, $r \sim 3500$ to 4600 km, and the corresponding exobase distances can vary from $r_x \sim 3900$ to 4300 km (e.g., Cui et al.,

2011, *Table 1*; Westlake et al., 2011, *Fig. 4*). When considering the theoretical Jeans formula for N_2 , CH_4 and H_2 over this temperature range, the Jeans parameters for all species will vary by a factor of 2, but the Jeans escape rates for heavier species increases significantly at higher temperatures because of exponential dependence of the Jeans parameter. As discussed in Section 2, the Jeans rates for CH_4 and N_2 even at higher temperatures are still orders of magnitude smaller than pre-Cassini non-thermal escape estimates. However, because H_2 has a small Jeans parameter and large scale height over this temperature range in Titan's upper atmosphere, it is difficult to characterize the effect of thermal or non-thermal processes on its density vs. altitude in the thermosphere. With the DSMC simulations I can isolate the effect of heat conduction on thermal escape in Titan's upper atmosphere.

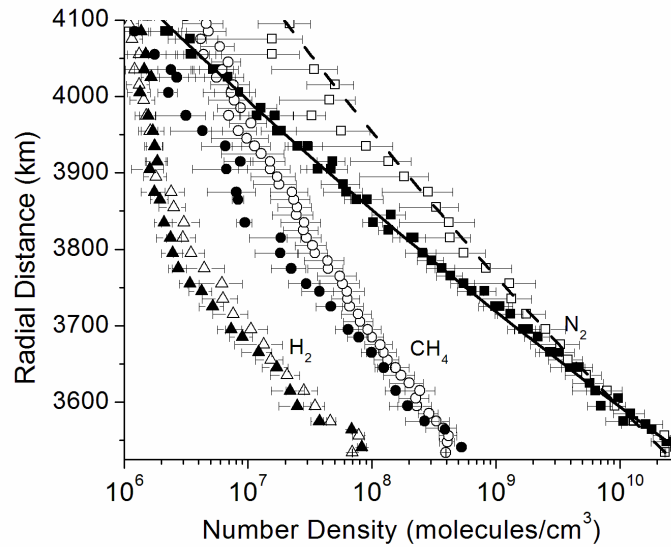


Figure 4-9: Averaged INMS densities for inbound Cassini trajectories.

The density data N_2 (squares), CH_4 (circles) and H_2 (triangles) was acquired from Magee et al., (2009) and Westlake et al., (2011). The filled shapes represent INMS measurements taken when Titan orbited in low ion density regions of Saturn's magnetosphere, referred to as the lobe, and the open shapes represent measurements taken during its orbits in high ion density regions, referred to as the plasma sheet (e.g., Rymer et al., 2009; Westlake et al., 2011). Solid curve (lobe) and dashed curve (plasma sheet) are hydrostatic density profiles obtained from Equation 2-1 using $r_0 = 3548$ km, $n_0 = 2.39 \times 10^{10}$ N_2/cm^3 , $T = 118$ K and $r_0 = 3548$ km, $n_0 = 2.02 \times 10^{10}$ N_2/cm^3 , $T = 161$ K respectively.

Westlake et al. (2011) showed the varying INMS density profiles of N_2 could be attributed to the effects of plasma heating (e.g., Rymer et al., 2009; Simon et al., 2010) on Titan's upper atmosphere. They fit the averaged N_2 densities obtained during periods of high and low plasma flux bombardment on Titan's upper atmosphere, referred to as the plasma sheet and lobe respectively, and inferred the temperatures $T \sim 161$ K and $T \sim 132$ K. The data from that study are shown in Figure 4-9 for inbound trajectories of the spacecraft. The outbound data are still being analyzed to account for sticking of molecules to the chamber walls during each pass. The effect of plasma heating suggested

by the *averaged* density profiles in Figure 4-9 is least evident in the molecular hydrogen density profiles. This is presumably because of rapid diffusion due to its lighter mass. As discussed in Section 2, the H_2 densities cannot be fit with the hydrostatic approximation, as the escape rate is sufficient that the upward flow through the thermosphere is restricted by the background N_2 .

Assuming steady state diffusion, Equation 2-7 has been used to fit the INMS data resulting in escape rates ϕ_D of $1.0 - 1.2 \times 10^{28} H_2/s$ and $2.5 - 2.7 \times 10^{27} CH_4/s$ (e.g., Cui et al. 2008, 2009; Yelle et al. 2006, 2008). These rates are significantly larger than the corresponding Jeans rates. Yelle et al. (2008) suggested that the known non-thermal processes occurring in the upper atmosphere could not sustain a large CH_4 loss rate. Cui et al. (2008) roughly reproduced the above H_2 escape rates by applying a kinetic model in the 13 moment approximation, and they also concluded H_2 escape was diffusion limited and non-thermal effects were not necessary to reproduce the INMS density profiles. Strobel (2008, 2009, 2010) used the SHE model to obtain the thermal escape rates, $9.2 \times 10^{27} H_2/s$ and $1.7 \times 10^{27} CH_4/s$, both consistent with diffusion model results. More recently, Cui et al. (2011) used a diffusion model to examine a much broader INMS data set, obtained for 32 flybys. They now concluded that the H_2 exospheric density structure is temporally affected by Titan's interaction with Saturn's magnetosphere plasma environment, and they inferred H_2 escape rates that are similar to the corresponding Jeans rates for varying exospheric temperatures.

4.4.2 3-component DSMC results for Titan's atmosphere

A series of DSMC simulations were performed using the INMS averaged inbound densities for the plasma sheet and lobe encounters shown in Figure 4-9, which included

all three species and is referred to as the 3-component DSMC simulations as described earlier. The simulations were started at a radial distance just below that at which H_2 appears to diffusively separate from N_2 , i.e. $r_0 = 3685$ km in Figure 4-9. At this distance the lower boundary densities are taken to be, $n(r_0) = n_0(N_2, CH_4, H_2) = 2.1 \times 10^9 \text{ cm}^{-3}$, $9.5 \times 10^7 \text{ cm}^{-3}$ and $8.5 \times 10^6 \text{ cm}^{-3}$, consistent with the averaged INMS data. I extracted the temperatures $T_0 = 118$ K and 161 K for the lobe and plasma sheet conditions respectively by fitting N_2 INMS density profiles in Figure 4-9 to the isothermal hydrostatic density profile given in Equation 2-1. The Knudsen numbers are $Kn = 8.4 \times 10^{-3}$ and 6.6×10^{-3} at the lower boundary for the lobe and plasma sheet respectively. Heating by solar radiation within the simulation domain is neglected. That is, the dominant heating is assumed to occur below r_0 . The corresponding simulation results and exobase parameters are given in Table 4-3.

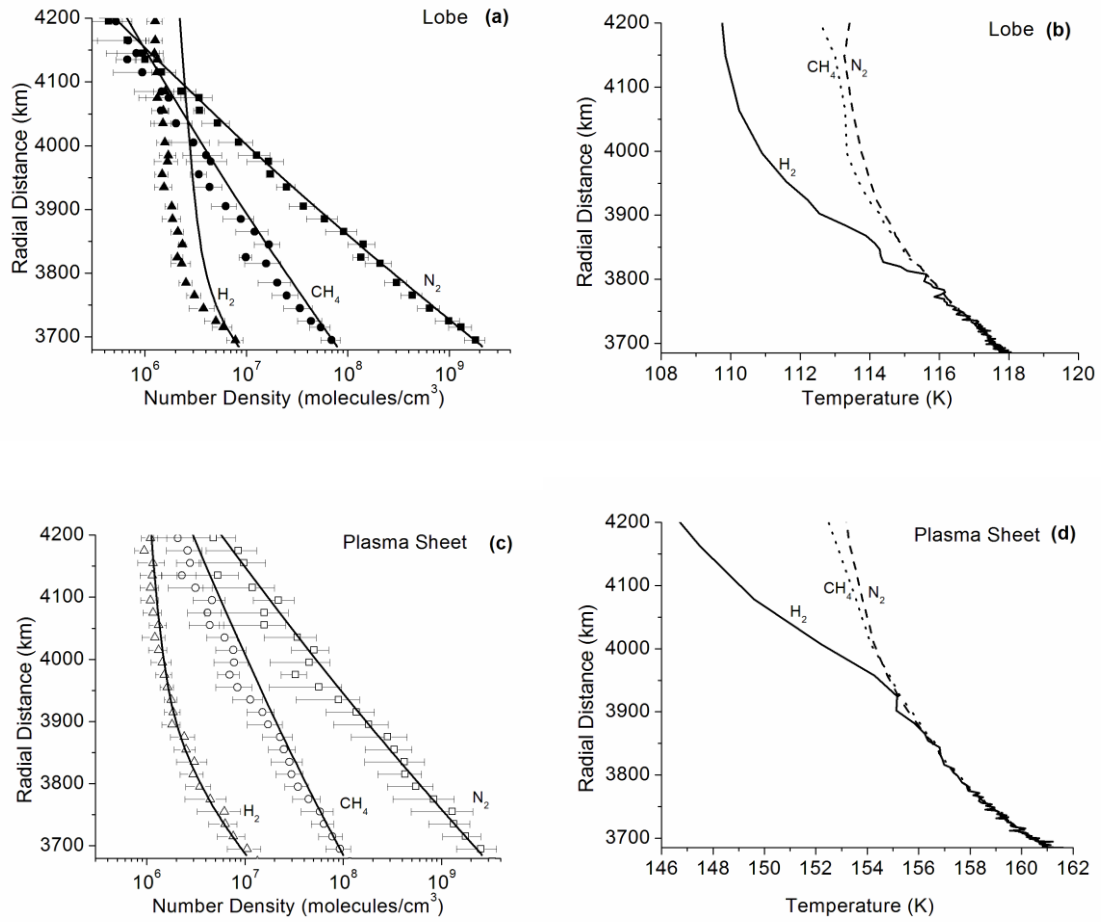


Figure 4-10: Multi-component DSMC results compared to INMS data.

Density (a, c) and temperature (b, d) versus radial distance: INMS density data for N_2 (squares), CH_4 (circles) and H_2 (triangles) are shown for the lobe (filled shapes) and plasma sheet (open shapes). The DSMC results for density (solid curves) are compared to the INMS data and shown in the left panel, and the DSMC results for the temperature of N_2 (dashed curve), CH_4 (dotted curve) and H_2 (solid curve) are shown on the right panel. The lower boundary conditions are: $r_0 = 3685$, $n_0 = (N_2, CH_4, H_2) = 2.1 \times 10^9 \text{ cm}^{-3}$, $9.5 \times 10^7 \text{ cm}^{-3}$ and $8.5 \times 10^6 \text{ cm}^{-3}$, and $T_0 = 118 \text{ K}$ (lobe) and 161 K (plasma sheet).

The 3-component DSMC simulations for Titan's atmosphere are computationally demanding as a result of the small H_2 mixing fraction $f_{H_2}(3685 \text{ km}) = n_{H_2}/n_{N_2} = 0.004$.

The DSMC simulations were performed using the VHS-LB collision model.

Approximately 600,000 representative particles were used to model the atmosphere with a total 6300 particles in the lower boundary cell of which ~ 25 are representative H_2

particles. At every time step we re-distribute velocities to all particles in bottom cell, according to a Maxwell Boltzmann velocity distribution, so that over the duration of the simulation the velocity distribution is well sampled. For example, in the lobe simulations, the statistical scatter in the temperature in the lower boundary cell was $T_{N_2} = 118 \pm 0.04$, $T_{CH_4} = 118 \pm 0.07$ and $T_{H_2} = 118 \pm 0.3$. The fluctuations in the H_2 temperature are greatest near the bottom of the simulation domain where it is a trace species, and in the upper most regions, $r > 4300$ km, where H_2 begins to dominate, the N_2 and CH_4 temperatures fluctuate significantly.

After 3×10^7 steps, at a time step of 0.1 seconds, the DSMC simulations obtained density profiles for N_2 and CH_4 that are similar to both the averaged INMS lobe (Figure 4-10(a)) and plasma sheet (Figure 4-10(c)) data without requiring significant escape, consistent with the simulations with the HS results discussed in Section 4.1. Again it was found that over the duration of the simulation no nitrogen or methane representative particles escaped the simulation domain. If one representative particle would have escaped over the simulation time, the escape rate would have been $\sim 10^{-20}$ CH_4/s several orders of magnitude smaller than the rate inferred from the diffusion equations for CH_4 . This result confirms that for characteristic temperatures in Titan's exosphere CH_4 cannot escape thermally at the proposed rates. Even for the highest temperatures inferred by the INMS density data, i.e. $T \sim 200$ K (e.g., Westlake et al., 2011), the Jeans parameter for methane is $\lambda_{CH_4} \sim 20$, which is much larger than the value suggested for hydrodynamic escape as discussed in Section 4.3 (e.g., Volkov et al., 2011a, b). Although the DSMC simulation reproduces the plasma sheet H_2 densities very accurately, simulations of the lobe data set do not. I find that the H_2 densities diffusively separate from the N_2 densities

at altitudes ~ 3700 km which is approximately 100 km below that seen in the averaged INMS lobe H_2 . In both simulations, the H_2 density profiles began to separate from N_2 at altitudes where the $n_{\text{N}_2} \sim 10^9 \text{ cm}^{-3}$.

In contrast to the DSMC result for N_2 and CH_4 shown in Figure 4-3, H_2 escape causes adiabatic cooling of all three species as shown in Figure 4-10(b, d). That is, the density gradients for N_2 and CH_4 are less steep than the hydrostatic law as a result of the cooling. We derive a nominal exobase distance of $r_x \sim 4000$ km and 4100 km for the lobe and plasma sheet encounters respectively using an average mean free path and a mass averaged scale height. Below the exobase the H_2 temperatures separate from those of N_2 and CH_4 at $r \sim 3800$ km and ~ 3900 km for the lobe and plasma sheet respectively, reaching a maximum difference of about ~ 10 K at 4200 km. Lastly both simulations (lobe, plasma), obtained hydrogen escape rates similar to the Jeans rate, $1.0 \times 10^{28} \text{ H}_2/\text{s}$ ($\sim 1.1 \times \text{Jeans}$) for the lobe and $1.4 \times 10^{28} \text{ H}_2/\text{s}$ ($\sim 1.1 \times \text{Jeans}$) for the plasma sheet, evaluated using the corresponding H_2 densities ($2.9 \times 10^6 \text{ cm}^{-3}$, $1.2 \times 10^6 \text{ cm}^{-3}$), N_2 temperatures (114 K, 154 K) and average exobase altitudes. The N_2 temperature is used to calculate the H_2 Jeans rates as it is the dominant species at the exobase and collisionally populates the tail of the H_2 velocity distribution.

Table 4-3: 3-Component DSMC exobase parameters

	N₂	CH₄	H₂
Lobe: $r_x = 4000$ km			
n_x (cm ⁻³)	1.55×10^7	4.67×10^6	2.86×10^6
T_x (K)	113.9	113.5	111.2
λ_x	64	37	4.6
ϕ_J (H ₂ /s)	2100	4.2×10^{14}	9.0×10^{27}
ϕ_{DSMC} (H ₂ /s)	0	0	1.0×10^{28}
Plasma: $r_x = 4100$ km			
n_x (cm ⁻³)	1.48×10^7	4.93×10^6	1.22×10^6
T_x (K)	153.6	153.2	148.5
λ_x	46	27	3.3
ϕ_J (H ₂ /s)	8.9×10^{10}	9.9×10^{18}	1.3×10^{28}
ϕ_{DSMC} (H ₂ /s)	0	0	1.4×10^{28}

The lower boundary conditions are: $r_0 = 3685$, $n_0 = (\text{N}_2, \text{CH}_4, \text{H}_2) = 2.1 \times 10^9 \text{ cm}^{-3}$, $9.5 \times 10^7 \text{ cm}^{-3}$ and $8.5 \times 10^6 \text{ cm}^{-3}$, and $T_0 = 118 \text{ K}$ (lobe) and 161 K (plasma sheet).

Because the 3-component DSMC simulations are computationally expensive, reducing the statistical scatter by including more particles or performing simulations for altitudes deeper in the atmosphere is challenging. Therefore, as discussed earlier, I modified the code to dynamically track the H₂ molecules in a stationary background N₂ gas; these simulations are referred to as DSMC-H₂. The simulations were completed in significantly less time and provided better statistics. In the DSMC-H₂ simulations, several hundred representative molecules composed the H₂ density in the bottom cell and several thousand at the nominal exobase. Therefore, the fluctuations in the temperature are approximately an order of magnitude smaller. Although the N₂ and CH₄ temperatures and densities are affected by H₂ escape, for simplicity, the densities are taken directly from the INMS data or hydrostatic fits.

The DSMC-H₂ simulations of the averaged INMS data sets are started more than 200 km deeper in the atmosphere than the 3-component DSMC simulations. This computational domain encompassed the complete data set ranging from 3500 – 4600 km using approximately 200,000 -400,000 representative molecules. The lower boundary conditions in the new simulations are now: $r_0 = 3548$ km and $n_0(\text{H}_2) = (7.98 \times 10^7 \text{ cm}^{-3}, 6.53 \times 10^7 \text{ cm}^{-3})$, $Kn_0 = (9.1 \times 10^{-4}, 6.1 \times 10^{-4})$ and $T_0 = (118 \text{ K}, 161 \text{ K})$ for the lobe and plasma sheet respectively. The mixing ratio for these conditions is now $f_{\text{H}_2} = 0.003$, which is a significant decrease from that at 3685 km, and the new lower boundary distance is more than two N₂ scale heights below that used earlier.

The simulations were performed for 2.4×10^8 steps with a time step of $dt = 0.005$ s for a total time of 1.2 million seconds. As indicated in Figure 4-11(a), the exobase distances are essentially the same as those obtained using the 3-component DSMC simulations, ~4000 km and ~4100 km for lobe and plasma sheet respectively. The DSMC-H₂ molecular hydrogen temperature profile is seen to cool with altitude as a result of escape, and again is seen to depart from the fixed N₂ and CH₄ temperatures below the exobase (Figure 4-11(a)). The temperatures for N₂ and CH₄ in the DSMC-H₂ simulations are few degrees higher at the exobase than the 3-component DSMC simulations, 4 and 10 K for the plasma sheet and lobe respectively, because N₂ and CH₄ are not permitted to cool during the simulation. The escape rates are now $1.3 \times 10^{28} \text{ H}_2/\text{s}$ and $1.4 \times 10^{28} \text{ H}_2/\text{s}$, both ~0.93 x Jeans, for the lobe and plasma sheet using the corresponding exobase parameters: $n_x(3.4 \times 10^6 \text{ cm}^{-3}, 1.3 \times 10^6 \text{ cm}^{-3})$ and $T_x(118 \text{ K}, 161 \text{ K})$. Likewise, escape rates are slightly smaller than the Jeans rate as N₂ is not allowed to cool in these simulations.

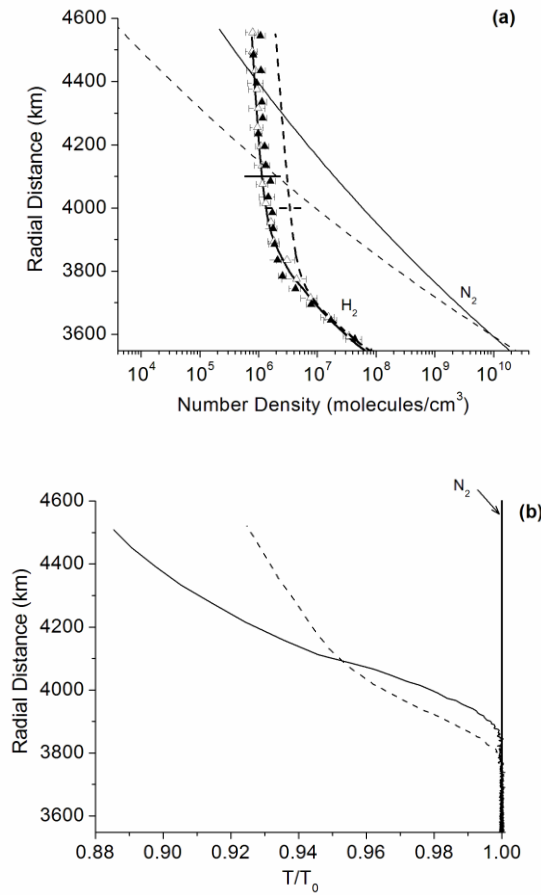


Figure 4-11: Density profiles for DSMC-H₂ simulations.

DSMC-H₂ simulations: (a) Lobe (dashed curves) and plasma sheet (solid curves). H₂ densities compared to data: lobe (filled triangles) and plasma sheet (open triangles). Hydrostatic N₂ profiles are included. The respective exobase altitudes are marked by the horizontal lines. (b) Temperature profiles ($T(r)/T_0$) for the lobe $T_0 = 118$ K (dashed curve) and plasma sheet $T_0 = 161$ K (solid curve) results. The lower boundary is $r_0 = 3548$ km: $n_0(\text{N}_2, \text{H}_2) = (2.39 \times 10^{10}, 7.98 \times 10^7 \text{ cm}^{-3})$ for the lobe and $(2.02 \times 10^{10}, 6.53 \times 10^7 \text{ cm}^{-3})$ for the plasma sheet.

For the plasma sheet case, the DSMC-H₂ and the 3-component DSMC simulations produce consistent results. Both simulations lead to the same escape rates, and at $r = 3700$ km the densities differ by $< \sim 20\%$. The DSMC-H₂ lobe simulation resulted in an escape rate $\sim 30\%$ larger than the 3-component DSMC result. This

difference is attributed to the onset of diffusive separation occurring at lower altitudes in the DSMC-H₂ simulations. In both simulations of the lobe, the H₂ density profile follows its own scale height down to distances as low as $r = 3700$ km. However, in the DSMC-H₂ lobe simulations at 3700 km the density is 1.3 times larger than that in the 3-component DSMC simulation providing a larger inventory of escaping molecules. This suggests that H₂ is not well mixed even at $r \sim 3685$ km, the lower boundary of the 3 component simulations. Therefore, in the following, I primarily compare the DSMC-H₂ results to the INMS data because these simulations are conducted at altitudes well into the region where H₂ should be well mixed with N₂. In spite of the change in the escape rate, the disagreement with averaged INMS lobe densities remains and does not appear to be a simulation artifact. These results contrast with the *averaged* INMS data set (Figure 4-9) for which the H₂ densities profiles are very similar for the plasma sheet and lobe temperatures.

Table 4-4: DSMC-H₂ results for T_{N_2} (100 – 200 K)

DSMC-H ₂ : T_{N_2}	100 K	125 K	150 K	175 K	200 K
$\phi_{\text{DSMC}} (\times 10^{-28} \text{ H}_2/\text{s})$	1.24	1.48	1.48	1.45	1.35
$r_x = 4150 \text{ km}$					
$n_x (\times 10^{-6} \text{ cm}^{-3})$	4.5	2.5	1.4	0.84	0.62
λ_x	5.1	4.1	3.4	2.9	2.5
$\phi_{\text{DSMC}}/\phi_{\text{J}}$	0.80	0.93	0.95	0.94	1.03

The lower boundary is $r_0 = 3548$ km and $n_0(\text{N}_2, \text{H}_2) = (2.39 \times 10^{10}, 7.98 \times 10^7 \text{ cm}^{-3})$. For simplicity the Jeans rates are evaluated at 4150 km for all results using the corresponding T_{N_2} .

It is seen that the simulated H₂ density profiles diffusively separate from the background gas at lower altitudes for lower temperatures than what appears to be shown

by the *averaged* INMS density data sets. This is confirmed by a series of simulations for a range of temperatures in Titan's upper atmosphere $T_{\text{N}_2} = 100 - 200 \text{ K}$ ($\lambda_0 = 5 - 2.5$) resulting in very different H_2 density profiles as seen in Figure 4-12a. At $r = 4150 \text{ km}$, the simulation using $T_{\text{N}_2} = 200 \text{ K}$ resulted in a density approximately 1 order of magnitude smaller than that from a simulation using $T_{\text{N}_2} = 100 \text{ K}$.

There appears to be a slight maximum in the escape rate using $T_{\text{N}_2} = 150 \text{ K}$ ($\lambda_0 \sim 3.4$). As shown by the production of escaping molecules in Figure 4-12b, at the higher temperatures diffusion limits the altitudes from which H_2 can escape, and when molecular escape is permissible the inventory of escaping molecules is depleted. Therefore, for a given T_{N_2} and f_{H_2} there is a competition between the inventory of escaping molecules and their ability to diffuse through N_2 resulting in the maximum escape rate. The exobase distances for these simulations range from $r_x \sim 3900 - 4300 \text{ km}$, however for simplicity I take the exobase distance as $r_x \sim 4150 \text{ km}$ when calculating the theoretical Jeans rates which are compared with the DSMC- H_2 rates in Table 4-4.

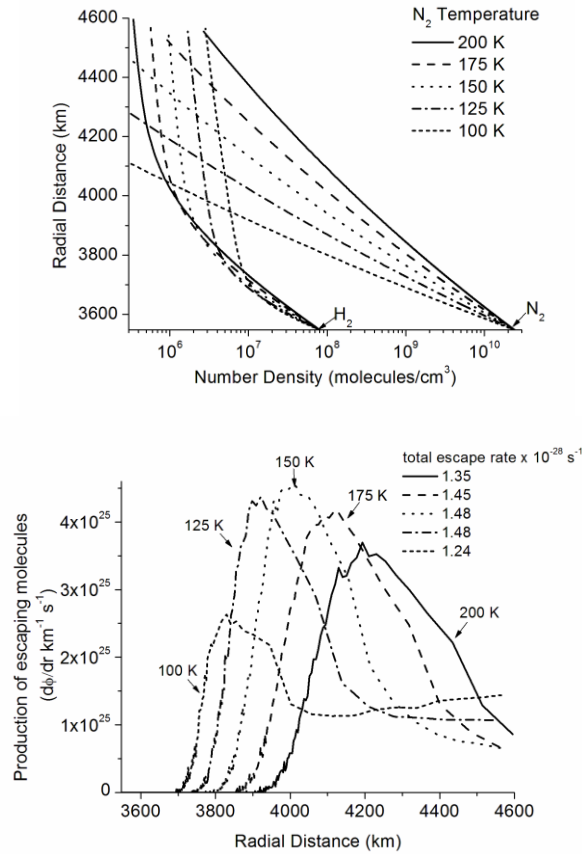


Figure 4-12: DSMC-H₂ simulations showing the effect of diffusion at various T_{N_2} .

(a) DSMC-H₂ density profiles for $T_0 = 100$ K (short dashed curve), $T_0 = 125$ K (dashed dotted curve), 150 K (dotted curve), 175 K (dashed curve) and 200 K (solid curve). The N₂ hydrostatic density profiles are plotted with the same curve style. At colder temperatures H₂ diffusively separates from N₂ at lower altitudes. The averaged INMS density data does not show this trend. (b) Corresponding production of escaping H₂ molecules versus radial distance: lower boundary conditions: $r_0 = 3548$ km, $n_0(N_2, H_2) = (2.39 \times 10^{10}, 7.98 \times 10^7 \text{ cm}^{-3})$.

To examine the discrepancy between the DSMC results and the averaged INMS data we also compared our model results to individual INMS data sets. For example, in an investigation of individual INMS passes, Cui et al., (2011) concluded that the H₂ exospheric density showed temporal variations with the changing plasma environment on dynamical time scales of 10^3 s ($<10^{-3}$ of a Titan day). In addition, Bell et al. (2011)

concluded the response of the molecular nitrogen density profiles to varying magnetospheric energy input occurred on a timescale of $\sim 10^6$ s (~ 0.5 of a Titan day for heating and ~ 0.6 of a Titan day for cooling). Even though the INMS data sets are generally obtained typically one to several Titan days apart and at different times of the day (e.g., Figure 2-5), a qualitative comparison to the steady state DSMC-H₂ results is insightful. The T18 flyby ($T_{N_2} \sim 130$ K) and T19 flyby ($T_{N_2} \sim 140$ K) occurred approximately 1 Titan day apart, with plasma conditions for the T18 flyby classified as lobe and conditions for the T19 flyby as plasma sheet. The N₂ and H₂ densities vs. altitude for these flybys are shown in Figure 4-13a. Molecular hydrogen appears to diffusively separate from the background N₂ at lower altitudes for the T18 flyby. However this pattern is not distinctly noticeable for the entirety of the data set. For example, the T36 flyby ($T_{N_2} \sim 188$ K) and T39 flyby ($T_{N_2} \sim 120$ K) (e. g. Cui et al., 2011 *Table 1*) both classified as plasma sheet, show only a slight difference in the H₂ density profiles even though the difference between the T_{N_2} for these flybys is more than 60 K (Figure 4-13b).

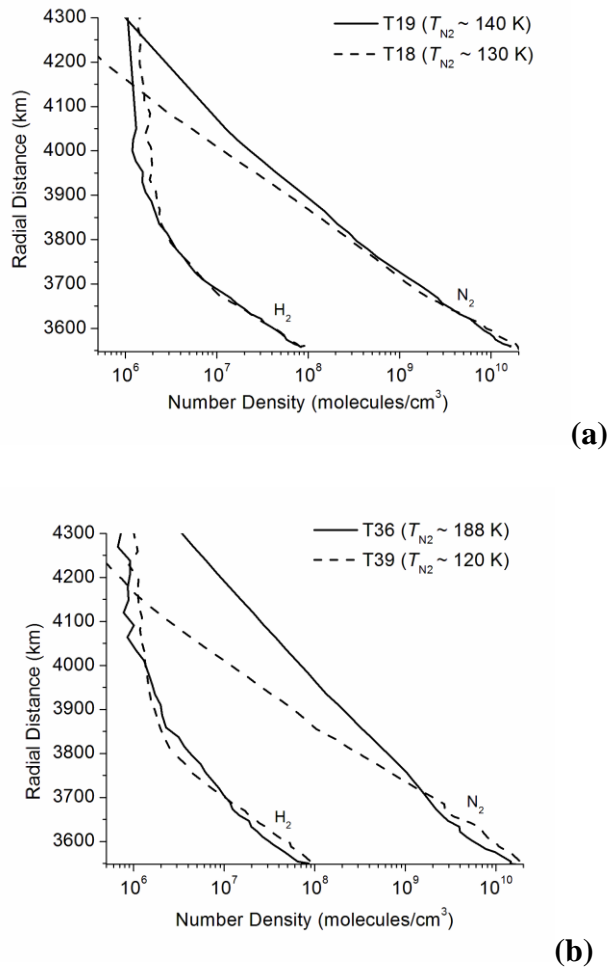


Figure 4-13: Individual INMS N_2 and H_2 density profiles.

(a) The T19 flyby (solid curves) and T18 flyby (dashed curves) qualitatively agree with the DSMC- H_2 trend, that H_2 diffusively separate more efficiently for colder temperatures. (b) The T36 flyby (solid curves) and T39 flyby (dashed curves) do not indicate any difference between the H_2 density profiles even though the N_2 density profiles are significantly different. T_{N_2} is indicated within the parenthesis.

The above comparisons show that the small temporal variations of the H_2 densities in Titan's atmosphere are more apparent in the individual INMS density data sets rather than the averaged data set (e.g. Bell et al., 2011; Cui et al., 2011). Therefore, I carried out simulations of the density profiles obtained during the T41 flyby, classified as a lobe encounter ($T_{N_2} \sim 112$ K), and the T29 flyby, classified as plasma sheet encounter

($T_{\text{N}_2} \sim 145$ K). The data from these passes appear to indicate H_2 diffusively separates at lower altitudes with lower temperatures of the background N_2 gas. Although H_2 diffusively separates at lower altitudes for T41, consistent with the results in Figure 4-12, in Figure 4-14 it is again seen that the lobe densities are not reproduced.

For qualitative analysis, we added heat according to the non-thermal energy deposition rates for Titan's upper atmosphere (e.g., Michael et al., 2005), in test DSMC simulations of a single component N_2 atmosphere to consider the effect of heating on the H_2 density profile. It was assumed that all of the deposited heat went into the translation energy of molecules. I found depositing the plasma energy as heat, and not in the non-thermal processes discussed earlier, only had a modest effect on the profiles and the temperature increased by less than 3 degrees. Since this heat is transferred to H_2 predominantly via collisions with N_2 , the effect on H_2 would also be small. However, it is important to note, above the exobase the H_2 densities eventually become comparable or dominate N_2 , so more detailed simulations of the interaction with the plasma are needed. For instance, if for the lobe cases H_2 was removed rapidly at high altitudes by ionization, transport or some other loss process, the simulations would agree better with the data.

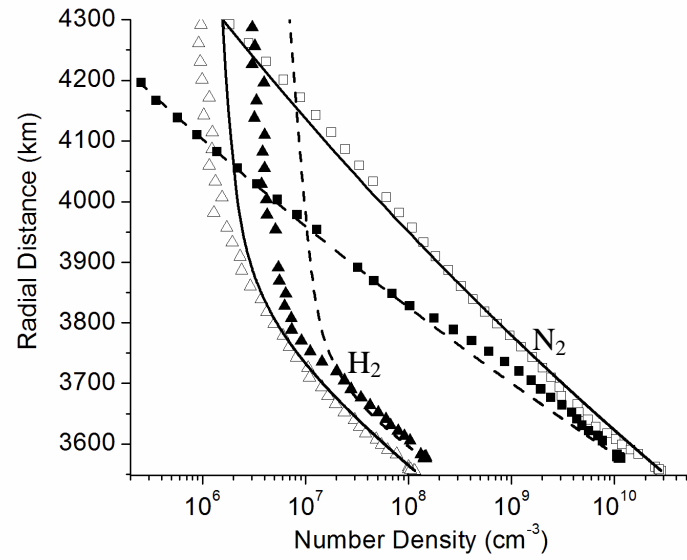


Figure 4-14: DSMC results compared to T29 and T41 flybys.

INMS density data for N_2 (squares) and H_2 (triangles) for individual Titan flybys T29 (open shapes) and T41 (closed shapes) classified as plasma sheet and lobe encounters respectively. These INMS data sets show H_2 diffusively separating from N_2 at lower altitudes when the temperature is colder. DSMC- H_2 : T29 $T_{N_2} = 145$ K (solid curves) and T41 $T_{N_2} = 112$ K (dashed curves). For T29 and T41 respectively, the lower boundary conditions are $r_0 = 3556$ km and 3576 km; n_0 (N_2 , H_2) = $(2.85 \times 10^{10}, 1.15 \times 10^8)$ cm^{-3} and $(1.15 \times 10^{10}, 1.42 \times 10^8)$.

4.4.3 Comparison of DSMC and Diffusion model results

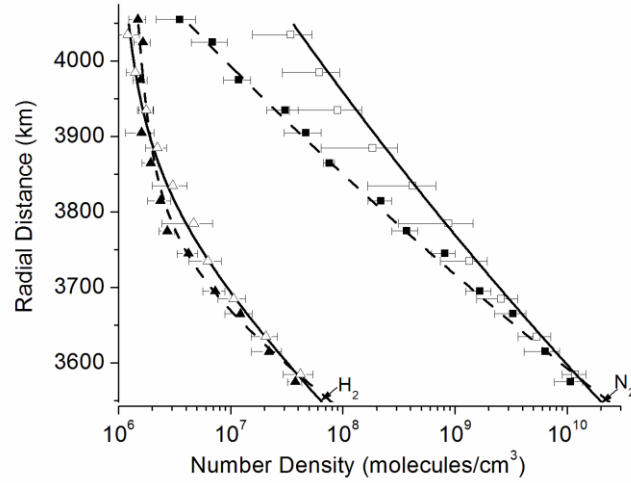


Figure 4-15: Diffusion model fits of the INMS data.

The fits to the plasma sheet (dashed curve) and lobe (solid curve) are plotted against the averaged INMS H₂ densities plasma sheet (open triangles) and lobe (filled triangles).

While it is possible to fit the INMS data with the diffusion equation the DSMC simulation results are in disagreement (i.e. Figure 4-12 and Figure 4-15). The averaged INMS lobe and plasma sheet density profiles have been fit to the diffusion equation by assuming escape rates $\phi_D \sim 6.68 \times 10^{27} \text{ H}_2/\text{s}$ and $5.95 \times 10^{27} \text{ H}_2/\text{s}$ respectively. Both these rates are approximately 97% of the diffusion limited escape rates for (e.g., Equation 2-8), (lobe $\phi_{DL} = 6.9 \times 10^{27} \text{ H}_2/\text{s}$, plasma $\phi_{DL} = 6.1 \times 10^{27} \text{ H}_2/\text{s}$). My DSMC simulations can reproduce the INMS plasma sheet density profile but give a thermal escape rate of $\phi_{DSMC} = 1.4 \times 10^{28} \text{ H}_2/\text{s}$. This indicates the diffusion model might significantly underestimate the escape rate when constrained to INMS data. However, I find that the diffusion and DSMC-H₂ can be made consistent if the diffusion equation is scaled by ϕ_{DSMC}/ϕ_D .

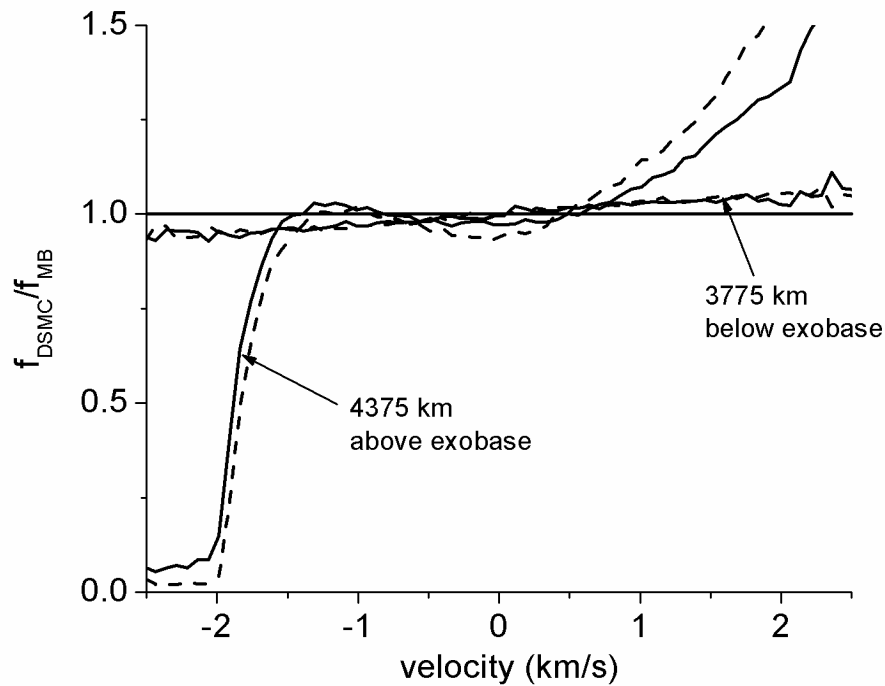


Figure 4-16: DSMC- H_2 velocity distributions.

Radial velocity distributions normalized to a Maxwell Boltzmann distribution for the plasma sheet (dashed curves) and lobe (solid curves) simulations at 3775 km T_{H_2} (~ 161 K and ~ 118 K) and at 4375 km T_{H_2} (~ 145 K and ~ 110 K) respectively.

Lastly, in the DSMC model, diffusion and escape occur concomitantly and the distribution of velocities becomes non-Maxwellian below the exobase. However, in using the diffusion equations Equation 2-6 and Equation 2-7 it is assumed the distributions are nearly Maxwellian at all altitudes and, typically, the temperature of the diffusing species is assumed to be equal to that of the background gas. Even at altitudes below the nominal exobase the DSMC velocity distribution for the minor species, H_2 , is enhanced in upward radial velocities and depleted in downward radial velocities for speeds larger than the escape speed (Figure 4-16). Chamberlain and Smith, (1971) and Cui et al., (2008) also

showed this difference can lead to discrepancies between the escape rates obtained by kinetic models as compared to diffusion models.

5. Conclusions and Future Work

A primary goal of the Cassini mission to Saturn has been to characterize the escape processes and escape rates occurring in Titan's atmosphere. To this end, neutral density data for Titan's upper atmosphere measured by the INMS instrument has been used with computational models to estimate the escape rate. Several continuum models have inferred significant escape rates to match the methane density profiles, but the rates vary drastically between models. These models can reproduce the INMS CH₄ density data for a range of eddy diffusion coefficients and molecular escape rates dependent upon whether escape is assumed to be driven by non-thermal or thermal processes. Furthermore, even though the molecular hydrogen escape rates are roughly consistent between models, it is unclear whether escape is diffusion limited or powered by enhanced heating in the exosphere. Lastly, the continuum models cannot characterize how the H₂ densities respond thermally to exospheric temperatures which can vary by up to ~ 100K depending on the magnetosphere and solar illumination environment.

The limitations of these models, which solve the diffusion equation or the Navier Stokes fluid equations, are well known. Therefore, the inferred escape rates require verification using a kinetic Monte Carlo model or higher moments from the Boltzmann equation. For example, using the continuum models the escape rate is essentially an independent parameter constrained by how well the equations reproduce the INMS density data. In addition, these models are most applicable to gas flows which do not

significantly depart from equilibrium. However, molecular escape occurs from the most rarefied regions of the atmosphere in which the velocity distribution can deviate significantly from a Maxwellian. Therefore, extending the continuum solutions to the exobase and above can be problematic. In particular, it has been suggested that methane escapes from Titan's atmosphere at rates orders of magnitude larger than the Jeans rate by a process referred to as slow hydrodynamic escape. In such models, the Navier Stokes equations are solved assuming the Fourier description of thermal conduction is efficient into the exobase region driving a supersonic expansion of atmosphere.

In this dissertation study, I used the DSMC model to consider the thermal escape of molecules from Titan and Pluto to compare with density data, SHE model results and solutions obtained using the diffusion equation. The DSMC model is a molecular kinetic approach in which the atmosphere flow is modeled using a set of representative molecules that are tracked in the planetary gravitational field and subject to mutual collisions. Molecular escape is inherent to the model, and the atmospheric properties are derived from the evolution of the local velocity distribution due to heat conduction through the lower boundary and escape from the top boundary. There are no assumptions about the density and temperature at infinity, as is the case with fluid models. I applied the DSMC model over a limited range of altitudes where the atmosphere flow transitions from being collisional to collisionless for each body studied.

My DSMC simulations gave consistent results with the INMS density profiles for Titan's upper atmosphere without requiring the large escape rates for CH₄ and N₂ suggested by an application of the SHE model in Strobel (2008a, 2009, 2010). In fact, methane cannot escape Titan thermally for the characteristic exosphere temperatures

because it is strongly bound gravitationally, $\lambda_x \sim 30$. Even at $\lambda_x \sim 10$, I showed that the escape rates were only ~ 1.4 times the theoretical Jeans rate (Tucker and Johnson, 2009; Tucker et al., 2012). Using such simulations, I also showed the escape rate cannot be strongly constrained using fits to density versus altitude data below the exobase. Driven by these results the community modeling the upper atmosphere of Titan has concluded that, as suggested prior to the Cassini mission, the effect of heating from interaction of charged particles in Saturn's magnetosphere with Titan's extended atmosphere has a bearing on the N_2 and CH_4 extended density profiles and escape rates.

It is quite exciting that the ideas I have worked on will soon be further tested by the expected New Horizon spacecraft encounter with Pluto. Pluto's atmosphere, which has $\lambda_x \sim 10$, has been suggested to undergo hydrodynamic escape by several authors (e.g., McNutt, 1989; Krasnopolsky, 1999; Strobel, 2008a; Tian and Toon, 2005). Therefore, in collaboration, primarily with fellow student Justin Erwin, a combined fluid/DSMC approach was used to model the thermal escape from Pluto's atmosphere. These hybrid simulations were carried out for a case in which the heating in the upper atmosphere was neglected and then for a case roughly representing UV heating of the upper atmosphere at solar minimum conditions. For lower boundary conditions leading to $\lambda_0 = 23$ and $Kn(r_0) \sim 10^{-6}$, a fluid model *can* obtain accurate temperatures densities and gas velocities up to the exobase. But this is the case *only* if the escape flux and energy flux out the top of the atmosphere are equal to that obtained from a kinetic simulation of the exobase region. In fact, the total energy flux through the system cannot be determined independently for finite $Kn(r_0)$ using a fluid calculation, because it depends on knowing the flow in the non-equilibrium region of the exosphere. For both cases it was again shown that thermal

escape rate was within a factor of two of the Jeans rate and the flow never went supersonic. Our fluid/DSMC simulations result in rates that were a factor 10 and 1.5 less than the published SHE escape rates for the two cases. However, the fluid/DSMC results for atmospheric density, flow velocity and temperatures in the upper atmosphere differed drastically indicating that obtaining a reasonable escape flux is not a good constraint for successfully describing the structure of the upper atmosphere.

Solar maximum conditions are expected to occur in 2013, so that the New Horizon encounter with Pluto and Charon in 2015 will occur somewhere between solar maximum and minimum conditions. At a distance from the sun of 33 AU and assuming the same heating efficiency and cooling process, this results in a net heating rate used in Equation 2-13 of $\beta_0 \sim 2.5 \times 10^{-3} \text{ erg cm}^{-2} \text{ s}^{-1}$, which is 1.7 times that used here ($\sim 1.5 \times 10^{-3} \text{ erg cm}^{-2} \text{ s}^{-1}$). Therefore, accurate simulations of the atmospheric density at the New Horizon encounter distance 10000 km from Pluto, and the atmospheric structure and the escape rates expected during the encounter will require the use of a fluid/kinetic model such as that described here.

The above results are also relevant to hydrodynamic models of escape from exoplanet atmospheres. These are often based on the fact that the model results are close to the energy limited escape rate. In this limit, the entire energy budget obtained from absorption of solar radiation over narrow region of the thermosphere is converted into heat and drives an adiabatic expansion of the atmosphere (e.g., Lammer et al., 2009; McNutt, 1989; Watson et al., 1981). Ignoring the gravitational effect of Charon, the escape rate we obtain for Pluto during solar minimum conditions is $\sim 84\%$ of the energy-

limited escape rate, $(4\pi r_0^2 \beta_0)/(\lambda_0 k T_0)$. This has suggested to some that fluids models can accurately describe Pluto's upper atmosphere, which is shown here to be incorrect.

The DSMC simulations for thermal escape from the atmospheres of Titan and Pluto were supplemented by our groups' detailed DSMC study of atmospheric structure and escape for the set of parameters (Kn_0, λ_0) , as led by A. Volkov. These parameters were varied from values that corresponded to escape occurring as a bulk outflow to those that correspond to escape on a molecule by molecule basis (Volkov et al., 2011 a,b). Surprisingly, it was determined that for a single component atmosphere for molecular interactions described by HS collisions and for $Kn(r_0) \ll 1$, thermal escape transitioned from being hydrodynamic in nature to evaporative in nature over a narrow range of Jeans parameters. These simulations also confirmed my Titan and Pluto simulations: i.e., for $6 < \lambda_0 < 15$ the escape rate was 1.7 – 1.4 times the Jeans rates. Similar results were found using the VHS and VHS-LB collision cross sections. In this work we also pointed out that the published SHE model's use of the Fourier thermal conductivity significantly overestimates the transfer of heat in the exosphere region.

Consistent with the above, my DSMC simulations showed the H_2 escapes rates at Titan would only be enhanced by a factor $\sim 1.1 - 1.4$ times the Jeans rates. Because the simulated hydrogen density vs. altitude profile was not consistent with the *averaged* INMS H_2 density profile for the so-called lobe encounters, but diffusion models could produce agreement, I carried out further studies. These DSMC simulations showed that molecular hydrogen diffusively separated at lower temperatures than suggested by the INMS data sets analyzed in this study and by others. Surprisingly, the *averaged* inbound INMS density profiles for molecular hydrogen are seen to be very similar for the so-

called lobe and plasma sheet data. In both data sets H_2 appears to begin diffusively separating from the N_2 densities above $r \sim 3800$ km. The DSMC simulation, possibly fortuitously, reproduces the H_2 densities for the plasma sheet data, but when applied to the lobe data set, the DSMC densities diffusively separate above $r \sim 3700$ km leading to H_2 densities at higher altitudes that are larger than that in the averaged data set.

The temperature of the gas is a critical parameter but is, unfortunately, not independently measured and, as shown in Figure 4-11, is significantly different for H_2 and the background gas in the escape region. Rather the temperatures used were extracted by assuming the hydrostatic approximation applies in the region in which the flow speed is negligible. Therefore, the use of a value for T extracted from an average of highly variable density profiles is not necessarily representative. Since the encounter labeled T29 was a plasma sheet encounter and T41 a lobe encounter, I examined them individually. Similar to my DSMC simulations, these two data sets suggest, that for lower temperatures the H_2 densities diffusively separate more efficiently from N_2 than suggested by the averaged INMS lobe data set. However, even for this individual set of data the thermal DSMC- H_2 simulation cannot reproduce the INMS densities.

Additional modeling is required to determine the possible loss processes associated with the interaction of Saturn's plasma with H_2 in Titan's upper atmosphere and the effect of horizontal transport on the H_2 density profiles. Cui et al. (2011) found that the INMS H_2 density data above the exobase in its entirety showed little global variability possibly suggestive of transport. Furthermore, above $r \sim 5000$ km they showed the density data showed little vertical variability between flybys. However, they suggested that the vertical variability in the region $r \sim (4000 - 5000)$ km in H_2 density

profiles in flybys like T18 and T19 were a temporal response the magnetospheric heating with the variability occurring on timescales of $\sim 10^3 - 10^5$ s. Müller-Wodarg et al. (2008) showed global transport of CH_4 below the exobase was important, and at the altitude, $r \sim 3425$ km, where photolysis is most efficient and is occurring on a timescale of $\sim 10^7$ s, they estimated a global transport timescale of $\sim 10^4$ s. Possibly horizontal transport has an effect on the H_2 density profiles above $r = 3548$ km the lower boundary used in DSMC- H_2 simulations for Titan. Clearly there are outstanding issues that might be solved by considering additional data and by using 2 or 3 dimensional simulations. However, based on the work discussed, modeling the data correctly will require molecular kinetic simulations of the transition region of Titan's upper atmosphere, which is one of the most extended in our solar system. Success in describing Titan's upper atmosphere will provide guidance for other bodies that are only studied by remote sensing.

References

- Ailbert, Y., Mousis, O., 2007. Formation of Titan in Saturn's subnebula: constraints from Huygens probe measurements. *Astronom Astrophys* 465, 1051-1060.
- Atreya, S. K., Adams, E.Y., Niemann, H.B., Demick-Montelara, J.E., Owen, T.C., Fulchignoni, M., Rerri, F., Wilson, E.H., 2006, Titan's methane cycle, *Planet Space Sci.* 54, pp 1177- 1187.
- Atreya, S. K., Lorenz, R. D., Waite, J. H. 2009 Titan from Cassini Huygens. Chapter 7 Volatile Origin and Cycles: Nitrogen and Methane. Springer, New York.
- Banks, P. M., Kockarts, G., 1973. *Aeronomy*. Academic Press, New York, Part B Chap. 14-16.
- Bar-Nun, A. Klienfeld, I. Kochavi, E. 1988. Trapping of gas mixtures by amorphous water ice. *Phys Rev B* 38, 7749-7754.
- Bell, J.M., Bougher S.W., Waite Jr., J.H., et al., 2010a. Simulating the one-dimensional structure of Titan's upper atmosphere: 1. Formation of the Titan Global Ionosphere and Thermosphere Model and benchmark simulations. *J. Geophys. Res.* 115, E12002, pp 1-20.
- Bell, J.M., Bougher, S.W. Waite Jr., J.H., et al., 2010b. Simulating the one-dimensional structure of Titan's upper atmosphere 2. Alternative scenarios for escape. *J. Geophys. Res.* 115, E12018, pp 1- 20.
- Bell, J.M. Westlake, J., Waite Jr., J.H., 2011. Simulating the time-dependent response of Titan's upper atmosphere to periods of magnetospheric forcing. *Geophysical Research Letters* 38, L06202 pp 1-4.

- Bertaux, J.L., Kockarts, G., 1983. Distribution of Molecular Hydrogen in the Atmosphere of Titan. *J. Geophys. Res.* 88, A11 pp 8716 - 8720.
- Bird, G. A., 1994. *Molecular Gas Dynamics and the Direct Simulation of Gas Flows*. Clarendon Press Oxford, New York, pp. 218-256.
- Bockelée-Morvan, D., Crovisier, J., Mumma, M. J., Weaver, H. A., 2004. The Composition of Cometary Volatiles. *Comets II*, 391-423.
- Bondi, A., 1964. The nature of the chemical bond. *J. Phys. Chem.* 68, p 441.
- Brecht, S.H., Luhmann, J.G., Larson, D.J., 2000. Simulation of the Saturnian magnetospheric interaction with Titan. *J. Geophys. Res.* 105, pp. 13119 - 13130.
- Brinkmann, 1970. Departures from Jeans escape rate for H and He in the Earth's atmosphere. *Planet Space Sci.* 18, pp. 449 – 478.
- Chamberlain, J.W., Campbell, F.J., 1967. Rate of evaporation of a non-Maxwellian Atmosphere. *Astrophys. J.* 149, p. 687 – 705.
- Chamberlain, J. W., 1960. Interplanetary Gas. II. Expansion of a model of the Solar Corona. *Astrophys. J* 131, pp. 47-56.
- Chamberlain, J. W., 1961. Interplanetary Gas. III. Hydrodynamic Model of the Corona. *Astrophys. J* 133, pp. 675-687.
- Chamberlain, J. W., 1963. Planetary Coronae and Atmospheric evaporation. *Planet. Space Sci.* 11, pp. 901-960.
- Chamberlian, J.W., and Smith, G.R., 1971. Comments on the rate of evaporation of a non-Maxwellian atmosphere. *Planet. Space Sci.* 19, pp. 675 – 684.
- Chapman, S. and Cowling, T. G., 1970. *The Mathematical Theory of Non-uniform Gases* 3rd edition. Cambridge University Press, New York, Chapter 10.

- Coates, A.J., Crary, F.J., Young, D.T., Szego, K., Arridge, C.S., Bebesi, Z., Sittler, E.C., Jr., Hartle, R.E., Hill, T.W., 2007. *Geophys Res. Lett.* 34 p. L24S05.
- Cordier, D., Mousis, O., Lunine, J. I., Moudens, A., Vuitton, V., 2008. Photochemical enrichment of deuterium in Titan's atmosphere: new insights from Cassini-Huygens. *Astrophys. J* 689, L61-L64.
- Cravens, T. E., Keller, C. N., Ray, B., 1997. Photochemical sources of non-thermal neutrals for the exosphere of Titan. *Planet Space Sci.* 45, 889-896.
- Cui, J., Yelle, R. V., Volk, K., 2008. Distribution and escape of molecular hydrogen in Titan's thermosphere and exosphere. *J. Geophys. Res.* 113, E10004.
- Cui, J. and 12 other colleagues, 2009. Analysis of Titan's neutral upper atmosphere from Cassini Ion Neutral Mass Spectrometer measurements. *Icarus* 200, 581-615.
- Cui, J., Yelle, R. V., Müller-Wodarg, I. C. F., Lavvas, P. P., Galand, M., 2011. The implications of H₂ variability in Titan's exosphere. *J. Geophys. Res.* 116, p. A11324.
- Dandouras, I., Garnier, P., Mitchell, D. G., Roelof, E. C., Brandt, P. C., Krupp, N., Krimigis, S. M., 2009. Titan's exosphere and its interaction with Saturn's magnetosphere. *Phil. Trans. R. Soc. A* 367, pp. 743-752.
- De La Haye, V., Waite Jr., J.H., Johnson, R.E., et al., 2007a. Cassini Ion and Neutral Mass Spectrometer data in Titan's upper atmosphere and exosphere: Observation of a suprathermal corona. *J. Geophys. Res.* 112, A07309.
- De La Haye, V., Waite Jr., J.H., Cravens, T.E., Nagy, A.F., Yelle, R.V., Johnson, R.E., Lebonnois, Robertson, I.P., 2007b. Titan's corona: The contribution of exothermic chemistry. *Icarus* 191, 236-250.

Elliot, J. L., and 19 colleagues, 2007. Changes in Pluto's Atmosphere: 1988-2006.

Astrophys. J. 134, 1-13.

Gan, L. Keller, C. N., Craven, T. E., 1992. Electrons in the ionosphere of Titan. J.

Geophys Res 97, 12,137-12,151.

Garnier, P., Dandouras, I., Toubanc, D., Roelof, E. C., Brandt, P. C., Mitchell, D. G.,

Krimigis, S. M., Krupp, N., Hamilton, D. C., Dutuit, O., Wahlund, J.-E., 2008.

The lower exosphere of Titan: Energetic neutral atoms absorption and imaging. J.

Geophys. Res. 113, A10216.

Garnier, P., Dandouras, I., Toubanc, D., Brandt, P. C., Roelof, E. C., Mitchell, D. G.,

Krimigis, S. M., Krupp, N., Hamilton, D. C., Dutuit, Waite, H., 2007. The

exosphere of Titan and its interaction with the Kronian magnetosphere: MIMI

observations and modeling. Planet Space Sci. 55, pp. 165 - 173 A10216.

Greaves, J. S., Helling, Ch., Friberg, P. 2011. Discovery of carbon monoxide in the

upper atmosphere of Pluto. [2011arXiv1104.3014G](https://arxiv.org/abs/2011arXiv1104.3014G).

Grevesse, N. Asplund, M., Sauval, J., 2005. The new solar composition. In: Alcan, G.,

Richard, O., Vauclair, S., (eds) Element stratification in stars: 40 years of atomic

diffusion. EAS publications series, 21-30.

Gruzinov, A., 2011. The rate of thermal atmospheric escape, arXiv:1101.1103v1 [astro-

ph.EP] p. 5.

Hartle R.E., et al., 2006. Preliminary interpretation of the Titan plasma interaction as

observed by the Cassini plasma spectrometer: comparison with Voyager I.

Geophys Res Lett. 33.

- Hersant, F., Gautier, D., Tobie, G., Lunine, J.I., 2008. Interpretation of the carbon abundance in Saturn measured by Cassini. *Planet. 52*, pp. 623-641.
- Hunten D. M., 1973. The Escape of Light Gases from Planetary Atmospheres. *J. Atmos. Sci.* 30, 1481-1494.
- Hunten, D. M. and Watson, A. J., 1982. Stability of Pluto's Atmosphere. *Icarus* 51, 665-667.
- Jeans, J. H., 1916. *The Dynamical Theory of Gases: The Outer Atmosphere*. Cambridge University Press, 351- 363.
- Johnson, R. E., 1990. *Energetic charged particle interactions with atmospheres and surfaces*. Springer, Berlin.
- Johnson, R. E., 1994. Plasma-induced Sputtering of an Atmosphere. *Space Sci Rev* 69, 215-253.
- Johnson, R. E., 2004. The magnetospheric plasma-driven evolution of satellite atmospheres. *Astrophys. J.* 609, L99-L102.
- Johnson, R. E., 2009. Sputtering and heating of Titan's upper atmosphere. *Phil. Trans. R. Soc. A* 376, pp. 753-771.
- Johnson, R. E., 2010. Thermally Driven Atmospheric Escape. *Astrophys. J.* 716, 1573-1578.
- Johnson, R. E., Combi, M. R., Fox, J. L., Ip, W.-H., Leblanc, F., McGrath, M. A., Shematovich, V. I., Strobel, D. F., Waite, J. H., 2008. Exospheres and Atmospheric Escape. *Space Sci. Rev.* 139, pp. 355-397.

- Johnson, R. E., Tucker, O. J., Michael, M., Sittler, E. C., Smith, H. T., Young, D. T., Waite, J. H., 2009. Titan from Cassini Huygens. Chapter 15 Mass Loss Processes in Titan's Upper Atmosphere. Springer, New York.
- Krasnopolsky, V. A., 1999. Hydrodynamic flow of N₂ from Pluto. J. Geophys. Res. 104, 5955-5962.
- Krasnopolsky, V.A., 2010. A photochemical model of Titan's atmosphere and ionosphere. Icarus 201, pp. 226 – 256.
- Lammer, H., Bauer, S. J. 1993. Atmospheric Mass Loss from Titan by sputtering. Planet. Space Sci. 41, 657-663.
- Lammer, H. Stumptner, W. Bauer, S.J., 1998. Dynamic escape of H from Titan as a consequence of sputtering and induced heating. Planet. Space Sci. 46, pp. 1207 – 1213.
- Lammer, H., Stumptner, W. Molina-Cuberos, G. J., Bauer, S. J., Owen, T., 2000. Nitrogen isotope fractionation and its consequence for Titan's atmospheric evolution. Planet Space Sci 48, 529-543.
- Lammer, H., et al., 2009. Determining the mass loss limit for close-in exoplanets: what can we learn from transit observations? Aston. Astrophys. 506, pp. 399-410.
- Lebonnois, A., Bakes, E. L. O and McKay, C. P., 2003. Atomic and molecular hydrogen budget in Titan's atmosphere. Icarus 161, pp. 474-485.
- Lellouch, E., de Bergh, C., Sicardy, B., Ferron, S., Käufl, H.-U., 2010. Detection of CO in Triton's atmosphere and the nature of surface-atmosphere interactions. A & A 512, L8.
- Lewis, J. S., 1971. Chemistry of the outer solar system. Space Sci Rev 14, 401-410.

- Loeffler, M.J., Baragiola, R.A., 2012. Blistering and explosive desorption of irradiated ammonia-water mixtures. *Astrophys. J.* 744:102, pp. 1-7.
- Lunine, J. Choukroun, M. Stevenson, D., Gabriel, T. 2009. Titan from Cassini Huygens. Chapter 3 The Origin and Evolution of Titan. Springer, New York.
- Lunine, J. I., Yung, Y. L., Lorenz, R. D., 1999. On the volatile inventory of Titan from isotopic abundances in nitrogen and methane. *Planet Space Sci* 47, 1291 – 1303.
- Ma, Y., Nagy, A.F., Cravens, T.E., Sokolov, V., Hansen, K.C., Wahlund J-E, Crary, F.J., Coates, A.J., Dougherty, M.K., 2006. Comparisons between MHD model calculations and observations of Cassini flybys of Titan. *J. Geophys. Res.* 111.
- Magee, B. A., Waite, J.W., Mandt, K.E., Westlake, J., Bell, J., Gell, D.A., 2009. INMS-derived composition of Titan's upper atmosphere: Analysis methods and model comparison. *Planet. Space Sci.* 57, pp. 1895 – 1916.
- Mandt, K. E., Waite, J. H., Lewis, W., Magee, B. A., Bell, J. M., Lunine, J. I., Mousis, O., Cordier, D., 2009. Isotopic evolution of the major constituents of Titan's atmosphere based on Cassini data. *Planet Space Sci* 57, 1971 – 1930.
- Marconi, M.L., Dagum, L., Smyth W.H., 1996. Hybrid fluid/ kinetic approach to planetary atmospheres: An example of an intermediate mass body. *Astrophys. J.* 469, 393-401.
- Marten, A., Hidayat, T., Biraud, Y., Moreno, R., 2002. New millimeter heterodyne observations of Titan: vertical distributions of nitriles HCN, HC₃N, CH₃CN and the isotopic ratio ¹⁵N/¹⁴N in its atmosphere. *Icarus* 158, 532-544.
- Mauk, B.H., D.C. Hamilton, T.W. Hill, G.B. Hospodarsky, R.E. Johnson, C. Paranicas, E. Roussos, C.T. Russell, D.E. Shemansky, E.C. Sittler, R.M. Thorne,

- "Fundamental Plasma Processes in Saturn's Magnetosphere", Chapter 11 in *Saturn from Cassini-Huygens* (ed. M.K. Dougherty) pp 281-331 (2009).
- McKay, C. P. Scattergood, T. W., Pollack, J.B., Borucki, W. J., van Ghysseghem, H. T., 1988. High-temperature shock formation of N₂ and organics on primordial Titan. *Nature* 322, 520-522.
- McNutt, R. L., 1989. Models of Pluto's Upper Atmosphere. *Geophys. Res.* 16, 1225-1228.
- Michael, M., Johnson, R. E., 2005. Energy deposition of pickup ions and heating of Titan's atmosphere. *Icarus* 175, 263-267.
- Michael, M., Johnson, R. E., Leblanc, F. Liu, M. Luhmann, J. G., Shematovich, V. I., 2005. Ejection of nitrogen from Titan's atmosphere by magnetospheric ions and pick-up ions. *Icarus* 175, 263-267.
- Mousis, O., Gautier, D., Bockelée-Morvan, D., 2002. Turbulent model of the Saturn subnebula: implications for the origin of methane in Titan's atmosphere. *Icarus* 156, 162-175.
- Müller-Wodarg, I. C. F. and Yelle, R. V., 2002. The effects of dynamics on the composition of Titan's upper atmosphere. *Geophys. Res.* 29 p2139.
- Müller-Wodarg, I. C. F., Yelle, R. V., Cui, J., Waite, J.H. Jr, 2008. Horizontal structures and dynamics of Titan's thermosphere. *J. Geophys. Res.* 113 p. E10005.
- Niemann, H. B., and the GCMS team, 2005. The abundances of the constituents of Titan's atmosphere from the GCMS instrument on the Cassini Huygens probe. *Nature* 438, 779-784.
- Öpik, E.J., 1963: Selective escape of gases. *Geophys. J. Roy. Astron. Soc.*, 7, 490-509.

- Owen, T., 2000. On the origin of Titan's atmosphere. *Planet Space Sci* 48, 747-752.
- Owen, T., Encrenaz, T., 2003. Elemental Abundances and Isotope Ratios in the Giant Planets and Titan. *Space Science Reviews* 206, 121-138.
- Owen, T., MaHaffy, P. R., Niemann, H. B., Aterya, S., Wong, M., 2001. Protosolar Nitrogen. *Astrophys. J.* 553, L77-L79.
- Parker, E. N., 1958. Dynamics of the Interplanetary Gas and Magnetic Fields. *Astrophys. J.* 128, 664-676.
- Parker, E. N., 1964a. Dynamical Properties of Stellar Coronas and Stellar Winds. I. Integration of the Momentum Equation. *Am. Astron. Soc.* 139, 72-92.
- Parker, E. N., 1964b. Dynamical Properties of Stellar Coronas and Stellar Winds. II. Integration of the Heat-Flow Equation. *Am. Astron. Soc.* 139, 93-122.
- Prinn, R. G., Fegley, B., 1981. Kinetic Inhibition of CO and N₂ reduction in the circumplanetary nebulae: implications for satellite composition. *Astrophys J* 249, 308-317.
- Rymer, A.J., Smith, H.T., Wellbrock, A., Coates, A.J., Young, D.T., 2006. Discrete classification and electron energy spectra of Titan's varied magnetospheric environment, *Geophys. Res. Lett.*, 36, p. L15109.
- Sekine, Y., Genda, H., Sugita, S., Kadono, T., Matsui, T., 2011. Replacement and late formation of atmospheric N₂ on undifferentiated Titan by impacts. *Nature Geoscience* 4, 359-362.
- Shematovich, V. I., Johnson, R. E., Michael, M., Luhmann, J. G., 2003. Nitrogen Loss from Titan. *J. Geophys Res* 108, E085087, E6, 1-11.

- Shizgal, B., Blackmore, R., 1986. A collisional kinetic theory of a plane parallel evaporating planetary atmosphere. *Planet Space Sci.* 34, pp. 279-291.
- Sillanpaa, I., Kallio, E., Jarvinen, R., Schmidt, W., Mursula, K., Vippola, J., Tanskanen, P., 2006. Hybrid simulation study of ion escape at Titan for different orbital positions. *Adv Space Res.* 38, pp. 799-805.
- Simon, S., Wennmacher, A., Neubauer, F.M., Bertucci, C.L., Kriegel, H., Saur, J., Russell, C.T., Dougherty, M.K., 2010. Titan's highly dynamic magnetic environment: A systematic survey of Cassini magnetometer observations from flybys TA – T63. *Planet. Space Sci.*, 58, pp. 1230 – 1251.
- Sittler, E.C., et al., 2010. Saturn's magnetospheric interaction with Titan as defined by Cassini encounters T9 and T18: New results. *Planet. Space Sci.* 58, pp. 327 – 350.
- Spitzer, L. Jr., 1949. *The Atmospheres of the Earth and Planets.* Univ. of Chicago Press, Chicago, Illinois pp. 213-249.
- Strobel, D. F., 2008a. N₂ escape Rates from Pluto's atmosphere. *Icarus* 193, 612-619.
- Strobel, D. F., 2008b. Titan's Hydrodynamically escaping atmosphere. *Icarus* 193, 588-594.
- Strobel, D.F., 2009. Titan's hydrodynamically escaping atmosphere: Escape Rates and Exobase Structure. *Icarus* 202, 632—641.
- Strobel, D. F., 2010. Molecular hydrogen in Titan's atmosphere: Implications of the measured tropospheric and thermospheric mole fractions. *Icarus* 208, 878-886.
- Strobel, D. F., Shemansky, D. E., 1982. EUV emissions from Titan's upper atmosphere: Voyager I encounter. *J Geophys Res* 87, 1361-1368.

- Tian, F., 2009. Thermal escape from super Earth atmosphere in the habitable zone of M stars. *Astrophys. J.* 703, 905–909.
- Tian, F. and Toon, O. B., 2005. Hydrodynamic escape of nitrogen from Pluto. *J. Geophys. Res.* L18201-L18205.
- Trafton, L., 1980. Does Pluto have a Substantial Atmosphere? *Icarus* 44, 53-61.
- Tucker, O. J., Erwin, J. T., Volkov, A. N., Cassidy, T. A., Johnson, R. E., 2011. Escape from Pluto's atmosphere: Fluid/DSMC hybrid simulation. *Proc. 27th International Symposium on Rarefied Gas Dynamics*, Pacific Grove, USA, 2010, AIP Conf. Proc. 759 1333, pp. 1145–1150.
- Tucker, O. J. and Johnson, R. E., 2009, Thermally driven atmospheric escape: Monte Carlo simulations for Titan's atmosphere. *Planet Space Sci.* 57, 1889-1894.
- Tucker, O. J., Erwin, J. T., Deighan, J. I., Volkov, A. N., Johnson, R. E., 2012. Thermally driven escape from Pluto's atmosphere: combined fluid/kinetic model. *Icarus*, 217, pp. 408 – 415.
- Volkov, A. N., Johnson, R. E., Tucker, O. J. and Erwin, J. T. 2011a. Thermally-driven atmospheric escape: Transition from hydrodynamic to Jeans escape. *Astrophys. J.* 729, L24 1-5.
- Volkov, A. N., Tucker, O. J., Erwin, J. T. and Johnson, R. E., 2011b. Kinetic Simulations of Thermal escape from a single component atmosphere. *Phys. Fluid* 23, 066601 1-16.
- Vuitton, V., Yelle, R.V., McEwan, M.J., 2007. Ion chemistry and N containing molecules in Titan's upper atmosphere. *Icarus* 191, 722.

- Wahlund, J.-E., et al., 2005. Cassini Measurements of Cold Plasma in the Ionosphere of Titan, *Science* 308, pp. 982-986.
- Waite, J. H., et al., 2005. The Cassini Ion and Neutral Mass Spectrometer (INMS) Investigation. *Space Sci. Rev.* 114, 113-231.
- Watson, A. J., Donahue, T. M., Walker J. C. G., 1981. The Dynamics of a Rapidly Escaping Atmosphere: Applications to the Evolution of Earth and Venus. *Icarus* 48, 150-166.
- Westlake, J. H., Bell, J. M., Waite, J. H., Johnson, R. E., Luhmann, J. G., Mandt, K. E., Magee, B. A., Rymer, A. M., 2011. Titan's thermospheric response to various plasma environments. *J. Geophys. Res.* 116. A03318.
- Wilson, E. H., Atreya, S.K., 2004. Current state of modeling the photochemistry of Titan's mutually dependent atmosphere and ionosphere. *J. Geophys. Res.* 109, p. E06002.
- Yelle, R. V., 2004. Aeronomy of extra-solar giant planets at small orbital distances. *Icarus* 170, 167-179.
- Yelle, R.V., Borggren, N., de la Haye, V., Kasprzak, W.T., Niemann, H.B., Müller-Wodarg, I. C. F., and Waite Jr., J.H., 2006. The vertical structure of Titan's upper atmosphere from Cassini Ion Neutral Mass Spectrometer measurements, *Icarus* 182, pp. 567–576.
- Yelle, R. V. Cui, J. and Müller-Wodarg I. C. F., 2008. Eddy diffusion and methane escape from Titan's atmosphere, *J. Geophys. Res.* 113, p. E10003.
- Young, E. F. and 13 colleagues, 2008. Vertical Structure in Pluto's Atmosphere from the 2006 June 12 Stellar Occultation. *Astrophys. J.* 136, 1757-1769.